**Netherlands Institute of Applied Geoscience TNO**
*- National Geological Survey*

Princetonlaan 6
P.O. Box 80015
3508 TA Utrecht

www.tno.nl

T +31 30 2564750
F +31 30 2564755
info@nitg.tno.nl

**TNO report**

# The evolution of groundwater quality around pumping-station Holten, The Netherlands, simulated by means of the multi-component geochemical transport model PHT3D

| | |
|---|---|
| Date | December, 2004 |
| Author(s) | Linda Ruijpers |
| Supervision | Bas van der Grift (TNO-NITG)<br>Boris van Breukelen (Vrije Universiteit Amsterdam)<br>Jasper Griffioen (TNO-NITG) |
| No. of copies | 16 |
| Number of pages | 100 |
| Number of appendices | 4 |

# Contents

# Figures

# Tables

# Acknowledgements

I would like to thank Henning Prommer for greatly helping me during my internship. Whenever I sent him an e-mail, he was always willing to answer my questions and give useful advises. When he happened to be in Holland we met in Delft; the resulting talk with him clarified matters!
Alice Buijs helped me with taking groundwater samples in the observation wells in and around Holten. She carefully taught me how to handle the different pumps and how to treat the pumped groundwater. Furthermore, Bertil van Os and Erik van Vilsteren are acknowledged for carrying out the chemical analyses on the groundwater samples. The drinking water company Vitens and Statistics Netherlands (CBS) are thanked for providing me with a large amount of field data.
I would also like to express my gratitude to Annemieke Marsman, who several times converted my recharge series for the model input to grid files compatible for PHT3D. Also Aris – "Ik schrijf er wel even een scriptje voor!" – Lourens was always ready to help me with running the model on supercomputer beowulf.
Last but not least, I would like to thank my supervisors Bas van der Grift, Jasper Griffioen and Boris van Breukelen. Whenever I had questions they took their time to help me. I am grateful that they enabled me to carry out this interesting research at NITG-TNO.

# Summary

The research as described in this Master's thesis follows an earlier study carried out by NITG-TNO and Royal Haskoning (Griffioen et al., 2003). The latter study examined the influence of various land use functions and changes in land use functions on groundwater quality by means of the reactive transport model RT3D (Clement, 1997). The load at surface level resulting from the various land use functions formed the input for the model. The reactive transport was calculated in three dimensions for the most important groundwater quality parameters, nitrate, sulfate and chloride and incorporated only nitrate reduction as a geochemical process. As some significant differences between measured and simulated concentrations remained, the current study was set up in order to calculate three-dimensional reactive transport by means of the more sophisticated reactive transport model PHT3D (Prommer et al., 2003). PHT3D couples the three-dimensional transport simulator MT3DMS (Zheng and Wang, 1998) with the geochemical model PHREEQC-2 (Parkhurst and Appelo, 1999) and is therefore able to model various geochemical processes and consider the composition of the groundwater as a whole (multi-component geochemical modeling). Again, the load at surface level resulting from the various land use functions formed the input for the model. However, besides nitrate, sulfate and chloride, other components, e.g., sodium, potassium, calcium and magnesium, were included in the model. Furthermore, in addition to nitrate reduction, cation exchange, aqueous complex formation, dissolution and precipitation processes and other redox processes were incorporated in the model as geochemical processes. The area around the groundwater pumping station near Holten, The Netherlands, served as pilot in both studies.
Aim of the PHT3D study is to check the reactive transport calculations of RT3D and reveal the error causing the differences between measured and simulated concentrations. Moreover, it is attempted to make accurate estimates of the load at surface level for the other components and to ascertain the hydrogeochemical processes occurring in the subsurface of the study area.

Before starting to build a three-dimensional model in PHT3D, a one-dimensional transport model is constructed in PHREEQC-2. According to Griffioen et al. (2003), calcite dissolution, pyrite oxidation and the precipitation of iron hydroxide are important hydrogeochemical processes occurring in the study area. Furthermore, they found that part of the groundwater was supersaturated with respect to siderite. In order to properly understand the hydrogeochemical processes in the aquifers in and around Holten and how they are related to each other, nine scenarios are studied in PHREEEQC-2. Input for the one-dimensional model comprises the load at surface level for nitrate, sulfate, chloride, sodium, potassium, calcium, magnesium and bicarbonate.
In general, from the one-dimensional model study it can be concluded that groundwater quality in the area around Holten depends on both the composition of the load at surface level and the reactive components in the aquifers. The one-dimensional model study furthermore showed that the equilibria of calcite, pyrite, siderite and iron hydroxide are strongly related to each other in the geochemical setting of the Holten aquifers.

Subsequently, a three dimensional reactive transport model, representing the subsurface of Holten and its surroundings, was constructed in PHT3D. The model covers an area of approximately 70 square kilometres and has a thickness of about 80 metres. As in PHT3D all chemical species which are possibly formed need to be specified in the

input, the load at surface level comprises besides sodium, potassium, calcium, magnesium, nitrate, sulfate and chloride, another eight components: nitrite, nitrogen gas, ammonium, hydrogen sulfide, methane, oxygen and iron (iron(II) and iron(III)). Moreover, in stead of bicarbonate, alkalinity is defined as carbonate in the PHT3D input. Finally, two more components, bromide (Br) and lithium (Li), are specified in order to neutralize electrical imbalances in the input.

As with the one-dimensional reactive transport model, the minerals calcite, pyrite, siderite and iron hydroxide form the reactive components in the three-dimensional PHT3D model. Furthermore, cation exchange is imposed as a hydrogeochemical process in the model.

Considering the nitrate, sulfate and chloride concentrations simulated by PHT3D and RT3D it becomes clear that with respect to nitrate and chloride, PHT3D yields better results than RT3D, whereas with respect to sulfate both PHT3D and RT3D do not fully represent the observed concentration changes in time. Furthermore, the three-dimensional model study in PHT3D shows results comparable to the one-dimensional model results: both the load at surface level and reactive components in the aquifers determine the groundwater quality in the area around Holten.

With respect to the reactive transport study carried out by Griffioen et al., it is concluded that for nitrate the differences between simulations and observations in RT3D were caused by the fact that, besides pyrite oxidation by nitrate reduction, no hydrogeochemical processes were incorporated in the model. The sulfate concentrations simulated in PHT3D do not show an improvement with respect to the sulfate concentrations simulated in RT3D. It is therefore for sulfate hard to determine the error which caused the differences between simulations and observations in RT3D. However, it is expected that the differences between simulated and observed sulfate concentrations in RT3D were caused by wrong estimates of the sulfate load at surface level or improper modeling of sulfate leaching from the unsaturated zone. For chloride, it is concluded that the differences between simulated and observed concentrations in RT3D were caused by wrong estimates of the load at surface level.

# 1 Introduction

## 1.1 Scope and aims

Recently, research about the influence of various land use functions and changes in land use functions on groundwater quality has been carried out by NITG-TNO and Royal Haskoning (Griffioen et al., 2003). Purpose of the research project was to develop a method in adjusting alterations in spatial planning, like house-building, agricultural changes, designation of drinking water supply areas and recreation and nature areas, to protection and control of groundwater systems. The area around the groundwater pumping station near Holten, The Netherlands, served as pilot in this study. Considered land use types were agricultural land, nature, urban areas and recreational areas.
In order to quantify the influence of current land use and changes in land use on groundwater quality, first a conservative transport model, MT3DMS (Zheng and Wang, 1998) was used. The three-dimensional transport model was based on a groundwater flow model constructed in MODFLOW (McDonald and Harbaugh, 1996). Then, a reactive transport model, RT3D (Clement, 1997), was used in order to calculate nitrate degradation during groundwater transport. Input for the transport models consisted of recharge concentrations of the most important groundwater quality parameters: nitrate, sulfate and chloride. Recharge concentrations were determined beforehand in MD-SAT (Van den Brink and Van Immerzeel, 2002), a model in which by means of data about the load at surface level resulting from different land use functions, the composition of groundwater recharge is calculated. Input for MD-SAT was calculated from CBS (Statistics Netherlands) data about atmospheric deposition and amounts and types of manure and fertilizers applied at agricultural lands, and consisted of yearly changing nitrate, sulfate and chloride loads at surface level. Subsequently, MD-SAT calculated to what extent the load at surface level changed during its transport towards the groundwater table, as a result of uptake by vegetation and degradation in the unsaturated zone. The model thereby takes into account different land use types, soil types and groundwater levels. Finally, the output generated by MD-SAT consisted of yearly changing and spatially variable nitrate, sulfate and chloride recharge concentrations.

The groundwater quality as observed in the pumping and observation wells near Holten in the period between 1900 and 2000 was roughly reproduced by the simulations of the reactive transport model (Griffioen et al., 2003). However, some significant differences between measured and calculated concentrations remained. According to the authors, wrong estimates of the surface load or improper modeling of unsaturated zone leaching are held responsible for this. Alternatiely, differences can be caused by the fact that only the process of nitrate reduction by pyrite oxidation was simulated in the model. Further hydrogeochemical processes, e.g. cation exchange, aqueous complex formation, precipitation and dissolution processes and other reduction and oxidation (redox) processes were not incorporated in the model. A fully geochemical approach where other components, e.g., sodium, potassium, calcium and magnesium, are included may allow to distinguish between these two types of error.

The main goal of this study, carried out under the authority of NITG-TNO, therefore, is to check the reactive transport calculations of RT3D by means of a more sophisticated

reactive transport model, PHT3D (Prommer et al., 2003) which couples the three-dimensional transport simulator MT3DMS with the geochemical model PHREEQC-2 (Parkhurst and Appelo, 1999). Furthermore, it is attempted to make more accurate estimates of the load of the components sodium, potassium, calcium and magnesium at surface level and the hydrogeochemical processes occurring in the subsurface.
By coupling MT3DMS to PHREEQC, PHT3D is able to model various geochemical processes and consider the composition of the groundwater as a whole (multi-component geochemical modeling), in contrast to RT3D, which can incorporate merely a few geochemical processes. In this study, geochemical processes taken into account are cation exchange, aqueous complex formation, dissolution and precipitation processes and redox processes.

## 1.2 Approach

First, in order to model the hydrogeochemical transport processes properly, an inventory is made about the spatial distribution of reactive components and possible geochemical processes occurring in the aquifers. Then, developments in land use resulting in the current distribution between agriculture, nature areas, recreation areas and urban areas are considered. The factors determining the yearly load at surface level resulting from the different land use types are examined as well. Furthermore, the time-dependent load at surface level is converted into recharge concentrations in order to link land use to groundwater quality.

Before starting to build a model in PHT3D, a one-dimensional transport model is constructed in PHREEQC-2. The one-dimensional model does not simulate a unique flow path but represents a vertical depth profile. Groundwater flow represents the vertical infiltration velocity of recharge water, whereas the composition of the recharge water results from the load at surface level.
First, a conservative one-dimensional transport model is set up, in order to study how chemical components are transported through the model while no geochemical processes are imposed. Secondly, a reactive one-dimensional transport model is developed by inserting the relevant geochemical processes in the conservative model.

After studying the several possible hydrogeochemical reactions and their relation to one another in the one-dimensional model, a three dimensional reactive transport model is constructed in PHT3D. The PHT3D-model represents the subsurface of Holten and its surroundings, thereby covering an area of approximately 70 square kilometers.

## 1.3 Outline of the report

The report consists of seven chapters. Chapter 2 describes the main geo-scientific features of the research area. The geology as well as the hydrogeological characteristics are set out. Furthermore, the hydrogeochemistry of the research area is considered in this chapter. Chapter 3 deals with the different land use types in the study area and the changes in land use over time. The load at surface level resulting from the different land use types is described as well.

In Chapter 4 the one-dimensional model study is set out, whereas Chapter 5 describes the three-dimensional reactive transport model. In Chapter 5, the MT3DMS part of the model is considered first. Then, it is explained how MT3DMS and PHREEQC-2 are coupled. Subsequently, the PHREEQC-2 part is set out, as well as the general model setup. Finally, the results of the modeling exercise are described.
Chapter 6 describes the general conclusions of the study and in Chapter 6, recommendations for further research, both with respect to field observations and modeling, are given.

Appendix A includes a list of Dutch translations of specific English terms, most of which are related to agriculture. Appendix B shows how the load data in kg $m^{-2}$ $year^{-1}$ are converted to moles $l^{-1}$. In Appendix C a short version of the input file used in PHREEQC-2 is included. In Appendix D, the location of the pumping wells is indicated on the topographical map.

# 2 Hydrogeology and hydrogeochemistry of the research area

Before the reactive transport model study was set up, an inventory was made about the spatial distribution of reactive components and geochemical processes playing a role in the local hydrogeology of Holten and its surroundings. This chapter first describes the geological characteristics of the study area. Then, the hydrogeology and the aquifer geochemistry are described. Subsequently, based on the observations, a conceptual model of the hydrogeochemistry is set out. Furthermore, the hydrogeochemistry is schematically represented in Figure 2.3.

## 2.1 Geology

The research area is located in and around Holten, in the eastern part of the Netherlands (Figure 2.1). The area is characterized by the Holterberg, a hill north of the village of Holten, which has an elevation of approximately 70 meters +NAP (above sea level). Another small hill, the Zuurberg, is located south of the village and has an elevation of approximately 30 meters +NAP. In the remaining part of the study area, surface level is relatively flat with respect to the hills and varies between 15 and 20 meters +NAP.
The Holterberg is an ice-pushed ridge and consists of thrusted sediments, whereas the lower parts of the area represent a former fluvioglacial area (Griffioen et al., 2002). A groundwater pumping station is located to the northeast of Holten (see Figure 5.1).

In the lower, relatively flat part of the research area, Tertiary marine sediments of the Breda Formation form the hydrological base at a depth of approximately 100 to 70 meters -NAP (below sea level). The sediments consist of green clay. On top of the Breda Formation, sandy sediments of the Oosterhout Formation form the deepest aquifer (Griffioen et al., 2002, Figure 2.2). The Tertiary Oosterhout Formation has a thickness of a few tens of meters, thereby reaching to approximately 5 meters -NAP. The sediments consist of fine sands containing glauconite and at some sites, clayey and loamy lenses with thicknesses of several meters occur.
A second aquifer is formed by the Urk Formation, which in turn lies on top of the Oosterhout Formation. The sediments of the Urk Formation consist of coarse sands deposited by the river Rhine and reach a thickness of about 15 meters. The Drenthe Formation on top of the Urk Formation forms part of the second aquifer as well. This formation comprises fluvioglacial sands varying in grain size from fine to coarse, and has a thickness of approximately 10 meters. The Drenthe Formation crops out south of the Holterberg and in the southern part of the study area.
No confining layers occur in between the deepest and second aquifer, whereas south of the Holterberg, a thin unit with a thickness of approximately 1 meter exists in between the Oosterhout and Urk Formation (Figure 2.2). The coarse and gravely deposits of this unit belong to the Peize Formation and originate from former Baltic rivers. The Peize Formation belongs to the second aquifer.
In the central part of the study area, the Drenthe Formation and part of the Urk Formation are intersected by a channel, which in turn is filled with sediments of the Twente Formation, outcropping at this site (Figure 2.2). The Twente Formation forms

the upper aquifer and consists of periglacial deposits, varying from silty clay to coarse, gravely sands.
No confining layers occur in between the second (middle) and upper aquifer. However, in the southern part of the study area, a loamy layer characterizes the top of the Urk Formation.

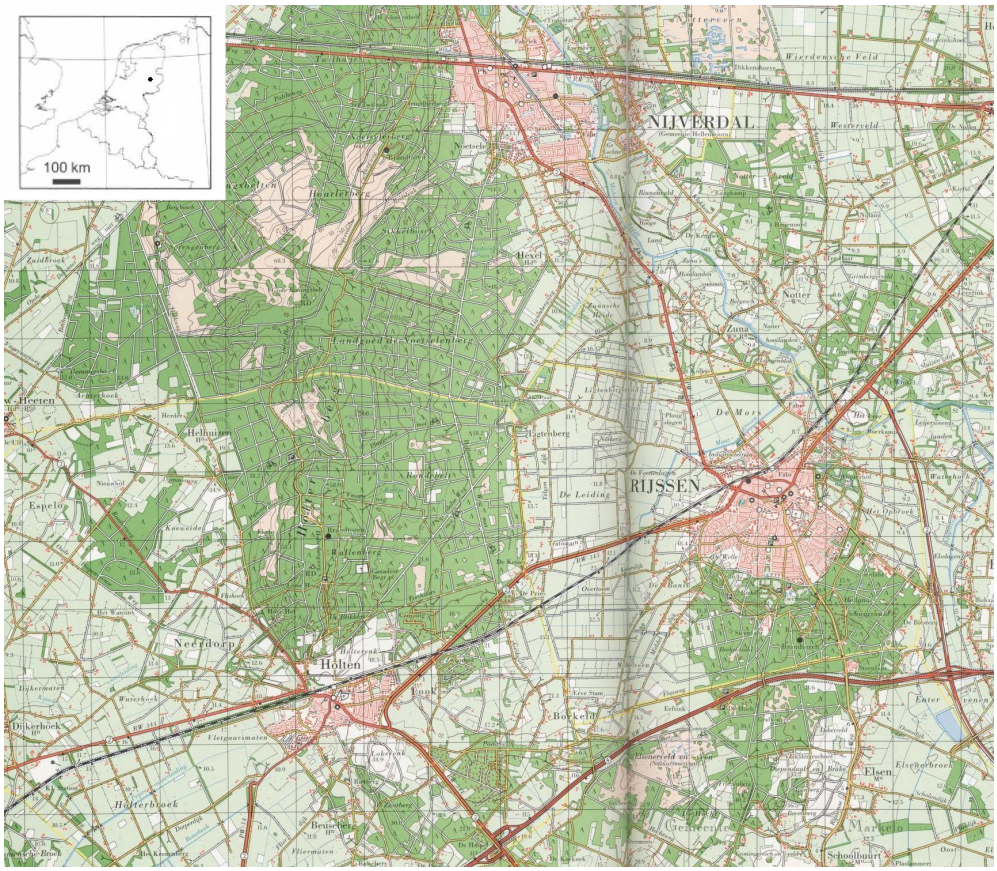


Figure 2.1 – Topographic map of Holten and its surroundings.

At the sites of the ice-pushed sediments of the Peize and Urk Formation, which form the Holterberg, the hydrological base (Breda Formation) lies at a depth of about 73 meters -NAP. The Oosterhout Formation on top of the Breda Formation has, in contrast to the flat parts of the study area, a thickness of only 16 meters at these sites (Figure 2.2). The thrusted Peize and Urk Formation reach a total thickness of approximately 90 meters. Furthermore, the Drenthe and Twente Formation are absent on top of the Peize and Urk formation.

## 2.2 Hydrogeology

As already mentioned above, the hydrological base in the study area is formed by the Breda Formation at a depth of approximately 70 to 100 meters -NAP. The research area is characterized by a phreatic groundwater system. Based on their geological origin, three aquifers are distinguished: the Twente Formation forms the upper or first aquifer, the Urk Formation, the Drenthe Formation and the Peize Formation constitute the

middle or second aquifer and the Oosterhout Formation forms the lower or third aquifer. At the sites of the ice-pushed ridges, the Urk and Peize Formations form both the first and second aquifer. Confining layers between the aquifers do not occur at a regional scale (Griffioen et al., 2002).

The first aquifer has a moderately high hydraulic conductivity and within the upper few meters local loamy or clayey lenses, originating from moraine deposits, can occur (Griffioen et al., 2002). The second aquifer in general has a very high hydraulic conductivity. However, due to lateral variations in grain size within the Urk Formation, the hydraulic conductivity is not uniform throughout the area. The third aquifer has a high hydraulic conductivity. In a part of the study area, the Oosterhout Formation is intersected by a channel filled with sediments of the Appelscha Formation. The sediments of the Appelscha Formation are coarser than the sediments of the Oosterhout Formation and therefore lateral variations in hydraulic conductivity and porosity occur in the third aquifer as well. The Breda Formation has a low hydraulic conductivity.
Anisotropy characterizes the hydraulic conductivity of the Urk and Peize Formations in the ice-pushed ridges (Griffioen et al., 2002). As the thrust acted in a W-E direction, the anisotropy is oriented N-S. The third aquifer (Oosterhout Formation) is, with respect to anisotropy, not affected by ice-thrusting. However, at the site of the ice-pushed ridges, the Oosterhout Formation has a thickness of only 16 meters and is located a few tens of meters deeper than in the lower areas (Figure 2.2).

In the lower, relatively flat parts of the research area, the unsaturated zone is approximately 3 to 6 meters in thickness. Infiltrating recharge water at surface level travels in less than three years to the groundwater table (Griffioen et al., 2003). However, the ice-pushed ridges are characterized by a thicker unsaturated zone. The unsaturated zone of the Holterberg has a maximum thickness of 50 meters and travel times of infiltrating recharge water to the groundwater table are approximately 10 years.

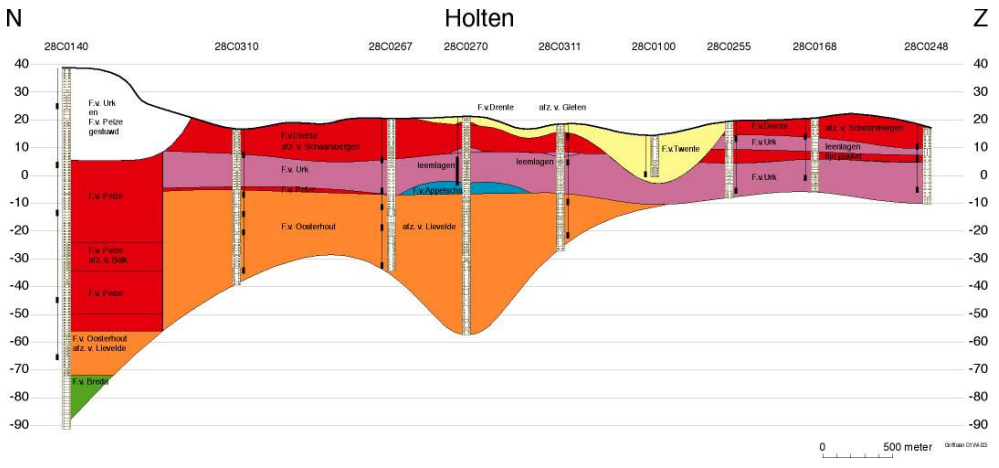


Figure 2.2 - Geologic N-S profile of the subsurface around Holten. Vertical scale is in meters, NAP (sea level) is represented by the zero level. Observation wells along the transect are displayed in the profile. After Griffioen et al., 2003.

## 2.3 Hydrogeochemistry

Besides texture and hydraulic conductivity, distinction with respect to hydrogeochemical characteristics is made as well between the three aquifers. The aquifers have different concentrations of solutes and minerals and the extent to which the aquifers are capable to exchange cations differs as well (Griffioen et al., 2003). As a result of these differences in sediment geochemistry between the aquifers, the hydrogeochemical processes occurring in each aquifer are different as well. A hydrogeochemical schematization of the aquifers in and around Holten is depicted in Figure 2.3.
Based on solute concentrations and pH and Eh values as observed in groundwater observation wells and based on measurements of aquifer compositions (NITG-TNO; Vitens), it is assumed that three hydrogeochemical processes are decently important in the hydrogeology of Holten (see also Griffioen et al., 2003). These processes comprise cation exchange, mineral dissolution or precipitation and reduction and oxidation (redox) processes. This will be set out in the next sections.

### *2.3.1 Cation exchange*

Cation exchange in the aquifers can be expected to occur because the aquifers have a Cation Exchange Capacity (CEC) and the cationic composition has varied considerably over time in the recharge water. The CEC is determined by the fractions of clay and organic matter in the sediment. In the third aquifer, clayey and loamy lenses with thicknesses of several meters exist and the organic matter content is relatively high. The CEC of the third aquifer, therefore, is relatively high and has a value of 38 meq/l (Griffioen et al., 2003; Figure 2.3). Furthermore, although the first and second aquifer mainly consist of fine to very coarse sands and have low clay content, and the fraction of organic matter in these aquifers is relatively low (Griffioen et al., 2003), cation exchange does occur in these aquifers. However, the CECs of the first and second aquifer are relatively low with values of 2.1 and 1.5 meq/l, respectively (Figure 2.3).

### *2.3.2 Calcite dissolution*

Observations from groundwater wells and measurements on aquifer material indicate that the second and third aquifer contain calcite, whereas in the first aquifer the calcite content is relatively small or even zero (Griffioen et al., 2003; Maas, 2002). The observations show that, if observed, the amounts of calcite in the first aquifer lie within the measurement noise and the groundwater is undersaturated with respect to calcite. Therefore, calcite is not taken into account in the first aquifer in the hydrogeochemical schematization in Figure 2.3.
Initial contents of calcite in the second and third aquifer are based on the weight percentages of calcite in these aquifers, as determined by Griffioen et al. (2003) and Maas (2002). As a result of acid rain caused by air pollution (Chapter 3) the recharge water became relatively acidic. Therefore, calcite in the second and third aquifer which is often found as (pieces of) shells will dissolve in the groundwater. The calcite dissolution creates a front: above the front the available calcite has been dissolved, whereas right below the front calcite is still present. During time, the calcite dissolution front shifts downward.

In the study area, the calcite dissolution front is, based on the calcite observations, expected in the second aquifer. However, it is unknown to which depth calcite has been dissolved in the second aquifer and therefore the shifting velocity of the calcite dissolution front can not be determined. Nevertheless, supposing that the second aquifer has a thickness of about 25 meters (Section 2.1) and the recharge water became, as a result of air pollution, acidic around 1950 (Chapter 3), the average velocity is roughly estimated in between 0 and 25 meters per ~50 years, or 0 and 50 cm/year.

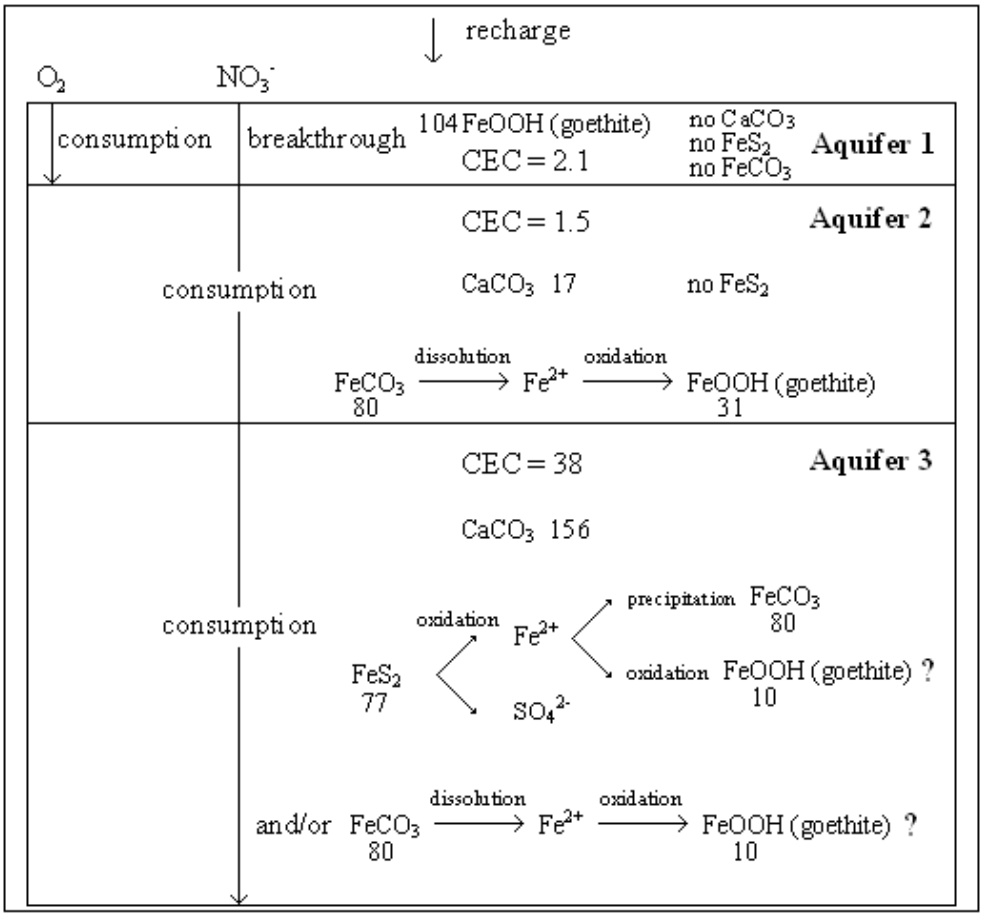


Figure 2.3 - Hydrogeochemical schematization of initial concentrations and processes as they are assumed to occur in the aquifers of Holten and its surroundings. Numbers are mineral contents in millimoles; CECs are in meq/l (Griffioen et al., 2003 and Maas, 2002). Soil organic material is not considered as a geochemical component.

In Figure 2.4, the pH of the groundwater is depicted in the N-S profile as displayed in Figure 2.2. Besides the pH value, Figure 2.4 shows whether the groundwater is undersaturated or saturated with respect to calcite. If the groundwater is undersaturated for calcite, the mineral will dissolve, whereas if the groundwater is saturated for calcite, a thermodynamic (unstable) equilibrium exists. Calcite equilibrium in combination with a neutral pH indicates that the subsurface is buffered with respect to pH. Furthermore, Figure 2.4 shows whether the groundwater is undersaturated or saturated with respect to siderite. This will be described later.

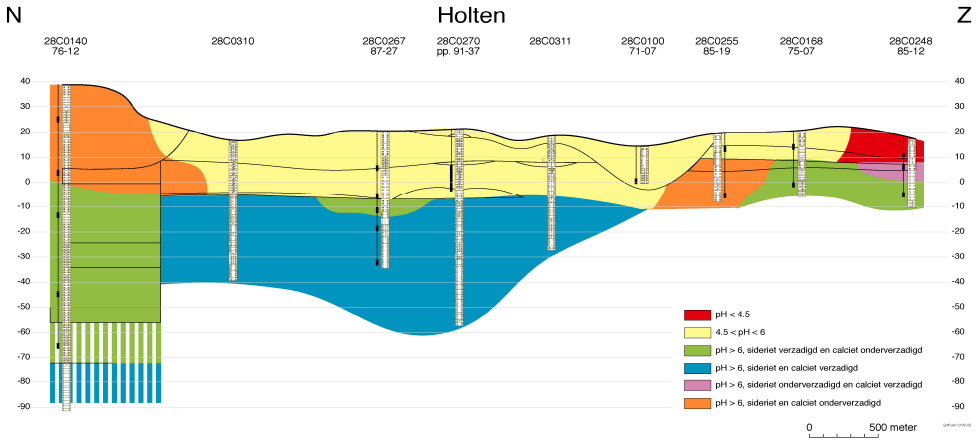


Figure 2.4 - pH values and Saturation Indices of calcite and siderite in the groundwater in a N-S profile across Holten and its surroundings. Vertical scale is in meters, NAP (sea level) is represented by the zero level. Observation wells along the transect are displayed in the profile. After Griffioen et al., 2003.

### 2.3.3 *Redox processes*

The occurrence of redox processes in an aquifer is determined by the presence of oxidizing (electron accepting) and reducing (electron donating) components. Observations in the study area show that oxygen ($O_2$) and nitrate ($NO_3^-$) are the most important oxidizing components, whereas reducing components comprise the minerals pyrite ($FeS_2$) and siderite ($FeCO_3$) and Soil Organic Matter (SOM; $CH_2O$) (Griffioen et al., 2003, Figure 2.3).
Figure 2.5 shows the redox state of the groundwater in the N-S profile as depicted in Figure 2.2. The upper groundwater is partly oxic, i.e., oxygen en nitrate are present, and partly suboxic, i.e., only nitrate is present. The deeper groundwater is characterised as iron-anoxic groundwater which means that iron is present, whereas oxygen and nitrate are absent. The third aquifer is iron-anoxic throughout the complete aquifer. In the second aquifer, the redox state laterally varies, whereas the first aquifer is characterised by oxic and suboxic groundwater.

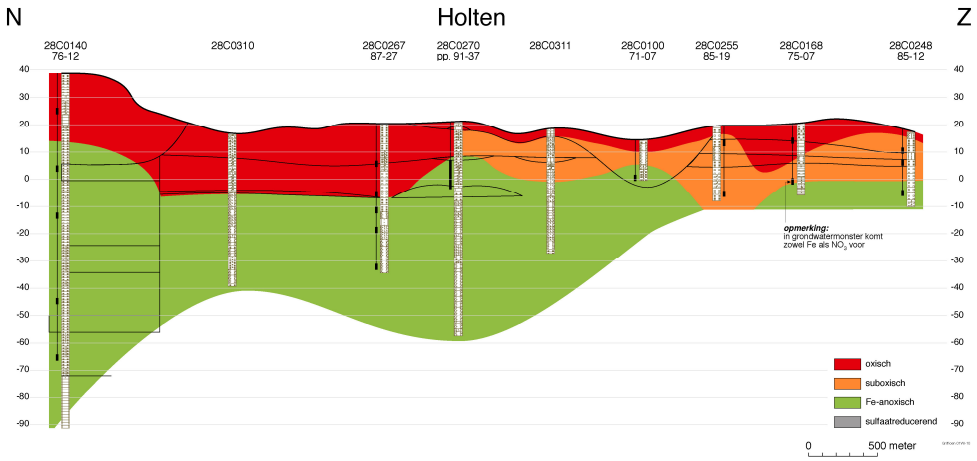


Figure 2.5 - Redox state of the groundwater in a N-S profile across Holten and its surroundings. Vertical scale is in meters, NAP (sea level) is represented by the zero level. Observation wells along the transect are displayed in the profile. After Griffioen et al., 2003.

Iron hydroxide content in the first aquifer is relatively large, whereas in the second and third aquifer iron hydroxide contents are smaller (Griffioen et al., 2003, Figure 2.3). Iron hydroxide reduction by reducing components, however, does not occur in the first aquifer, since in this aquifer oxygen is used as an electron acceptor. In the second and third aquifer, reduction of iron hydroxide may occur after nitrate has been consumed, although earlier studies in the area around Holten do not mention the occurrence of this redox process.

Furthermore, the sulfate ($SO_4^{2-}$) concentration in the second and third aquifer is in the order of 0.5 mmol/l (Figure 2.6a). Sulfate reduction thus may, if reducing components are available, occur in the study area after nitrate and iron hydroxides have been consumed. However, the observed sulfate concentrations in the second and third aquifer would be smaller if sulfate reduction occurred to a large extent. Moreover, comparing sulfate concentrations from 1950 (Figure 4.4) as they were calculated in the one-dimensional model (Chapter 4) to observed sulfate concentrations from 1985 until 2005 (Figure 2.6a), rather points to a sulfate increase during time in the second and third aquifer. Therefore, the occurrence of sulfate reduction is not considered an important redox process in the study area.

Finally, methane observations are not available and therefore it is not known whether methanogenesis occurs in the research area. However, as sulfate is still observed in the second and third aquifer methanogenesis is not (yet) likely to be an important redox process in the study area.

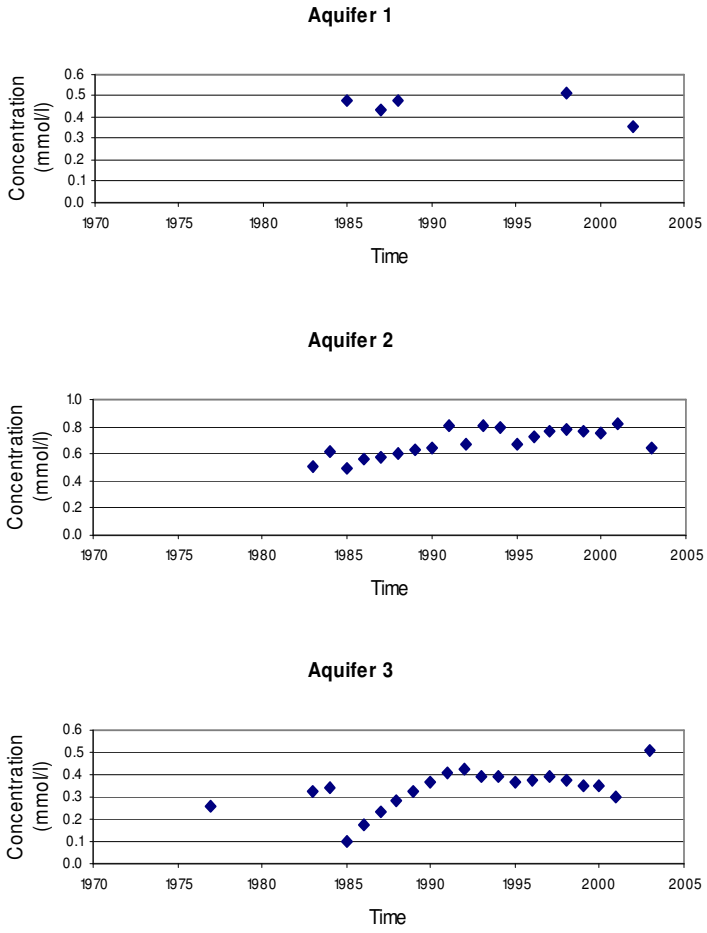


Figure 2.6a - Measurements of sulfate concentrations in observation and pumping wells in Aquifer 1, 2 and 3 (averaged).

It was already mentioned that oxygen is present in the first aquifer, whereas in the second and third aquifer it is nearly absent (Figure 2.4; Maas, 2002; NITG-TNO; Vitens). Clearly, the recharge water continually supplies oxygen to the first aquifer and during its transport through this aquifer the oxygen is consumed (Figure 2.3).
The occurrence of nitrate reduction depends on the amount of oxygen present in the aquifer. As oxygen is a stronger electron acceptor than nitrate, nitrate can only act as an electron acceptor when oxygen has (nearly) been consumed. Nitrate reduction, therefore, cannot, or only very slightly, occur in the first aquifer, whereas in the second and third aquifer nitrate plays an important role as electron acceptor (Figure 2.3).
Measurements of nitrate concentration in the observation wells, carried out from 1974 until 2004, show that in the first aquifer nitrate concentrations are in the same order of magnitude as nitrate concentrations in the recharge water (Figure 2.6b and 4.3; NITG-TNO; Vitens; due to the small amount of filters present in the first aquifer, only few measurements have been made in this aquifer). The second aquifer shows a slight decrease in nitrate concentrations with respect to the recharge water. However, the concentrations of nitrate in the groundwater in the third aquifer are rather low, while based on travel times calculated by the three-dimensional groundwater flow model (Chapter 1), the recharge water did contain nitrate during infiltration (Griffioen et al., 2003; see also Chapter 5 in which it is described that the reactive transport model results show that the travel time from the groundwater level to the pumping wells in the third aquifer is approximately 35 years, whereas in Chapter 3 it is described that nitrate was already part of the surface load in 1950). The nitrate concentrations in the third aquifer fluctuate around the detection limit, which varies between 0 and 0.5 mg per liter (0 and 8.1 micromoles per liter).
However, the age of the groundwater samples and therefore the year of infiltration of the water are not known, which makes comparison of recharge water quality to groundwater quality difficult (Chapter 4, section 4.2). It is therefore hard to estimate the amount of nitrate being reduced in the subsurface and the velocity of the reduction process.

Measurements in the study area show that there are considerable amounts of the mineral pyrite present in the sediments of the third aquifer whereas in the first and second aquifer no pyrite is observed (Maas, 2002). Furthermore, Griffioen et al. (2003) found that groundwater in the second and third aquifer is supersaturated with respect to siderite in a large part of the study area. In the first aquifer no siderite is observed.
As it is expected that the oxidation of SOM will, in contrast to pyrite, influence the hardness of the groundwater, taking into account SOM as a reductant is rather complex. Therefore, although the fact that SOM in the aquifers around Holten is an important electron donor, this component is left out of consideration in this study.

*Pyrite*

A commonly observed reaction in pyrite-containing aquifers in which nitrate-rich recharge water enters, is pyrite oxidation by nitrate reduction. It was already mentioned before that pyrite is present in the third aquifer. Since in the third aquifer pyrite is available and nearly no oxygen is present, the small nitrate concentrations in the groundwater suggest that nitrate, entering the third aquifer via the first and second aquifer, is reduced in combination with pyrite oxidation (see also Griffioen et al., 2003). The following reaction equation describes the process of nitrate reduction by pyrite oxidation (see also Figure 2.3):

$$5\ FeS_2 + 14\ NO_3^- + 4\ H^+ \ > \ 7\ N_2 + 5Fe^{2+} + 10\ SO_4^{-2} + 2\ H_2O \quad (1)$$

Equation (1) shows that besides $N_2$ and $Fe^{2+}$, $SO_4^{2-}$ is produced. Furthermore, the initial amount of pyrite in the third aquifer was based on the weight percentage of pyrite in the sediments determined by Maas, 2002 (Figure 2.3).

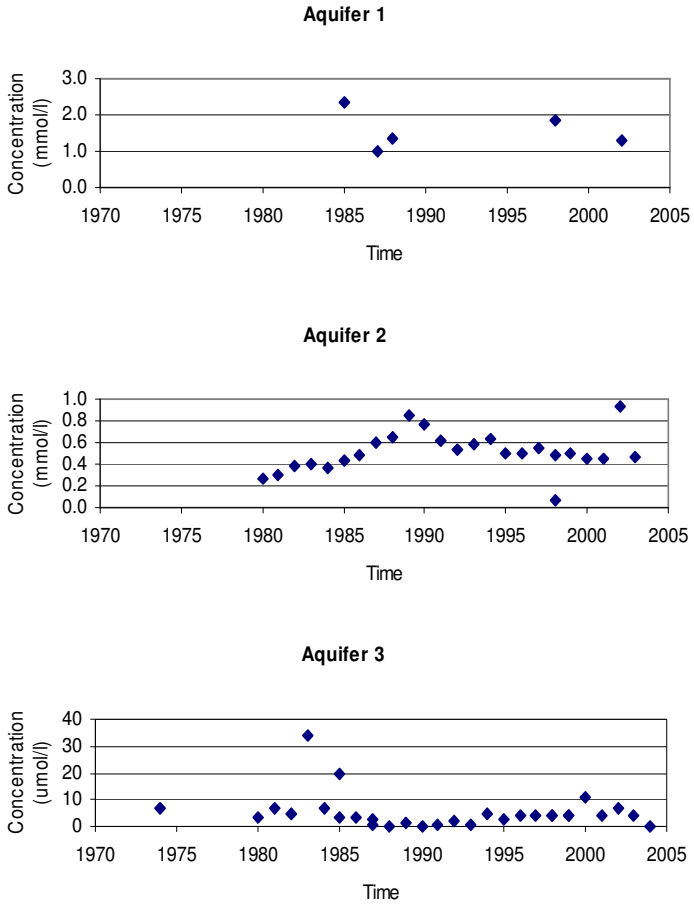


Figure 2.6b - Measurements of nitrate concentrations in observation and pumping wells in Aquifer 1, 2 and 3 (averaged). Mind that concentrations in Aquifer 3 are in µmol/l.

*Siderite*

According to Griffioen et al. (2003), the groundwater is supersaturated with respect to siderite in the second and third aquifer (Figure 2.4). Measurements of groundwater samples from observation wells suggest SI's of approximately 0.5 in these aquifers. This implies that the mineral siderite may either become oxidized (siderite dissolution and subsequent Fe(II) oxidation) or - if reduced iron is available - be formed (Figure 2.3). If siderite acts as an reducing component it competes with pyrite for nitrate.
Although in both the second and third aquifer siderite may become oxidized by nitrate, the nitrate concentration in the second aquifer has merely slightly decreased with respect to the recharge water (Figure 2.6b and 4.3). Obviously, in the second aquifer, siderite is only to a certain extent able to consume nitrate.

Initial siderite contents in the second and third aquifer are assumed, since data on siderite weight percentages are not available. Furthermore, it is assumed that in the first aquifer no siderite is present (Figure 2.3).

*Iron hydroxide*

As said before, pyrite oxidation yields $Fe^{2+}$ in the groundwater. A possible reaction following pyrite oxidation in groundwater containing nitrate is the precipitation of FeOOH in the form of crystalline goethite (Figure 2.3), which is described by the following reaction equation (Appelo and Postma, 1993):

$$10\ Fe^{2+} + 2\ NO_3^- + 14\ H_2O \quad > \quad 10\ FeOOH + N_2 + 18\ H^+ \qquad (2)$$

In this equation a combination of two processes is decribed: the first process oxidizes Fe(II) to Fe(III) by nitrate reduction and in the second process Fe(III) precipitates as FeOOH.
Iron hydroxide is observed in all aquifers (Griffioen et al., 2003) (although in the first and second aquifer it can not be formed as a result of pyrite oxidation). Initial contents of iron hydroxide in the three aquifers are based on weight percentages of the phase determined by Maas, 2002.

In accordance with goethite precipitation in the second and third aquifer, more siderite may dissolve, since the oxidation of Fe(II) according to equation (2) shifts the thermodynamic equilibrium in equation (3) to the right. Siderite dissolution in turn, may - if nitrate is available - result in more oxidation of Fe(II).

$$FeCO_3 \quad <> \quad Fe^{2+} + CO_3^{2-} \qquad (3)$$

However, the FeOOH mineral in the aquifer can also occur in the form of ferrihydrite (amorphous iron hydroxide), which is considerably more soluble than crystalline goethite. This implies that, as long as no supersaturation for Fe(II) occurs with respect to FeOOH, the reduced iron remains in solution and no FeOOH is precipitated. Moreover, as Fe(II) is still present, the siderite equilibrium in equation (3) may shift to the left, resulting in siderite precipitation rather than dissolution (Figure 2.3). The behavior of the mineral siderite thus depends on the solubility of the FeOOH mineral.

### *2.3.4 Conceptual model of the hydrogeochemistry*

Based on what is described above, a conceptual model of the hydrogeochemistry of the study area can be made. It was already mentioned that calcite dissolution occurs in the second and third aquifer. It is expected that the release of $Ca^{2+}$ as a result of calcite dissolution influences the cation exchange behavior, particularly in the third aquifer where the CEC is relatively high.
Furthermore, it was described that comparing nitrate observations in the aquifers to nitrate concentrations in the recharge water, indicates that only a small amount of nitrate is reduced in the second aquifer, whereas in the third aquifer nearly all nitrate is reduced. Obviously, the reducing components in the second aquifer, siderite and SOM, are only to a certain extent able to consume nitrate. It is therefore expected that siderite is in equilibrium in the second aquifer, which implies that the mineral FeOOH occurs in

the form of ferrihydrite rather than goethite. Furthermore, it is expected that SOM is reasonably inactive in the second aquifer.
The fact that nearly all nitrate becomes reduced in the third aquifer was earlier explained by the occurrence of pyrite oxidation. The occurrence of pyrite oxidation by nitrate reduction is subscribed by the increased sulfate concentrations in the third aquifer (equation (1); Figure 2.6a). However, it should be mentioned that sulfate concentrations in the aquifers increase as a result of the increased sulfate load at surface level as well (Chapter 3). Furthermore, it is expected that the oxidation of SOM contributes to the occurrence of nitrate reduction as well.
As was mentioned above, Griffioen et al. (2003) found that the groundwater in the second and third aquifer is supersaturated with respect to siderite. This observation also indicates that the FeOOH mineral is relatively soluble, since goethite precipitation would have consumed the iron(II). The supersaturation for siderite in turn, is the result of pyrite oxidation and calcite dissolution, releasing iron(II) and carbonate in the water. It is thus expected that pyrite is the main reducing component in the third aquifer; the occurrence of siderite as an electron donor is expected to play a minor part.

# 3 Determining the load at surface level

A central question in this study is to quantify the influence of various land use functions and changes in these functions on groundwater quality in the area around Holten. It is therefore important that the different land use functions, varying through time, are well defined. Furthermore, the load at surface level resulting from the different functions, due to atmospheric deposition, the application of fertilizers and manure in agricultural areas and the use of various substances, e.g., fuels, cleansing agents and salt for icy roads, in urban areas, needs to be determined. Finally, the time-dependent load at surface level is 'converted' into a recharge concentration in order to link land use to groundwater quality. A list of Dutch translations of specific English terms, most of which are related to agriculture, is included in Appendix A.

## 3.1 Land use types

Present-day land use in the area around Holten consists of agriculture, nature, i.e., forests, recreation and urban areas (Griffioen et al., 2003) and results from a land use evolution over centuries (Griffioen et al., 2002). The historical development of land use from about 1880 in this part of the Netherlands has been studied by means of topographical maps dating from the nineteenth and twentieth century. Results of this study have been documented extensively in Griffioen et al. (2002). In this study, it is described how the distribution of the various land use types changes in time.

In the current study, land use evolution in the period from 1950 until now is emphasized. When the various land use types and the resulting load at surface level are considered, a distinction is made between the land use types agriculture, nature and urban areas. Recreation areas are included as urban areas, since the load at recreational areas largely resembles the load at urban areas and the recreation resorts are permanently occupied (Griffioen et al., 2003). Figure 3.1 shows how the different land use types are currently distributed: agriculture takes up about 60 percent of the area, nature takes up about 30 percent of the area and urban areas, including recreation areas, take up about 10 percent of the area.

During the period 1950-1970, the land use type agriculture in the areas around Holten was equally divided into pasture and arable land. Arable land in turn consisted of potatoes, sugar beets and wheat. It is estimated that potatoes took up 25 percent, sugar beets took up 35 percent and wheat took up 40 percent of the arable land.
Around the year 1970, farmers started to grow maize at a considerable part of the arable land. During the period of 1970-1985, the portion of maize in the total area of arable land gradually increased at the expense of the portion of arable land used for potatoes, sugar beets and wheat. From 1985 until now no potatoes, sugar beets and wheat are grown anymore in the area around Holten. Moreover, the area covered with pasture increased at the expense of the arable land area.


Figure 3.1 - Current land use types in the area around Holten. Left picture is obtained from the topographic atlas 1:50000, right picture is the corresponding digital land use map, in which red and yellow represent agriculture (pasture and arable land, respectively), brown represents urban areas and green represents nature. Recreation areas are included as urban areas. The digital land use map is used in the three-dimensional model (Chapter 5).

Nature in the areas around Holten originally consisted of moorland (Griffioen et al., 2002). However, forestation throughout the nineteenth and twentieth century resulted in a nearly complete removal of the moorland. Present-day nature therefore comprises mainly forests (Griffioen et al., 2002).

The share of urban areas in the study area increased considerably in the period from 1950 until now. The village of Holten extended at the cost of agricultural areas and around the year 1976 several holiday parks were build in the area around Holten (Griffioen et al., 2002). Furthermore, a residential neighborhood developed during this time in the southern part of the forested area.

Changes in the distribution of crops within the land use type agriculture as described above are taken into account in the three-dimensional model calculation. However, although the shares of the land use types agriculture, nature and urban areas in the area around Holten varied during the period from 1950 until now, in the model merely the current land use distribution (Figure 3.1) is used during the calculation.

## 3.2 Load at surface level

As already mentioned, in determining the load at surface level, distinction is made between land use types. Discerning between land use types is important because the load at surface level differs considerably at the different land use types with respect to amounts as well as with respect to types of chemical components. Although the load at agricultural lands as well as in nature areas particularly consists of nitrate and sulfate, the amounts of nitrate and sulfate forming the load at agricultural lands is substantially

higher than these amounts in forests as a result of applying manure and fertilizers at agricultural lands. Furthermore, the load in urban areas is rather different from the load at agricultural lands and nature areas.

Many factors are taken into account in the determination of total load at surface level at the land use types agriculture and nature. Seven components, sodium (Na), potassium (K), calcium (Ca), magnesium (Mg), nitrate ($NO_3$), sulfate ($SO_4$) and chloride (Cl) form an important part of the load at surface level. Therefore, for these components yearly concentrations of the load are determined.
First, atmospheric deposition is taken into account in determining the total load at surface level. In calculating the load resulting from atmospheric deposition, nitrogen (N) and sulfur (S) are considered to be the most important components. However, sodium, potassium, calcium and magnesium are part of the atmospheric deposition as well. Since for chloride no data are available, this component is not taken into account. The amount of heavy metals in atmospheric deposition is relatively small with respect to the amounts of nitrogen, sulfur, sodium, potassium, calcium and magnesium (Coppoolse et al., 1993) and therefore, in this study, merely these six components are taken into account in the determination of atmospheric deposition.
Atmospheric deposition comprises dry and wet deposition. Dry deposition differs per land use type since the type of vegetation (grass, crops or forest) determines the amount of atmospheric particles trapped. With respect to wet deposition no distinction between land use types is made.

A second factor determining the total load at surface level is the use of manure on agricultural lands. Manure is divided into several elements in order to quantify the load per component. The main elements in manure are nitrogen, potassium ($K_2O$), chloride and organic matter (Van der Grift and Van Beek, 1996). A relatively small part of the manure consists of sulfur ($SO_3$), sodium ($Na_2O$), magnesium (MgO), phosphor ($P_2O_5$) and calcium (CaO). As is the case with atmospheric deposition, heavy metals are not taken into account since the amount of heavy metals in manure is relatively small (Hotsma et al., 1997).
In calculating the total load at surface level which results from applying manure, the type of cattle, i.e., horned cattle, porkers, breeding sows and poultry, and the different seasons, i.e., whether the cattle is at grass or in the stable, are taken into account, since the type and amount of load at surface level depends on these two factors (Van der Grift and Van Beek, 1996).

Thirdly, the use of fertilizers on agricultural lands is considered in the determination of total load at surface level. Four types of fertilizers are characterized: nitrogen fertilizers, phosphor fertilizers, potassium fertilizers and calcium fertilizers (Van der Grift and Van Beek, 1996). Each of these fertilizers contributes in different proportions to the seven components. Furthermore, data obtained from LEI-DLO (Agricultural Economic Institute – Agricultural Survey, Pronk, 1994) are used to determine the amounts of sodium, potassium, calcium, magnesium, nitrate, sulfate and chloride in the load as a result of applying fertilizers. Again, the amount of heavy metals in fertilizers is relatively small (Raven and Loeppert, 1997; Hotsma et al., 1997; Hotsma et al., 1999; Meeuwessen and Van Erp, 1995) and therefore these components are not taken into account in the determination of the load at surface level resulting from fertilizers.

In addition to the references mentioned above, data about atmospheric deposition and amounts and types of manure and fertilizers applied in the province of Gelderland are

assumed to be representative for the area around Holten. Therefore, these data, which are obtained from CBS (Statistics Netherlands), are used as well in determining the load at surface level resulting from the land use types agriculture and nature.

Besides sources, sinks determine the leaching to the groundwater of the several components mentioned above as well. For each component, load decreases as a result of uptake by vegetation. Uptake depends on crop type and therefore, in order to accurately determine the total uptake for the components, distinction is made between potatoes, sugar beets, wheat, maize and grass (Van der Grift and Van Beek, 1996).
For nitrate, a second sink is considered as part of this component is degraded in the unsaturated zone. The amount of degradation depends on the initial amount of nitrogen available in the root zone, which in turn depends on the amount and type of manure and fertilizers applied and the amount of atmospheric deposition. Furthermore, vegetation type, soil type and groundwater level influence the amount of nitrate degradation in the unsaturated zone (Beekman, 1998).

Summing the sources and sinks per component per year yielded for the area depicted in Figure 3.1 a 50-year record of the load at surface level for the period 1950-2000 at pasture, arable land and nature (Figure 3.2). In order to obtain concentrations, the load data in kg $ha^{-1}$ $year^{-1}$ were by means of the yearly recharge converted to moles $l^{-1}$ (Appendix B).

Chloride forms an important part of the load at surface level. However, data about the amount of chloride uptake by the different types of vegetation and crops are not available (Van der Grift, unpublished data) so that the sum of sources and sinks, i.e., the net load, could not be calculated for chloride. Therefore, data about yearly chloride load determined in an earlier study are used (Griffioen, unpublished data, Figure 3.2). In the study by Griffioen, load data were determined for the same period (1950-2000). Nevertheless, since no distinction between land use types was made in the study by Griffioen, the 50-year records of yearly chloride load concentrations are equal for the land use types pasture, arable land and nature.
Another important component in the load at surface level for which data are lacking, is bicarbonate ($HCO_3^-$). Therefore, bicarbonate load determined by Griffioen (unpublished data) is used as well. The data show that the bicarbonate load concentration is rather low, in the order of a few tens of micromoles per liter, and constant in time (Figure 3.2). A bicarbonate concentration in this order of magnitude agrees with a partial $CO_2$ pressure of $\sim 3 \cdot 10^{-4}$ atmosphere, indicating that the bicarbonate is in equilibrium with the atmosphere. Again, no distinction between the land use types pasture, arable land and nature was made.

The 50-year records of load at surface level for the different components and land use types (Figure 3.2) show temporal changes as a result of changes in land use functions. Moreover, increasing use of manure and fertilizers at agricultural land and air pollution caused an increase in the load at surface level from approximately 1950. Switches in environmental legislation around 1985 in turn decreased the load at surface level as the policy changes imposed restraints on the use of manure and fertilizers and the production of air polluting components.
The changes in load at surface level are most eminent for the land use types arable land and pasture as a result of considerable changes in the application of manure and fertilizers at agricultural lands during the period from 1950 until now. Although atmospheric deposition increased as well as a result of e.g. industrial processes and the

use of motor vehicles and decreased again due to restraining environmental legislation, the influence on the load at surface level due to atmospheric deposition is less distinct than that due to agricultural activities. Therefore, the changes in load at surface level are less eminent for the land use type nature.
Most components show a maximum load between the years 1980 and 1990. During the 1950s, concentrations of $Na^+$, $K^+$, $Ca^{2+}$ and $Mg^{2+}$, as well as concentrations of $NO_3^-$ and $Cl^-$ start to rise. Around the year 2000, $Na^+$, $K^+$ and $Ca^{2+}$ concentrations have decreased to approximately the same value as they had before the increase started. Concentrations of $Mg^{2+}$, $Cl^-$ and particularly $NO_3^-$ are higher in the year 2000 than before the increase started.
Sulfate concentration in the recharge water shows a somewhat different behavior: it starts to increase around the year 1950 and shows a peak during the 1960s. While decreasing until approximately 1975, the concentration starts to rise again, reaching a maximum around 1980 which is slightly lower than the first maximum. The first maximum in the sulfate concentration is due to atmospheric deposition, whereas the second maximum is due to the use of manure. In 2000, the sulfate concentration in the recharge water has reached approximately its value of 1950 again.

As already mentioned, load in urban areas is rather different from the load at agricultural lands and forests. Load in urban areas consisting of nutrients and chloride results from leaking sewer systems and the application of salt at icy roads. Furthermore, load in urban areas comprises aromatic components, either chlorinated or not, pesticides and hydrocarbons (Tauw, 1994). However, in this study, the latter components are left out of consideration and merely the eight components as described for the agricultural areas and nature (sodium, potassium, calcium, magnesium, nitrate, sulfate, chloride and bicarbonate) are taken into account.
As data about the load at surface level in urban areas are sparse, current groundwater quality in these areas is considered in the determination of the load at surface level. Griffioen et al. (2003) investigated urban groundwater quality by means of cluster analysis. Average composition of the cluster which best represented urban groundwater (indicated as ‘Cluster 1 (Sub)oxisch, licht zuur’ in Griffioen et al., 2003) is used as load at surface level in this study (Figure 3.2). It is furthermore assumed that the load in urban areas is constant during time.

In the area around Holten, travel time of the recharge water from surface level to water table is less than three years in the agricultural areas (Griffioen et al., 2003). This time lag is relatively small with respect to the total period (1950-2000) considered in this study. Therefore, the evolution of the recharge water composition through time closely follows the load at surface level. Consequently, both the one-dimensional and three-dimensional model use the yearly changing load at surface level as recharge concentrations.
However, at the Holterberg and the Zuurberg, groundwater tables are located deeper than in the rest of the study area and therefore travel times to the groundwater are longer. It should be mentioned here that the longer travel times are not taken into account in the conversion of the load at surface level to recharge concentrations at these sites.

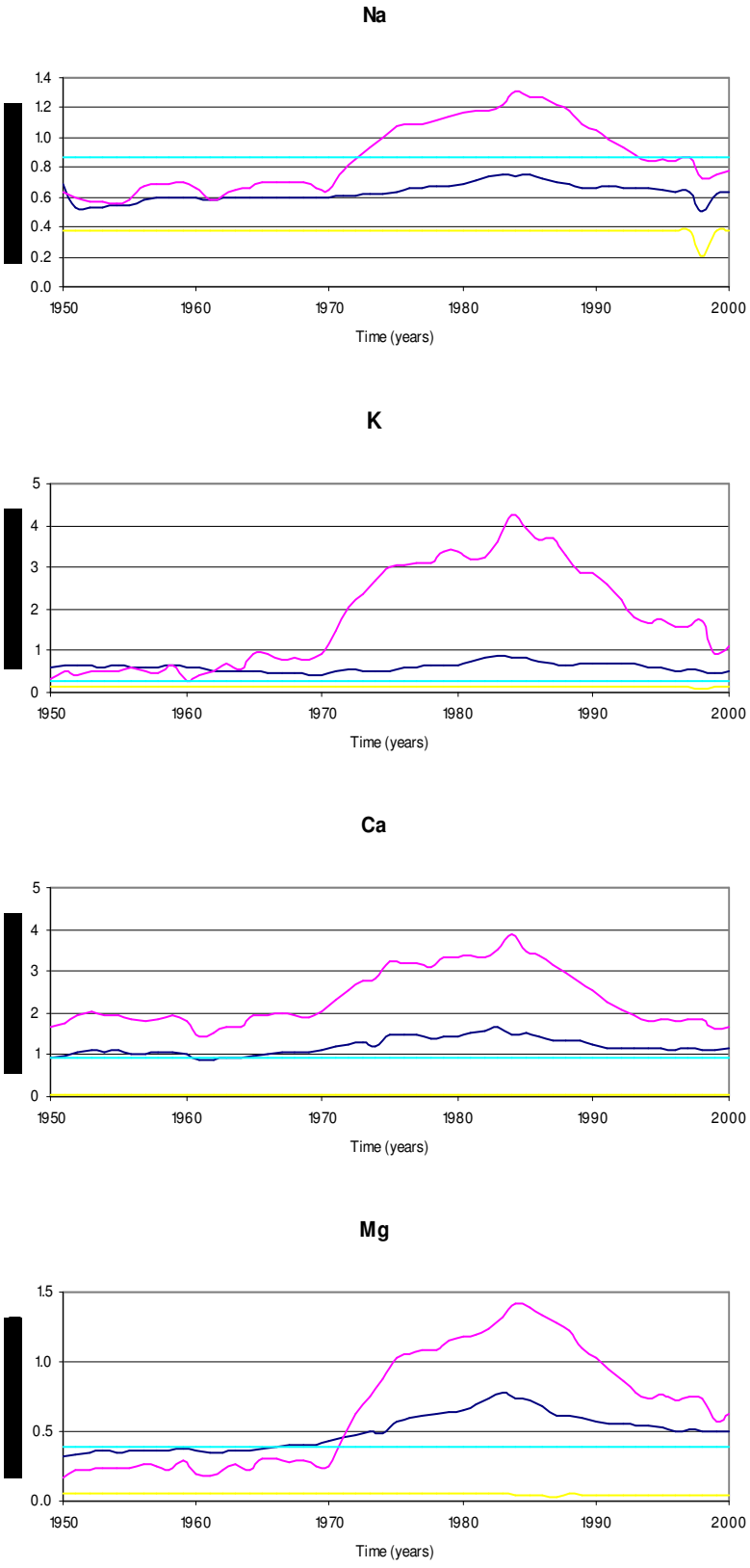


Figure 3.2 - Load at surface level at the four land use types. Dark blue, red, yellow and light blue represent pasture, arable land, nature and urban areas, respectively.

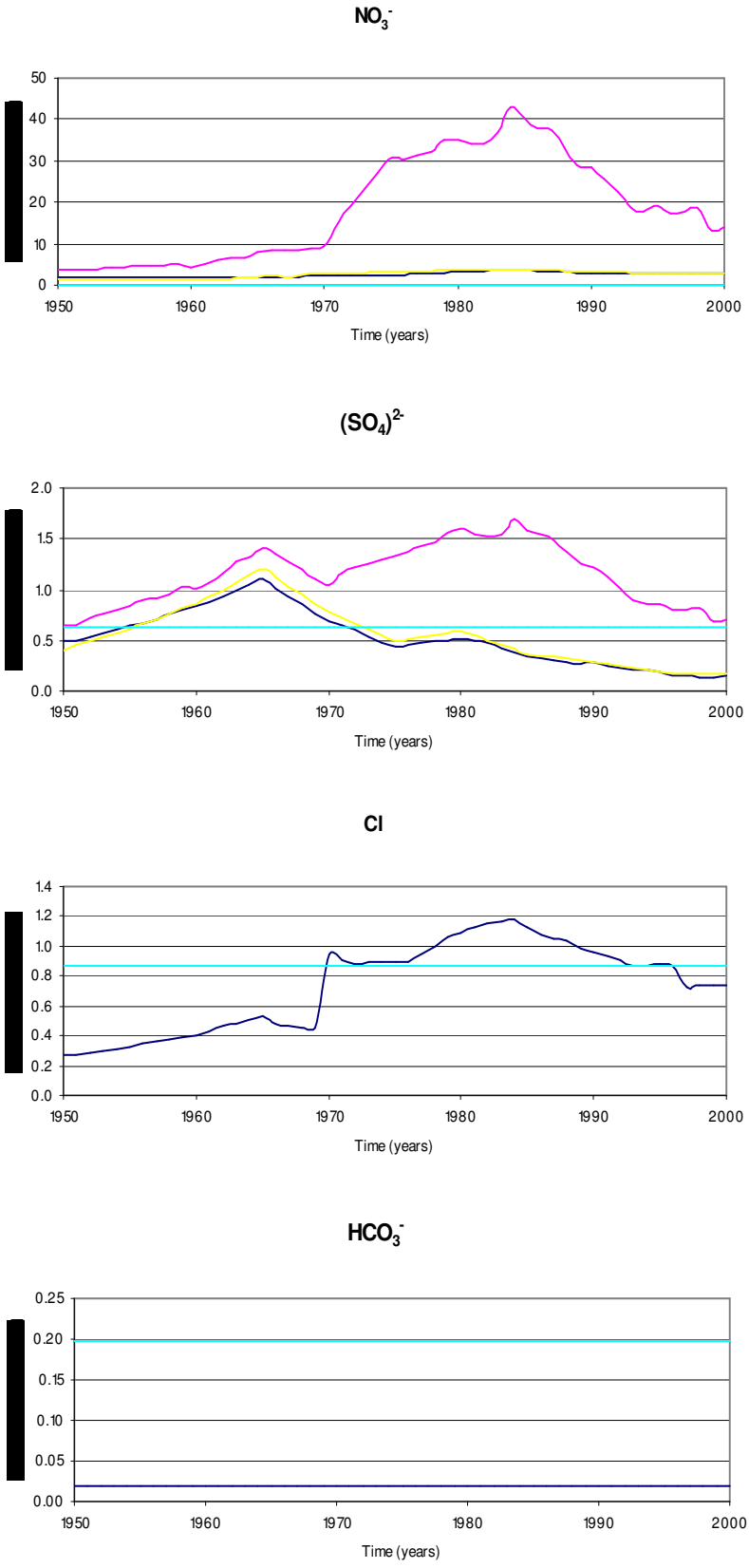


Figure 3.2 continued - Dark blue represents pasture, arable land and nature and light blue represents urban areas.

# 4 One-dimensional transport modeling in PHREEQC-2

In order to examine how solutes are transported through the subsurface and how they can be affected by hydrogeochemical processes in the local hydrogeology of Holten, a one-dimensional transport model was set up. The modeling was carried out in the geochemical model PHREEQC-2, which is a computer program for simulating chemical reactions and one-dimensional transport processes in aqueous systems (Parkhurst and Appelo, 1999).

## 4.1 Model setup

In PHREEQC-2, one-dimensional transport occurs in a column consisting of a number of cells. The column represents the flow path through the aquifer and each cell represents a solution with a specific composition (Figure 4.1). In the one-dimensional PHREEQC model in this study, the flow path comprises 200 cells, each having a length of 0.35 meter. The flow path does not simulate a unique streamline but represents a vertical depth profile. Three sets of cells represent the three aquifers present in the subsurface: cells 1-20 (Solution 1-20) represent the uppermost or first aquifer; cells 21-80 (Solution 21-80) represent the middle or second aquifer and cells 81-200 (Solution 81-200) represent the lower or third aquifer (Figure 4.1).
As already mentioned, the groundwater system is phreatic and although the flow model is divided into three aquifers, the subsurface can be considered one aquifer as the aquifers are not separated by low permeability layers (Chapter 2). Distinction between the aquifers is made since the hydrogeologic and hydrogeochemical characteristics of the aquifers are different (Figure 2.3; Table 4.1).
Recharge feeding the aquifers, resulting from the load at surface level and leaching from the unsaturated zone (Chapter 3), is modeled by means of a solution of which the solute composition changes yearly. The recharge solution is called Solution 0 (Figure 4.1) and is transported through the three aquifers along the one-dimensional flow path. The modeled groundwater flow represents the vertical infiltration velocity and amounts to 2 cells per year, which corresponds to 0.7 meter per year. The diffusion coefficients of all aqueous species have the default value of 0.3e-9 $m^2/s$ and the mechanical dispersion coefficient is set to 0 meter in each cell so that the hydrodynamic dispersion (diffusion + mechanical dispersion) only slightly obscures the hydrogeochemical results of the model.

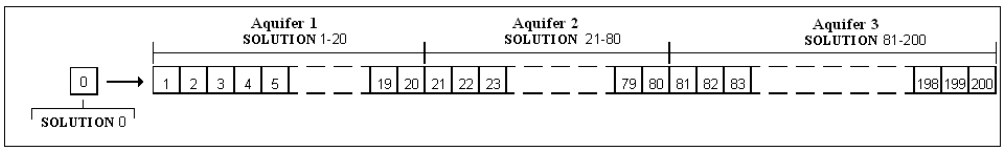


Figure 4.1 - Representation of the one-dimensional flow path in PHREEQC-2.

First, a conservative model, i.e., a model in which no hydrogeochemical processes occur, was set up. In this model, the solution representing the recharge unaffectedly flows through the aquifers. When the conservative model performed properly, hydrogeochemical processes were assigned to the aquifers according to the hydrogeological scheme as described in Chapter 2. The reactive model incorporates

cation exchange and mineral equilibria with, depending on the aquifer, calcite, pyrite, siderite and goethite (see also Table 4.1). This will be elaborated in the next sections.

Modeling conservative transport yields a 'feeling' in the (physical) flow pattern itself: it provides insight in when load at surface level arrives at a certain distance downstream and how the initial load is affected by hydrodynamic dispersion while no hydrogeochemical processes occur. Furthermore, results from the conservative model can be compared to reactive model results, which may yield a better understanding of the hydrogeochemical processes affecting the solute composition.

## 4.2 Calibration

In order to check whether a model properly represents the hydrogeochemical reactions occurring in the subsurface, model results are compared to measurements. Groundwater quality measurements in the area around Holten have been carried out in pumping wells and observation wells mostly during the 1980s and 1990s. In comparing modeled to measured groundwater quality and linking the groundwater quality to the load at surface level, it is important to know groundwater age and travel time. However, since groundwater age has never been determined in the area around Holten, only assumptions about the travel time of the groundwater can be made in this area.
In this one-dimensional model study, groundwater age is related to depth and the vertical flow velocity of 0.7 meter per year is based on a recharge of 250 mm per year and a porosity of 0.35. Whether in the field the isochrones are horizontal, i.e., each depth is related to a specific groundwater age (Figure 4.2), depends on the following factors. The aquifer needs to be phreatic and a uniform recharge over the area is required (Appelo and Postma, 1993). Furthermore, the aquifers need to be homogeneous. If these requirements are met groundwater age at depth *d* can be determined by means of the following equation (Appelo and Postma, 1993):

$$t = ((D*\varepsilon)/P) * \ln(D/(D-d)) \quad (4)$$

in which t is groundwater age [years]; D is aquifer thickness [m]; d is depth of the observation point [m]; ε is effective porosity [-] and P is precipitation surplus or recharge [m year$^{-1}$].

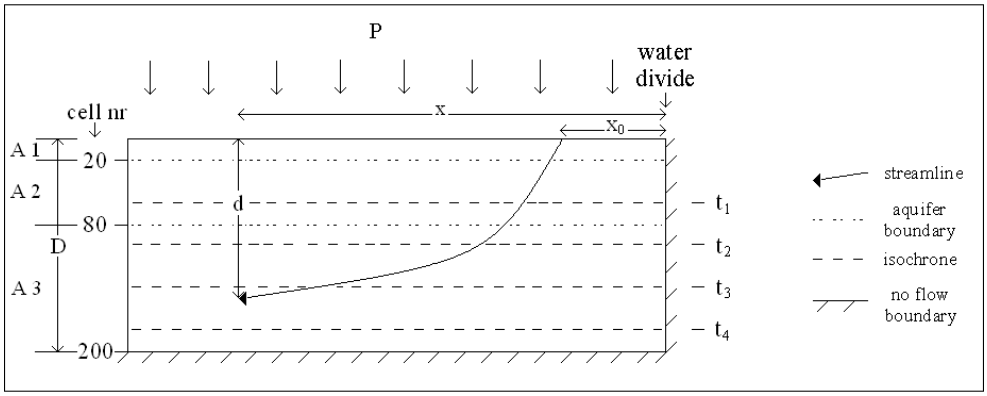


Figure 4.2 - Profile of a homogeneous, phreatic aquifer with horizontal isochrones. P represents recharge, A1, A2 and A3 are aquifer 1, 2 and 3 respectively (modified after Appelo and Postma, 1993).

However, although the aquifers in the study area are phreatic and the recharge is supposed to be approximately constant in space, there are two complications in assuming a groundwater age-depth relation according to equation (4) in the area around Holten. First, as mentioned in Chapter 2, lateral variations in grain size cause a heterogeneous hydraulic conductivity in the second aquifer, whereas local clayey and loamy lenses result in heterogeneous porosity and permeability in the third aquifer. Heterogeneity causes a distortion of the flow lines. A second complicating factor is the presence of abstraction wells in the study area, which at a certain distance may affect the flow lines. If the flow lines are affected, the groundwater age-depth relation as described in equation (4) does not apply. Therefore, assuming that groundwater age increases with depth according to equation (4) is unreal in the area around Holten. Flow lines extracted from the three-dimensional groundwater flow model set up for the study area (Chapter 1; Griffioen et al., 2003) indeed confirm that the groundwater age-depth relationship in equation (4) does not apply in the area around Holten.

Since it is not possible to deduce the age of the measured groundwater samples in this way, it is not feasible to compare the measurements at individual well screens to the one-dimensional model results. It is therefore decided that the one-dimensional model results are primarily used to study and understand the several possible hydrogeochemical reactions and their relation to one another, rather than to determine the exact hydrogeochemistry of the area's subsurface and to reproduce the measured groundwater composition.

## 4.3 Recharge composition

It was already mentioned in Chapter 3 that the one-dimensional model uses the yearly changing load at surface level as recharge concentrations. Figure 4.3 shows how the recharge concentrations of sodium, potassium, calcium, magnesium, nitrate, sulfate, chloride and bicarbonate change in time at the different land use types. In the one-dimensional model study, the recharge concentrations as determined for the land use type pasture were used.
Furthermore, different pH values are observed in the recharge water beneath the various land use types (NITG-TNO; Vitens). During time, however, an approximately constant pH value is observed in the recharge water beneath each land use type. In the PHREEQC input file, the pH value as observed beneath the land use type pasture is assigned to the recharge water. Moreover, the pH value is kept constant in time.

## 4.4 Initial aquifer composition

The initial water composition and pH in the aquifers, representing solute concentrations and pH values of the year 1950, are depicted in Figure 4.4 and Table 4.1. As can be seen, sharp boundaries exist between the solute compositions and pH values in aquifer 1, 2 and 3. Observations show that the initial pH value in groundwater strongly influences pH changes caused by redox processes and carbonate dissolution or precipitation processes (Griffioen et al., 2003). Therefore, it is important to accurately determine initial pH values in the groundwater in order to model the hydrogeochemical processes correctly.

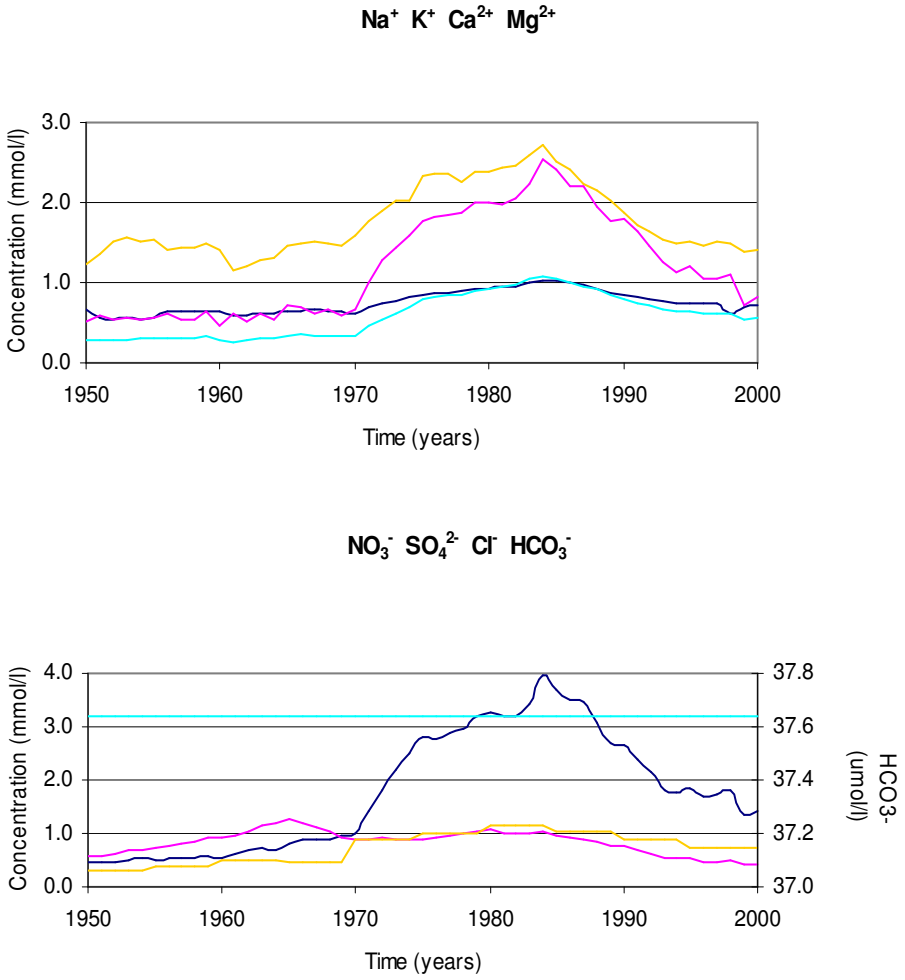


Figure 4.3 - Recharge composition changes in time. Dark blue, red, yellow and light blue represent in the upper graph Na, K, Ca and Mg, respectively and in the lower graph NO3, SO4, Cl and HCO3, respectively.

The initial solution composition of the aquifers is based on the results of a PHREEQC model in which 50 years of reactive transport was simulated from 1900 until 1950. The setup of this model was equal to the model as described in section 4.1. However, the composition of the recharge water from 1900 until 1950 was determined by means of observations from 1913 in wells located in the first aquifer (Griffioen et al., 2002) and was kept constant over the simulation period. The initial solution composition of the aquifers during the period of 1900-1950 as well as the cation exchange capacity and the initial amount of minerals present in the aquifers were based on measurements in observation wells and on measurements on aquifer material (Griffioen et al., 2002).
Besides the simulation results of the 1900-1950 model, for the first aquifer also the load at surface level of the year 1950 was taken into account in determining the initial solution composition. This was done in order to make a distinction between the different land use types.
The one-dimensional model results as described in this chapter are based on initial solution compositions determined for the land use type pasture (Table 4.1). Initial solution compositions, as well as solute concentrations and pH values of the recharge

water, as determined for the land use types arable land, nature and urban areas are used later on in the three-dimensional model (Chapter 5).

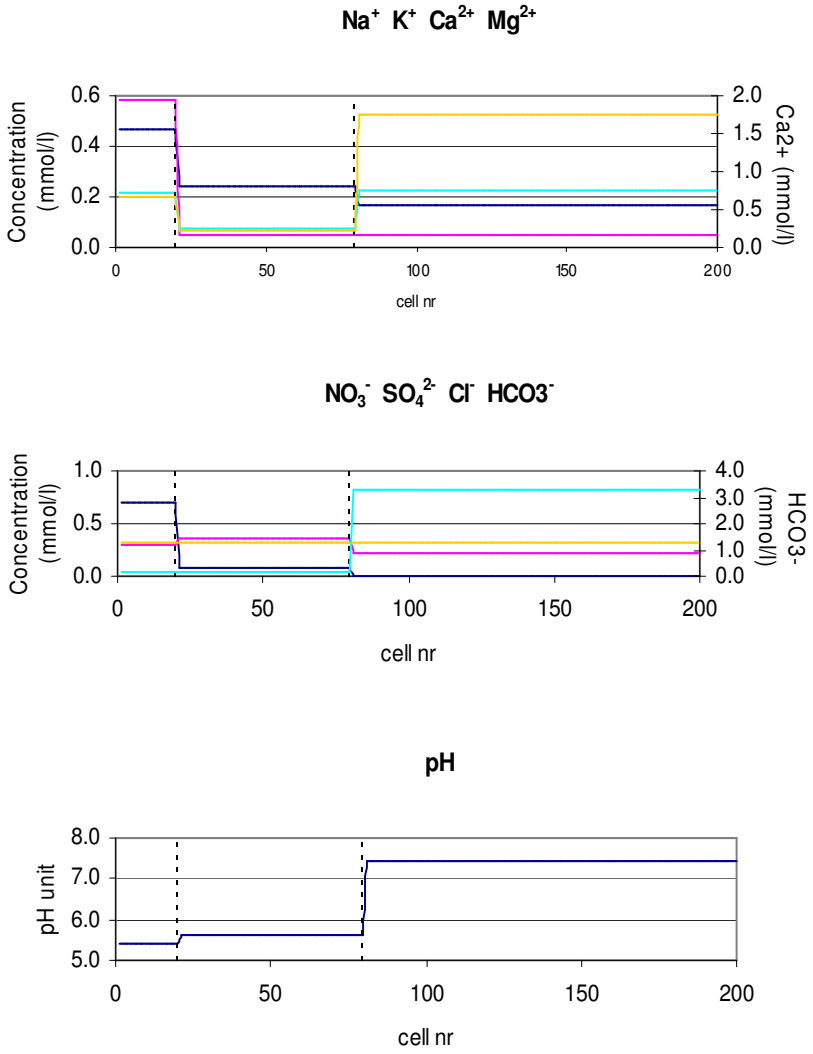


Figure 4.4 - Initial groundwater composition and pH in the three aquifers. Dark blue, red, yellow and light blue represent in the upper graph Na, K, Ca and Mg, respectively and in the middle graph NO3, SO4, Cl and HCO3, respectively. Dashed lines represent aquifer boundaries.

## 4.5 Conservative transport modeling

The model run starts in 1950 and simulates 50 years of conservative transport. Figure 4.5 shows the model results of the year 2000. Since the solute composition and pH in the aquifers as well as in the recharge water behave conservatively in this model, their spatial patterns from Figures 4.3 and 4.4 are recognizable in Figure 4.5. Essentially, the initial aquifer compositions in cells 1-200 are ‘pushed’ through the aquifers by the recharge water. When comparing Figures 4.4 with 4.5, it becomes clear that, after 50

years of transport (equivalent to 100 cells), the initial water composition and pH in cells 1-100 has been shifted to cells 101-200. Furthermore, Figure 4.5 shows that the hydrodynamic dispersion has smoothed the sharp boundaries initially present between the aquifers (Figure 4.4).
When Figure 4.3 is compared to Figure 4.5, it can be seen that the recharge water composition of 1950 has, after 50 years of transport, arrived in cells 99-100, whereas the recharge water composition of the year 2000 is present in cell 1-2. In other words, cells 1-100 in Figure 4.5 show in reversed order the solute concentration changes in the recharge water between 1950 and 2000 (Figure 4.3). As with the initial solute concentration and pH in the aquifers, also the yearly concentration changes in the recharge water visible in Figure 4.3 have become smoother in Figure 4.5 by hydrodynamic dispersion. Clearly, in the conservative model, the hydrochemistry along the flow path merely changes as a result of physical processes, i.e., advective transport and hydrodynamic dispersion.

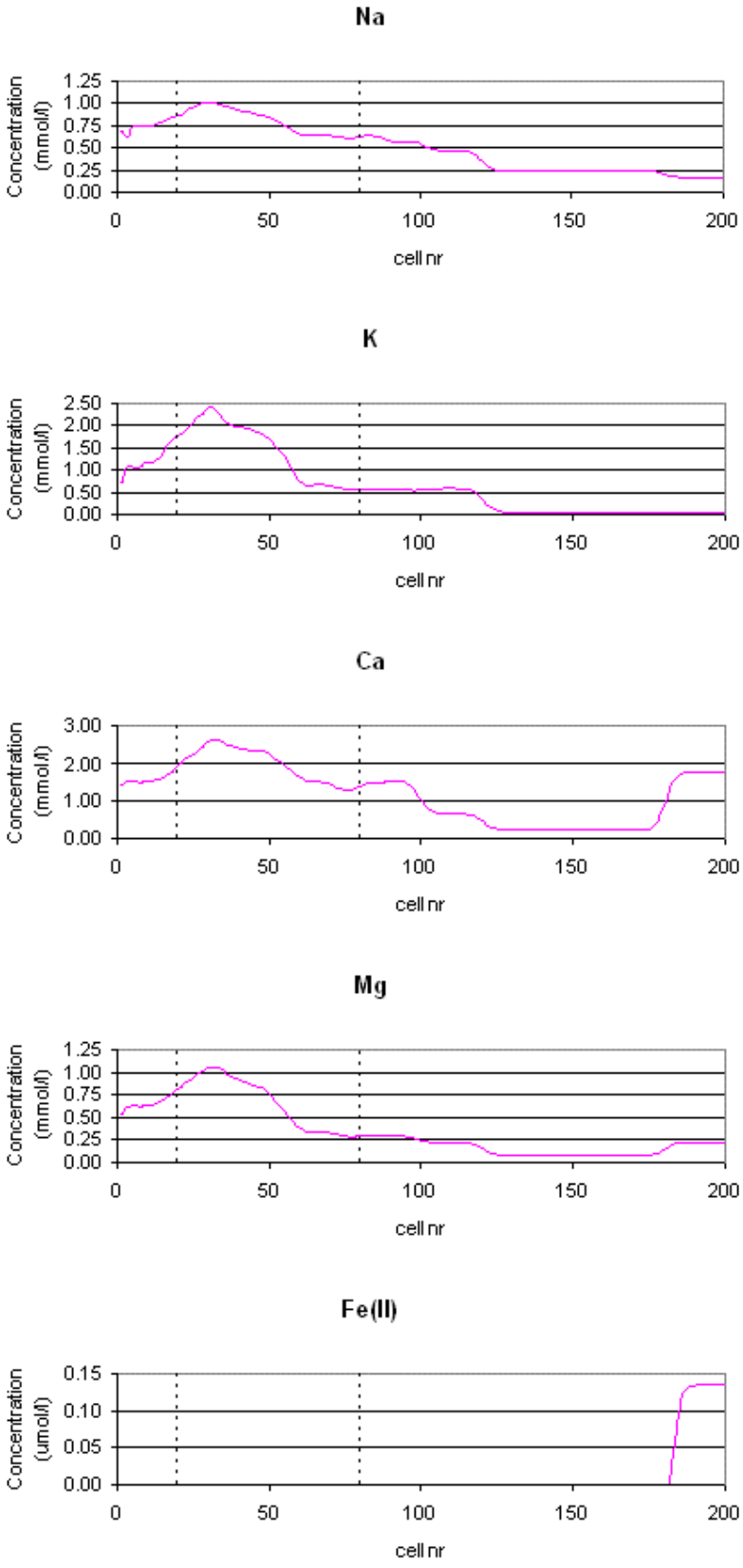


Figure 4.5 - Simulation results of the conservative transport model for the year 2000, i.e., after 50 years of conservative transport. Dashed lines represent aquifer boundaries.

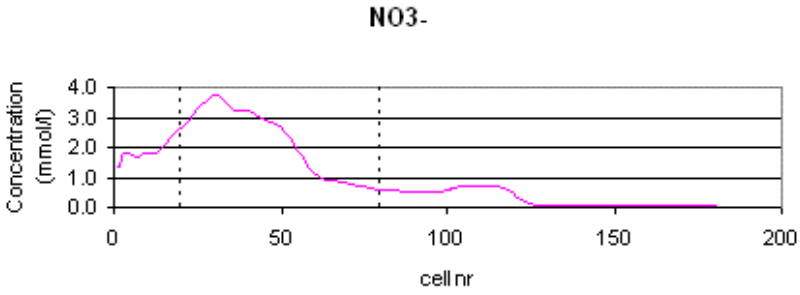


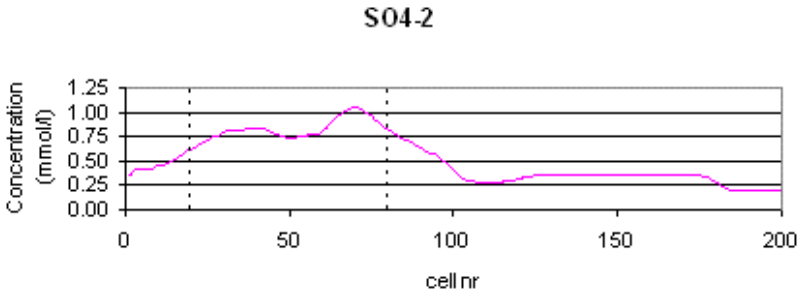


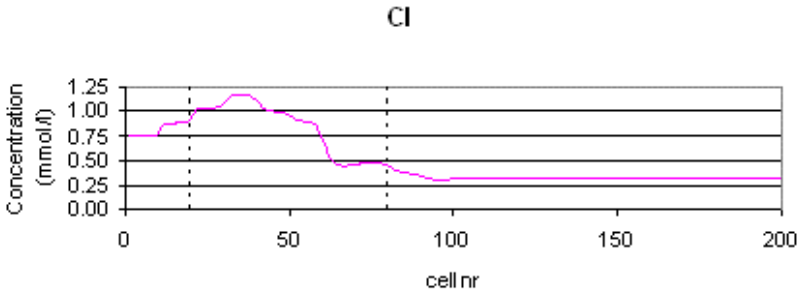


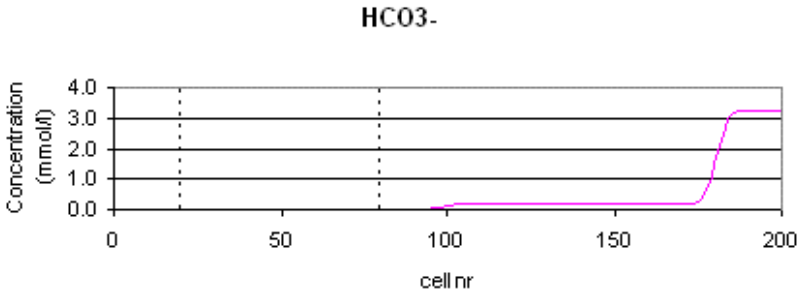


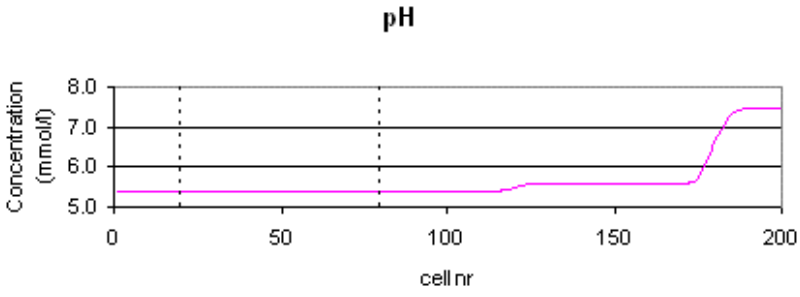


Figure 4.5 continued

## 4.6 Reactive transport modeling

In order to simulate reactive transport, the relevant hydrogeochemical processes (Chapter 2; Figure 2.3) are assigned to the three aquifers: cation exchange, mineral dissolution or precipitation and reduction and oxidation (redox) processes. In simulating cation exchange, the standard cation exchange coefficients from PHREEQC-2 were used. The simulation of dissolution or precipitation and redox processes occurs by means of imposing equilibrium phases.
It was already mentioned in Chapter 2 that the calcite content is relatively small or even zero in the first aquifer, whereas the second and third aquifer do contain calcite. In the one-dimensional reactive transport model, therefore, calcite dissolution was taken into consideration in the second and third aquifer, while in the first aquifer it was left out of consideration (Table 4.1; Figure 2.3). Furthermore, it was mentioned in Chapter 2 that the FeOOH mineral can occur in the form of crystalline goethite and in the form of ferrihydrite, where ferrihydrite has a higher solubility than crystalline goethite. The different solubilities of the FeOOH mineral are simulated by means of different SI's: if crystalline goethite is simulated, a SI of 0.0 (where log K = -1.0) is imposed, whereas if ferrihydrite is simulated, a SI of 3.0 is imposed. Finally, according to the groundwater measurements, siderite is assigned a Saturation Index (SI) of 0.5 in the second and third aquifer (Chapter 2).

Table 4.1 - Initial solution compositions in the aquifers as imposed in the reactive transport model. All components in mmol/l, CEC in meq/l. After Griffioen et al., 2003 and Maas, 2002.

| | **Aquifer 1** | **Aquifer 2** | **Aquifer 3** |
|---|---|---|---|
| Cells | 1-20 | 21-80 | 81-200 |
| pH | 5.4 | 5.6 | 7.5 |
| $Na^+$ | 0.47 | 0.24 | 0.17 |
| $K^+$ | 0.59 | 0.05 | 0.05 |
| $Ca^{2+}$ | 0.66 | 0.23 | 1.75 |
| $Mg^{2+}$ | 0.22 | 0.08 | 0.22 |
| $Fe^{2+}$ | - | 0.01 | 0.13 |
| $NO_3^-$ | 0.70 | 0.08 | - |
| $SO_4^{2-}$ | 0.31 | 0.36 | 0.23 |
| $Cl^-$ | 0.32 | 0.32 | 0.32 |
| $HCO_3^-$ | 0.20 | 0.19 | 3.36 |
| CEC | 2.1 | 1.5 | 38 |
| Calcite | - | 17 | 156 |
| Pyrite | - | - | 77 |
| Siderite | - | 80 | 80 |
| Goethite | 104 | 31 | 10 |

### *4.6.1 Simulation Results*

This section describes the simulation results of the reactive one-dimensional model. In the scenario described in the first part of this section, calcite equilibrium as well as siderite equilibrium are imposed in the second and third aquifer, pyrite equilibrium is present only in the third aquifer and FeOOH precipitation occurs - in case of

supersaturation - in all aquifers. In this scenario a SI of 0.0 was taken for the FeOOH mineral. The scenario is referred to as scenario CPSG 0 (number 8) in Table 4.2.
The scenario in which for the FeOOH mineral a SI of 3.0 was taken (CPSG 3, number 9 in Table 4.2) is described in the second part of this section. Moreover, simulation results of seven more scenarios (Table 4.2) are described in the second part of this section.

*Scenario CPSG 0*

The model run starts, as with the conservative transport model, in 1950 and simulates reactive transport for 50 years. Simulation results of the reactive transport model are visualized in Figure 4.6: solute concentration and pH values of the year 2000 are plotted along the flow path. The amounts of mineral dissolution or precipitation, either or not initiated by redox reactions, are plotted as well. Simulation results of the conservative model are depicted for reference.

By comparing the reactive and conservative model results with respect to the $Ca^{2+}$ concentration along the flow path in Figure 4.6, it can be seen that the amount of $Ca^{2+}$ in the groundwater present in cells 21-200 (aquifer 2 and 3) is higher in the reactive model simulation than in the conservative model simulation. The differences are in the order of millimoles and can be explained by calcite dissolution as a result of imposing calcite equilibrium in these aquifers in the reactive model (see also the results for calcite which are described further on).
At first sight, in cells 1-20 (aquifer 1) the reactive and conservative models appear to have approximately equal $Ca^{2+}$ concentrations. In this aquifer, conditions with respect to calcite in both models are equal (no calcite equilibrium). However, thorough inspection of the output files of both model calculations yields small differences - in the order of micromoles - in $Ca^{2+}$ concentrations in the first aquifer: in the conservative model there is slightly more $Ca^{2+}$ in the water than in the reactive model. These small differences are ascribed to cation exchange occurring in the reactive model, transferring the $Ca^{2+}$ from the groundwater onto the aquifer material. The process of cation exchange has buffered the amount of $Ca^{2+}$ in the groundwater in the second and third aquifer as well, since cation exchange is imposed in all aquifers.

In addition to $Ca^{2+}$ also $Na^+$, $K^+$, $Mg^{2+}$ and $Fe^{2+}$ in the water are subject to the process of cation exchange in the reactive model. In Figure 4.6, it can be seen that the reactive model results show $Na^+$, $K^+$, $Mg^{2+}$ and $Fe^{2+}$ concentrations different from those resulting from the conservative model. For $Na^+$, $K^+$, $Mg^{2+}$, the differences have to be attributed to cation exchange since no other processes are able to affect concentrations of $Na^+$, $K^+$ and $Mg^{2+}$ in the model. However, $Fe^{2+}$ concentrations are affected not only by cation exchange. This will be described further on.
The model results show that for $Na^+$ and $K^+$ retardation occurs in the upper part of the third aquifer (Figure 4.6). However, $K^+$ is considerably more retarded than $Na^+$: $K^+$ experiences a delay of 11 years (22 cells), whereas $Na^+$ experiences a delay of only 2.5 years (5 cells). This is explained by the fact that $K^+$ has a higher affinity to adsorb onto the aquifer material than has $Na^+$ (Parkhurst and Appelo, 1999) and therefore remains longer part of the exchanger.
Furthermore, $Mg^{2+}$ concentrations in the third aquifer are higher in the reactive model than in the conservative model. The process of cation exchange thus releases $Mg^{2+}$ into the groundwater. As can be seen in Figure 4.6, the $Mg^{2+}$ increase in the groundwater as a result of desorption occurs in nearly the complete third aquifer, whereas the $K^+$ and the $Na^+$ retardation occur only in the upper part of the third aquifer (Figure 4.6).

Therefore, with respect to $Na^+$, $K^+$ and $Mg^{2+}$, the effect of cation exchange is most eminent for $Mg^{2+}$. Furthermore, as appears from the observations, the release of $Ca^{2+}$ into the groundwater as a result of calcite dissolution has affected the exchange behavior of $Mg^{2+}$, $Na^+$ and $K^+$.

Considering the nitrate and sulfate evolution along the flow path in Figure 4.6, it can be seen that in the first aquifer and part of the second aquifer (until cell 37) nitrate as well as sulfate concentrations resulting from the conservative and reactive models are equal. From cell 37 on, clear differences in nitrate and sulfate concentration between the conservative and reactive model results are visible (Figure 4.6).
While in the results of the conservative transport model sulfate and nitrate concentrations reflect the smoothed load concentrations in cells 1-100, the reactive transport model results show abrupt decreases in nitrate and sulfate concentrations in cell 37, considerably below the boundary between the first and second aquifer (cells 20-21). Siderite concentrations resulting from the reactive model show that in the second aquifer siderite is dissolved (Figure 4.6). Apparently, as soon as nitrate-rich groundwater enters the second aquifer in which siderite is available, this mineral starts to act as an electron donor: it dissolves and the released Fe(II) is oxidized by nitrate. As can be seen, all nitrate entering the second aquifer is reduced.
The sulfate concentration drops from cell 37 as well, although the decrease is more gradual than the decrease in the nitrate concentrations. Inspecting the amount of reduced sulfur species indicates that the $HS^-$ concentration has increased. Obviously, sulfate is reduced in the second aquifer in the model. As siderite is the only possible electron donor in the second aquifer, the sulfate reduction occurs by siderite oxidation. However, although it occurs in the model, this redox process is not likely to occur in the field (Chapter 2).
Obviously, as the changes in nitrate and sulfate concentrations occur in cell 37 rather than in cell 21, in which the second aquifer starts, the siderite oxidation front has shifted downward after 50 years of reactive transport. This can also be seen in the siderite plot in Figure 4.6. The shifting of the front thus occurs in the model with a velocity of 16 cells per 50 years, corresponding to 11.2 cm/year. Above the front, in the uppermost cells of the second aquifer (cells 21-36), all available siderite, i.e., the initial amount imposed in the model, has been oxidized.
In the third aquifer (from cell 81) all sulfate is reduced. This is due to the fact that, besides siderite, pyrite equilibrium is imposed in this aquifer, resulting in the formation of pyrite. In cell 81, a pyrite formation front has formed. The reactive model results with this indicate that - in this setting - siderite is preferable to pyrite as an electron donor in the third aquifer. However, as is the case with siderite oxidation, pyrite formation is not likely to occur in the aquifers in and around Holten (Chapter 2). This will be discussed further on.

Furthermore, the model results show that the oxidized iron has precipitated in the form of crystalline goethite in cells 21-36 (equation (3), Figure 4.6). Downstream of cell 36, the siderite oxidation as well as the goethite precipitation abruptly decrease, both of which are explained by the fact that the available nitrate from the recharge water has been consumed in the upstream cells.
As can be seen, the siderite oxidation and goethite precipitation do not cease below cell 36, although all available nitrate has been consumed in this cell. It was already mentioned before that siderite oxidation occurs by sulfate reduction below cell 37. The fact that in cells 37-200 siderite oxidation by sulfate reduction as well as goethite formation occur has to do with the imposed minerals, their SI's and the resulting pe

shift in the model. Obviously, the combination of the mineral FeOOH with a relatively low solubility (SI = 0.0) with the mineral siderite with a relatively high solubility (SI = 0.5) forces a certain amount of siderite to dissolve, the released iron(II) to become oxidized and an almost equal amount of crystalline goethite to precipitate. The siderite oxidation occurs by sulfate reduction, as no other electron acceptor is available. However, as mentioned before, although they are simulated by the model, these processes are not likely to occur in the aquifers in and around Holten (Chapter 2).

In Figure 4.6 the Fe(II) concentrations (in µmol/l) resulting from the conservative and reactive model are depicted as well. Besides the process of cation exchange, also the imposed minerals affect the Fe(II) concentration in the reactive model. However, a nearly equivalent amount of Fe(II) which is released by siderite dissolution is oxidized and precipitated as goethite. Therefore, the fact that the Fe(II) concentrations in cells 37-185 are higher in the reactive than in the conservative model is ascribed largely to the process of cation exchange. Nevertheless, it should be kept in mind that the changes in the Fe(II) concentration are rather slight (Figure 4.6).

Figure 4.6 furthermore shows that the calcite dissolution front has, after 50 years of reactive transport, shifted downward to cell 45. The shifting of the calcite dissolution front is with a velocity of 25 cells per 50 years or 17.5 cm/year therefore faster than the shifting of the siderite oxidation front.

When the evolution of the pH and $HCO_3^-$ concentration along the flow path in Figure 4.7 is considered, it can be seen that cells 1-35 reflect the values of the recharge water. This observation is explained by the fact that in these cells, calcite and goethite, as they are absent, can not affect pH and $HCO_3^-$ concentration anymore. The relatively low pH value in cell 36 results from the $H^+$ released by goethite formation.
In cell 37 in the second aquifer, the pH abruptly rises, simultaneously with the decrease in nitrate and sulfate concentration and the siderite dissolution and goethite precipitation front. The pH increase is interpreted to be a result of the decrease in siderite dissolution and the subsequent Fe(II) oxidation and goethite precipitation (equations (4a) and (3), respectively). The formation of the mineral goethite following siderite dissolution produces $H^+$; when the goethite precipitation drops therefore, $H^+$ production drops as well and pH increases.
The $HCO_3^-$ concentration rises as well in cell 37, which is in turn a result of the changing pH values as the composition of aqueous carbonate species ($H_2CO_3$, $HCO_3^-$ and $CO_3^{2-}$) depends on pH (Appelo and Postma 1993). Rising pH values cause the amount of $HCO_3^-$ in the water to increase at the expense of $H_2CO_3$.
In cell 46, pH rises further, this time as a result of calcite dissolution. The $HCO_3^-$ concentration increases as well. However, from cell 46, the increasing $HCO_3^-$ concentration is not only due to pH increase: calcite dissolution releases $CO_3^{2-}$ into the groundwater which reacts with $H^+$, thereby forming $HCO_3^-$ as well.

The only component in the one-dimensional model which does not show differences in concentration between the conservative and reactive run, is chloride. This comes up to expectations, as in nature chloride behaves as a conservative component (Appelo and Postma, 1993).

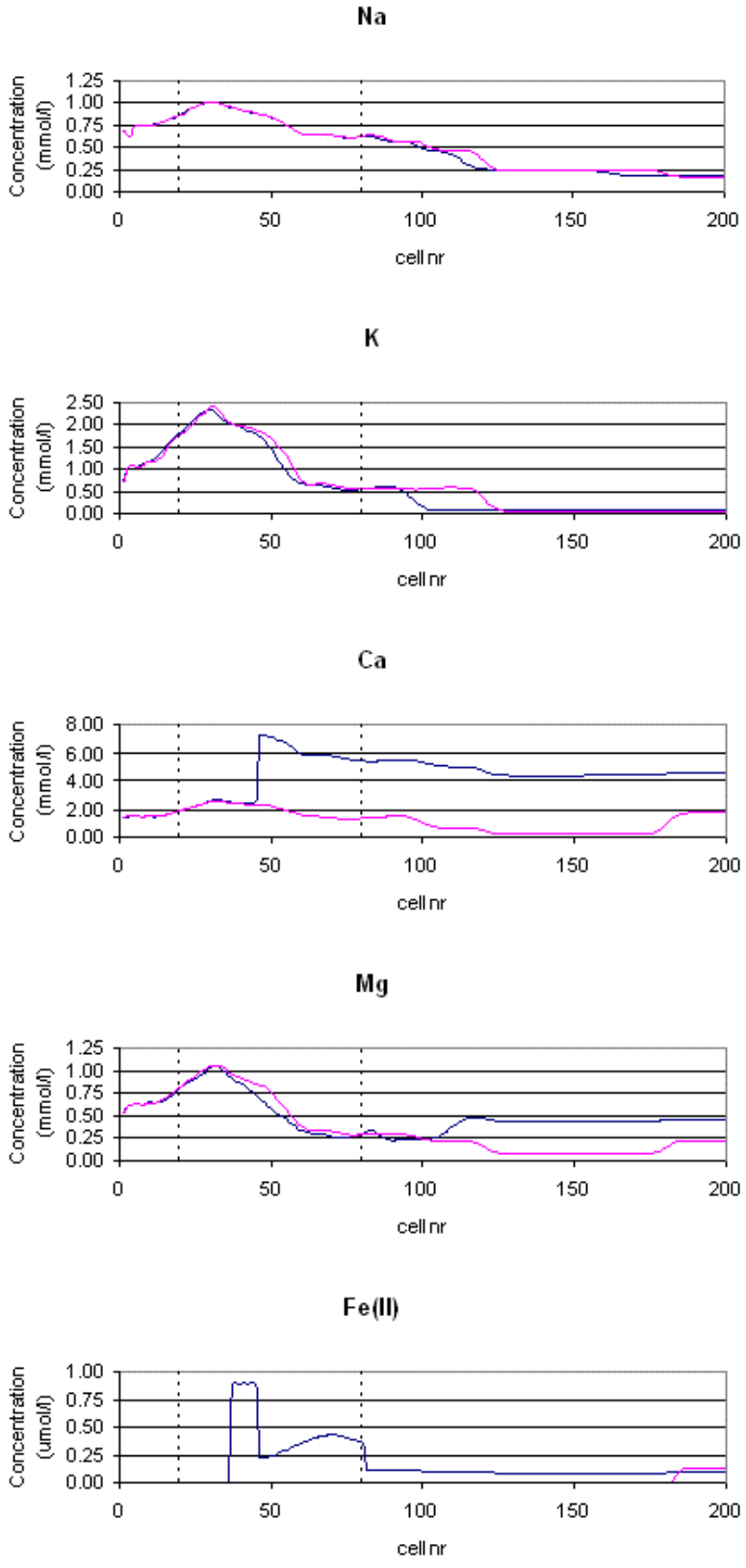


Figure 4.6 - Simulation results of the reactive transport model, scenario CPSG 0, (blue line) in the year 2000. Simulation results of the reactive transport model (red line) have been depicted for reference. Dashed lines represent aquifer boundaries.

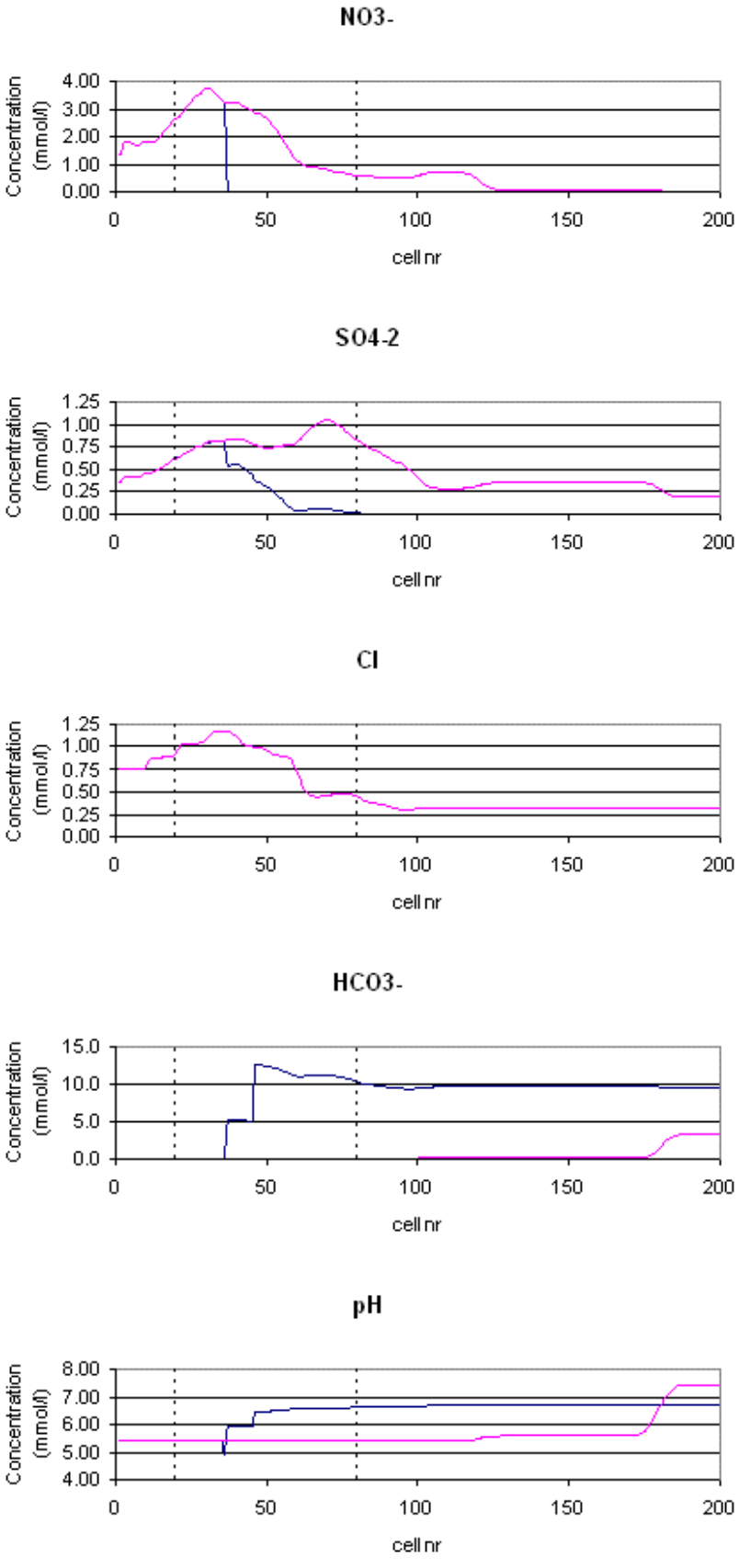


Figure 4.6 continued

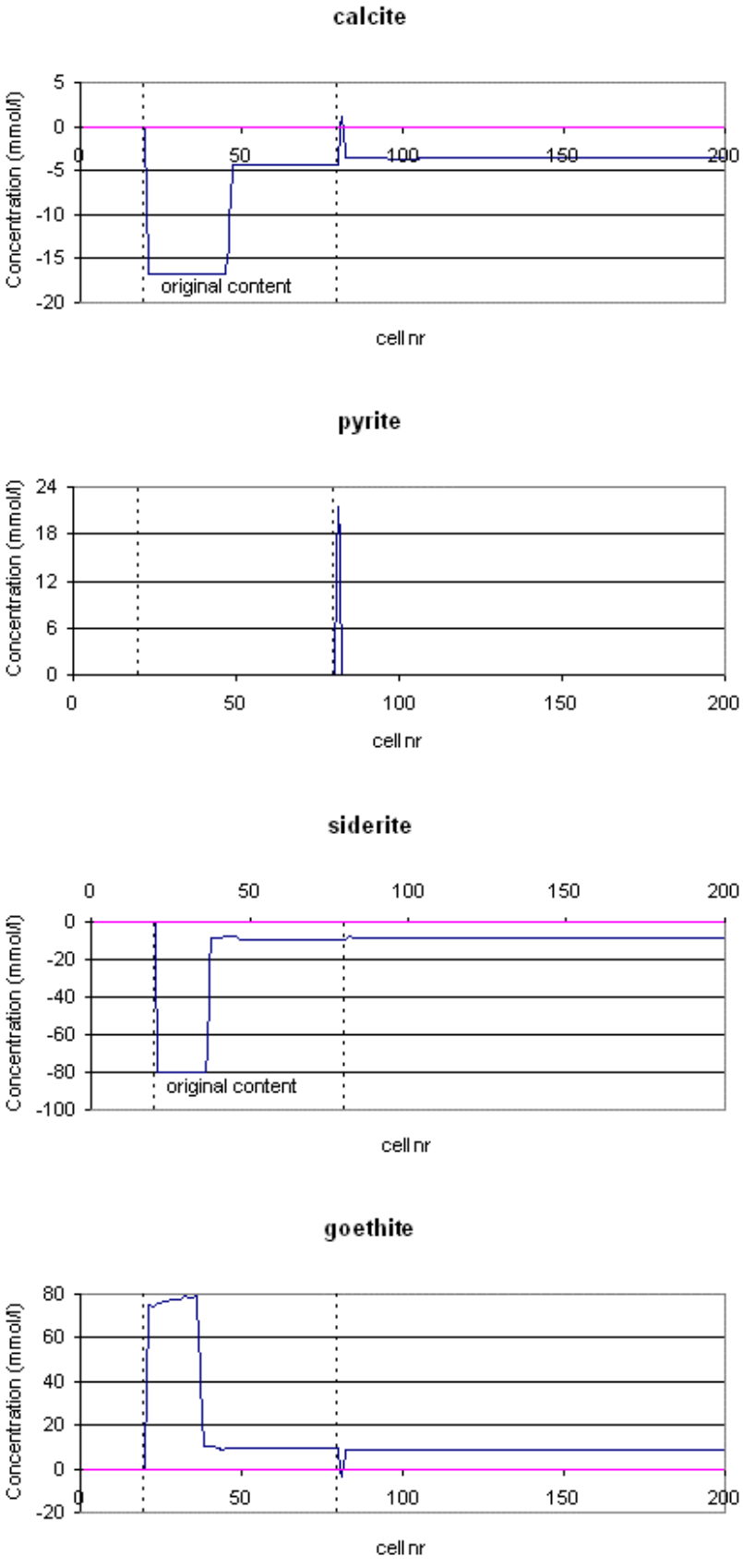


Figure 4.6 continued

*Different scenarios*

In order to better understand the processes of calcite dissolution and siderite, pyrite and goethite equilibrium and how they are related to each other, the one-dimensional reactive transport model was run several times with different scenarios (Table 4.2, Figure 4.7). In all scenarios, the hydrogeochemical processes occur in the second and third aquifer; in the first aquifer no processes are imposed.
In scenario C, only equilibrium with calcite is imposed (Table 4.2). Scenario CP models both calcite and pyrite equilibrium, while scenario CS combines calcite equilibrium with siderite equilibrium. In scenario CPG 0 and CPG 3, calcite, pyrite and FeOOH equilibrium are modeled, where the FeOOH mineral has a SI of 0.0 and 3.0 respectively. Scenario CPS models calcite, pyrite and siderite equilibrium, whereas in scenario CSG calcite, siderite and goethite equilibrium are combined. In scenario CPSG 0 and CPSG 3, calcite, pyrite, siderite and FeOOH equilibrium are imposed, where the FeOOH mineral has a SI of 0.0 and 3.0 respectively. Scenario CPSG 0 is the scenario as described above. The results of the nine scenarios were compared to each other, which yielded the following insights.

Table 4.2 – Different scenarios

| number | name | scenario | SI goethite |
|---|---|---|---|
| 1 | C | equilibrium with calcite, no redox | X |
| 2 | CP | equilibrium with calcite and pyrite | X |
| 3 | CPG 0 | equilibrium with calcite, pyrite and goethite | 0.0 |
| 4 | CPG 3 | equilibrium with calcite, pyrite and goethite | 3.0 |
| 5 | CS | equilibrium with calcite and siderite | 0.0 |
| 6 | CPS | equilibrium with calcite, pyrite and siderite | X |
| 7 | CSG | equilibrium with calcite, siderite and goethite | 3.0 |
| 8 | CPSG 0 | equilibrium with calcite, pyrite, siderite and goethite | 0.0 |
| 9 | CPSG 3 | equilibrium with calcite, pyrite, siderite and goethite | 3.0 |

Scenarios 1-6 all show approximately the same results with respect to calcite dissolution in the second aquifer (Figure 4.7). The calcite dissolution front in scenarios 1-4 is situated in cell 24, whereas in scenarios 5 and 6 it is situated in cell 26.
Most calcite in the second aquifer dissolves in scenarios 7 and 8; the dissolution fronts have arrived at cell 46 after 50 years of reactive transport. Scenarios 7 and 8 yield the same results in the second aquifer since the imposed conditions are equal in this aquifer. In scenario 9 the dissolution front is situated in cell 37. The combination of siderite and FeOOH equilibrium (scenarios 7-9) obviously creates more favourable conditions for calcite dissolution than does either siderite equilibrium (scenarios 5 and 6) or FeOOH equilibrium (scenarios 3 and 4). This can be explained by the fact that imposing FeOOH equilibrium effectively removes Fe(II) released by siderite dissolution from the water by precipitating the mineral FeOOH (equation (3)), thereby shifting the thermodynamic equilibrium of siderite dissolution to the right and causing more siderite to dissolve. If more Fe(II) is available by imposing siderite equilibrium, more FeOOH can precipitate. Oxidation of Fe(II) and subsequent precipitation of the mineral FeOOH produce $H^+$, which in turn cause calcite to dissolve. Combining FeOOH equilibrium and siderite equilibrium thus results in higher amounts of siderite dissolution, FeOOH precipitation and calcite dissolution.
The difference with respect to calcite dissolution between scenario 7 and 8 and scenario 9 (Figure 4.7) is ascribed to the higher solubility of the FeOOH mineral in scenario 9

(ferrihydrite) than in scenario 7 and 8 (crystalline goethite). Due to the higher solubility, a smaller amount of FeOOH precipitates, resulting in less calcite dissolution in scenario 9.

In the second aquifer, most FeOOH thus precipitates in scenario 7 and 8 as in these scenarios by siderite dissolution the largest amount of Fe(II) is available and the SI of FeOOH has a value of 0.0. The goethite precipitation front is situated in cell 37 in these scenarios.
Scenario 9 shows that the FeOOH precipitation front has arrived in cell 30, as, because of the higher solubility of the FeOOH mineral, FeOOH precipitates less easily compared to scenarios 7 and 8. In scenarios 3 and 4, a very slight amount of goethite – in the order of micromoles – precipitates since Fe(II) is only sparsely available.

Siderite dissolution in the second aquifer is highest in scenarios 7 and 8 as well. The siderite dissolution front has arrived in cell 37. In scenarios 5 and 6, imposed equilibria are equal in the second aquifer and, therefore, these scenarios yield the same results. The siderite dissolution front has arrived in cell 30 in these scenarios. Moreover, a small amount of calcite is precipitated in scenarios 5 and 6 in cells 27-29, since as a result of siderite dissolution, which releases $CO_3^{-2}$ in the water, calcite equilibrium shifts to the left (equation (5)).

$$CaCO_3 \quad > \quad Ca^{2+} + CO_3^{-2} \qquad (5)$$

The model results of the second aquifer of scenario 9 are equal to scenario 5 and 6, except for cells 31-37. While in cells 31-37 in scenarios 5 and 6 a small amount of siderite is dissolved, scenario 9 shows that a small amount of siderite precipitates in these cells. Obviously, below the FeOOH precipitation front in cell 30 in scenario 9, siderite precipitation is preferred rather than siderite dissolution as a result of the combination of siderite equilibrium and FeOOH equilibrium with SI 3.0. Imposing FeOOH with a relatively high solubility (SI = 3.0) in scenario 9 yields iron(II) in the water, thereby enabling siderite to precipitate, whereas in scenario 5 and 6, iron(II) is not available and the siderite equilibrium (equation (4)) is directed to the right.

In the third aquifer, equilibrium with the mineral pyrite is added to the calcite, siderite and FeOOH equilibrium. In order to inspect the model results properly, Figure 4.7b zooms in to cells 75-105, in which the boundary between the second and third aquifer is situated. All scenarios including pyrite equilibrium in the third aquifer, except scenario 8, indicate that pyrite is oxidized in cell 81 (scenarios 2, 3, 4, 6 and (to a smaller extent) 9, Figure 4.7b). In scenario 8, pyrite precipitates in cell 81. The ‘peaks’ in scenarios 2, 3, 4 and 6 represent the pyrite oxidation fronts, whereas the peak in cell 81 in scenario 8 indicates that in this scenario a pyrite precipitation front is formed (see also Figure 4.6).
Calcite, siderite and goethite show peaks in cell 81 as well (Figure 4.7b). In scenario 2, a calcite precipitation front is formed in cell 81. In accordance with the pyrite oxidation front in cell 81 in scenarios 3 and 4, a FeOOH precipitation front and a calcite dissolution front is formed. In scenario 6, a siderite precipitation front as well as a calcite precipitation front is formed in cell 81. Scenario 8 shows in accordance with the pyrite precipitation front a calcite precipitation and a goethite dissolution front. A slight dip occurs in cell 81 in the siderite dissolution (see also Figure 4.6).
In scenarios 5, 7 and 9 no peaks occur in cell 81. Scenarios 5 and 7 do not show distinct differences in mineral behavior between the second and third aquifer since pyrite equilibrium is not imposed in these scenarios and therefore no differences in imposed

equilibria exist between the second and third aquifer. Scenario 9 shows a calcite and siderite precipitation front, a pyrite oxidation front and a goethite dissolution front in cell 97. These fronts thus have extended more 'downstream' than the fronts in scenarios 2, 3, 4, 6 and 8. In scenarios 2, 3 and 4, in which no nitrate has been consumed in the second aquifer, all nitrate entering the third aquifer is consumed by pyrite oxidation in cell 81. In contrast to these scenarios, nitrate is not available for pyrite oxidation in the third aquifer in scenarios 6 and 9. Nevertheless, pyrite oxidation does occur: in scenario 6 in cell 81 and in scenario 9 in cells 81-200. This implies that there must be other electron acceptors oxidizing pyrite in this setting. Possibly, iron hydroxides are able to act as electron acceptor. In scenario 9, the presence of ferrihydrite indeed may explain the occurrence of pyrite oxidation. However, ferrihydrite is not available in scenario 6. A possible explanation is that different types of iron(III) species are formed as a result of iron(II) oxidation in de second aquifer. Subsequently, the iron(III) species are transported to the third aquifer, where they become reduced by pyrite oxidation. In cells 82-200 in scenario 6, no pyrite oxidizes or precipitates, which implies that the iron(III) species are directly reduced after entering the third aquifer in cell 81.
In scenarios 3, 4 and 8, pyrite and FeOOH are formed in cells 82-200 due to the imposed pyrite and FeOOH equilibrium.

The above data imply that combining FeOOH equilibrium with calcite and pyrite equilibrium in scenarios 3 and 4 inhibits pyrite to become oxidized (except in cell 81). Obviously, oxidation of in situ Fe(II) and the subsequent FeOOH precipitation is preferred to pyrite oxidation. The amount of pyrite precipitation as well as FeOOH precipitation is slightly larger in scenario 3 than in scenario 4, since in scenario 3 the SI of FeOOH is 0.0, while in scenario 4 the SI of FeOOH is 3.0. The amount of calcite dissolution is slightly larger as well in scenario 3 than in scenario 4.
However, when siderite equilibrium is added to calcite, pyrite and FeOOH equilibrium in the third aquifer (scenarios 8 and 9), pyrite oxidation does occur as long as FeOOH is relatively soluble. The difference between the scenario with a FeOOH SI of 0.0 and the scenario with a FeOOH SI of 3.0 is considerable: in scenario 8 pyrite precipitates, whereas in scenario 9 pyrite oxidizes. Therefore, sulfate is produced rather than reduced in scenario 9. Scenario 8 furthermore indicates that siderite oxidation and the subsequent precipitation of iron hydroxides is preferred to pyrite oxidation when the iron hydroxides are highly insoluble (crystalline goethite), whereas scenario 9 indicates that pyrite oxidation is preferred to siderite oxidation when the iron hydroxides are relatively soluble (ferrihydrite).
As in the study area pyrite oxidation is observed (Griffioen et al., 2003), scenario 9 better represents the aquifers in and around Holten than scenario 8. A difference between scenarios 8 and 9 also exists with respect to calcite behavior: in scenario 8, calcite dissolves in the third aquifer (except in cell 81, in which a small amount of calcite precipitates), while in scenario 9 calcite precipitates in the third aquifer.
Finally, the model results indicate that siderite equilibrium has no influence on the behavior of pyrite when no FeOOH equilibrium is imposed (scenario 2 and 6). In both scenarios, the same amount of pyrite is oxidized in cell 81. However, in scenario 2 pyrite oxidation occurs by nitrate reduction, whereas in scenario 6, as described earlier, pyrite oxidation occurs by the reduction of different types of iron(III) species.

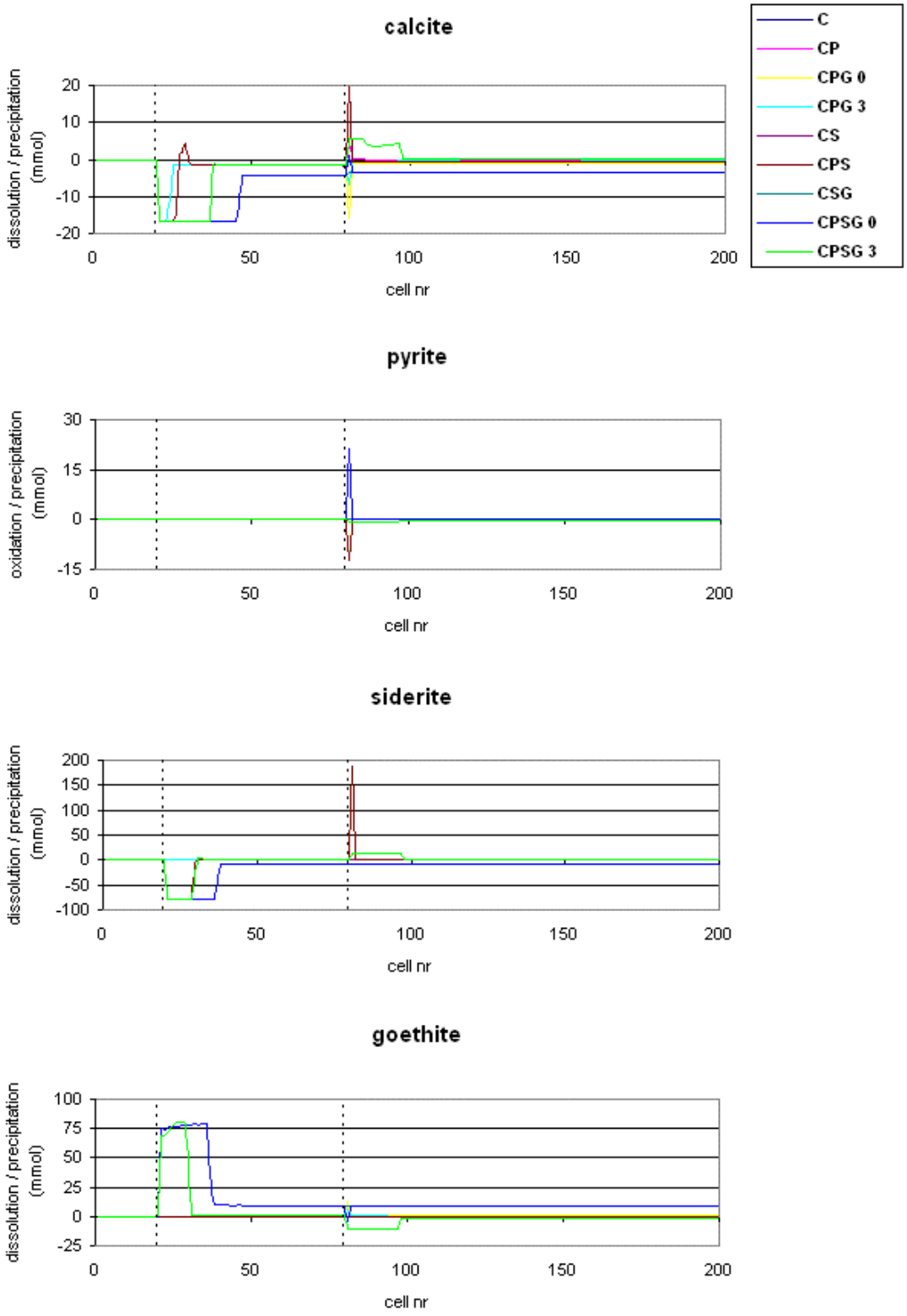


Figure 4.7a - Reactive model results for nine scenarios (see Table 4.2). Dashed lines represent aquifer boundaries.

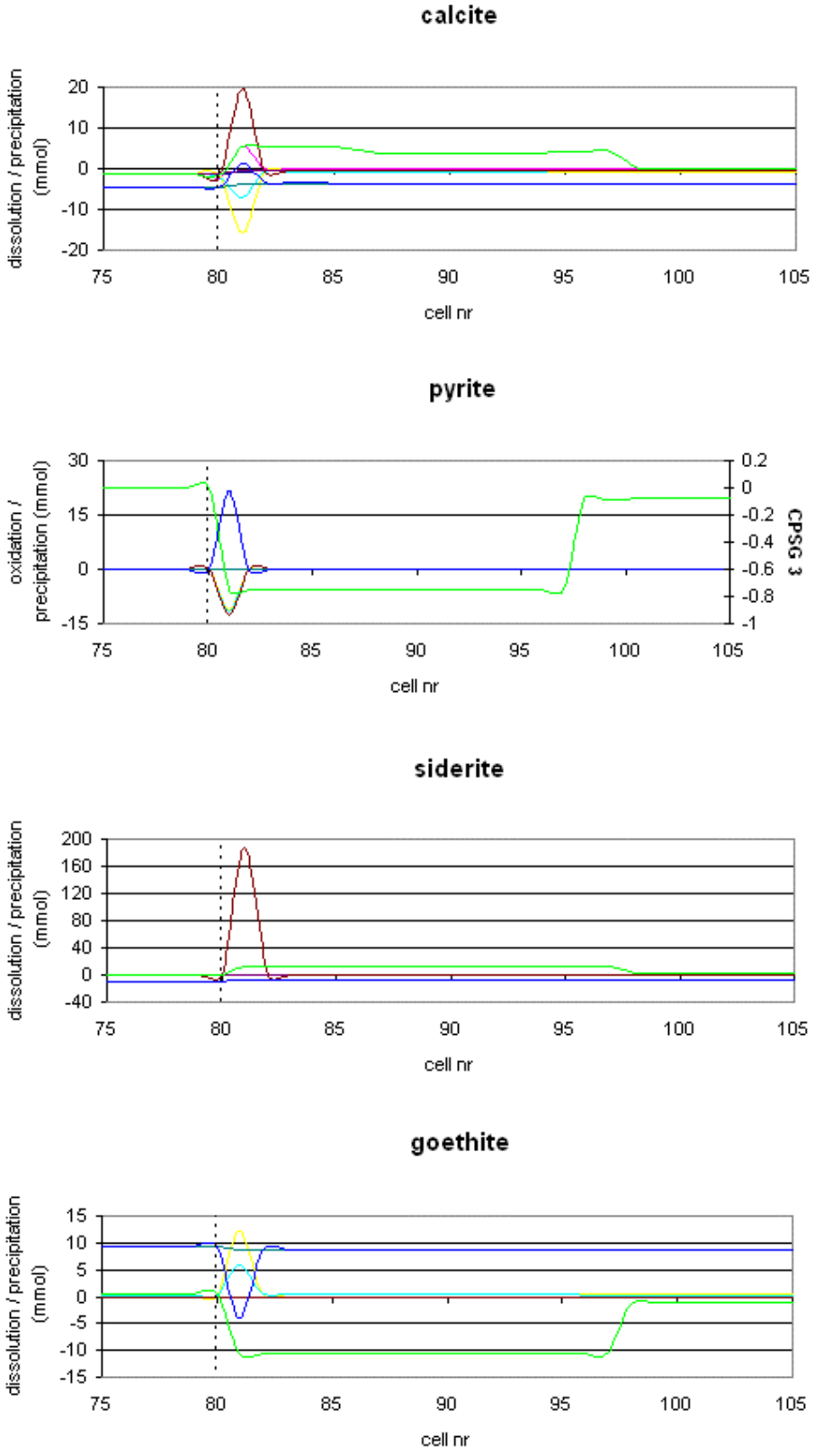


Figure 4.7b - Idem a, zoomed to cells 75-200. For legend, see Figure 4.7a. Dashed lines represent aquifer boundaries.

## 4.7 Conclusions and discussion

The nine scenarios carried out in the one-dimensional reactive model show that the equilibria of calcite, pyrite, siderite and the mineral FeOOH are strongly related to each other. Calcite behavior depends on the presence or absence of pyrite since the oxidation of pyrite consumes $H^+$. Siderite and FeOOH influence calcite behavior as during siderite dissolution or precipitation $CO_3^{2-}$ is produced or consumed, respectively, and FeOOH precipitation or dissolution produces or consumes $H^+$, respectively.
Furthermore, combining siderite and FeOOH equilibrium with calcite equilibrium results in an increase in calcite dissolution. Under these conditions, calcite behavior is determined by the solubility of FeOOH. Imposing a SI of 0.0 to FeOOH causes this mineral to precipitate and accordingly calcite to dissolve. Moreover, siderite dissolves accordingly with FeOOH precipitation in the form of crystalline goethite (scenarios 7 and 8). Imposing a SI of 3.0 to FeOOH implies that FeOOH is more soluble (scenario 9). As a result, FeOOH dissolves rather than precipitates, the released iron(III) is reduced to iron(II) and siderite precipitates. As was already mentioned, the iron reduction occurs by pyrite oxidation. Furthermore, calcite precipitates as a result of FeOOH dissolution.
As the solubility of the mineral FeOOH influences the behavior of siderite, it influences the behavior of pyrite as well. In the scenario without FeOOH equilibrium, pyrite oxidation is preferred to siderite oxidation (siderite dissolution and subsequent Fe(II) oxidation). However, equilibrium with FeOOH with SI = 0 'requires' Fe(II) for the precipitation of goethite, thereby forcing the siderite equilibrium to the right (equation (4)). Siderite thus acts as an electron donor and competes with pyrite in this case. Obviously, in this setting siderite dissolution and oxidation is preferred to pyrite oxidation. In contrast, equilibrium with the more soluble ferrihydrite (FeOOH with SI = 3) results in a siderite 'equilibrium' which is directed to the left (equation (4)), and therefore siderite precipitates rather than dissolves. In this case, pyrite is used as an electron donor and no competition between pyrite and siderite occurs.

In this context, it should be remarked that the SI of siderite, which has a value of 0.5, might influence the behavior of the minerals as well. A smaller SI of siderite would decrease its solubility, thereby hampering siderite to dissolve and act as an electron donor. The competition between the electron donors pyrite and siderite thus might depend on the solubility of siderite as well.

Although it is in this one-dimensional study unrealistic to compare field measurements to the model results, a considerable difference with respect to nitrate reduction in the second aquifer between the measurements and the model should be mentioned. Results of scenarios including siderite indicate that below the siderite dissolution front in the second aquifer, nitrate concentrations are zero. Field measurements however, show that in the second aquifer nitrate concentrations did not particularly decrease with respect to nitrate concentrations in the recharge water (Figure 2.6b and 4.3). Therefore, in the field, siderite dissolution and the subsequent oxidation of Fe(II) by nitrate occur only to a small extent. The fact that in the model nitrate concentrations are zero below the siderite dissolution front has to be ascribed to imposing mineral equilibria. In order to overcome this, the oxidation, dissolution and precipitation of the minerals should be modeled kinetically.
As appears from what is described above, siderite dissolution only occurs to a small extent in the field. Therefore, modeling FeOOH in the form of ferrihydrite is preferred

to modeling FeOOH in the form of crystalline goethite. Also with respect to the behavior of pyrite and sulfate, imposing ferrihydrite is more probable than imposing crystalline goethite: imposing ferrihydrite results - as observed in the field - in pyrite oxidation and accordingly sulfate increase (Figure 2.6a and 4.4), whereas imposing crystalline goethite results in sulfate reduction and pyrite precipitation. Scenario 9 thus best represents the expected behavior as described by the conceptual model in Chapter 2.

# 5 Three-dimensional transport modeling in PHT3D

After studying the several possible hydrogeochemical reactions and their relation to one another in the one-dimensional model (Chapter 4), a three dimensional reactive transport model, representing the subsurface of Holten and its surroundings, was constructed. Main aim of this modeling exercise is to quantify the influence of various land use functions and changes in land use functions on groundwater quality in the area around Holten. Moreover, it is aimed to deduce the geochemical processes occurring in the aquifers in and around Holten.
Griffioen et al. (2003) have modeled three-dimensional reactive transport in this area in an earlier study by means of RT3D (Clement, 1997). The modeling was carried out within the Integrated Transport Model (ITM) developed by NITG-TNO and KIWA (Van der Grift et al., 2003). ITM integrates various model codes, among which RT3D, in one program. An ArcView extension forms the graphical user interface for ITM, facilitating data input and visualization of output by GIS (Van der Grift et al., 2003).
Although the simulations in RT3D roughly reproduced groundwater quality as it was observed in the pumping and observation wells in the area around Holten, some significant differences between measured and calculated concentrations appeared (Griffioen et al., 2003). Therefore, in this study, the more sophisticated reactive transport model PHT3D is used in order to check the reactive transport calculations carried out in RT3D. The use of PHT3D occurs within ITM as well. Furthermore, this study attempts to estimate more accurately the load of the components sodium, potassium, calcium and magnesium at surface level and the hydrogeochemical processes occurring in the subsurface.

## 5.1 Model setup

The reactive transport model PHT3D couples the transport simulator MT3DMS (Zheng and Wang, 1998) with the geochemical model PHREEQC-2 (Parkhurst and Appelo, 1999) and is therefore able to model various geochemical processes occurring during groundwater flow (Prommer et al., 2003). PHT3D is able to consider the composition of the groundwater as a whole and carry out multi-component geochemical transport calculations, in contrast to RT3D, which can incorporate merely a few components and reactions.
The following sections describe the setup of PHT3D as it is used in this modeling exercise.

### *5.1.1 PHT3D: MT3DMS*

As already mentioned, PHT3D incorporates two models: a groundwater flow model and a geochemical model. The MODFLOW/MT3DMS part of PHT3D calculates the groundwater flow and non-reactive solute transport. In this study, groundwater flow is modeled in three dimensions.
The groundwater flow model was constructed for the RT3D study (Griffioen et al., 2003). The model is situated around Holten and covers an area of approximately 70 square kilometers (Figure 5.1). The model grid comprises 6984 cells formed by 97

columns and 72 rows. Cell size at and near the boundaries is 0.5 square kilometer (500 * 1000 meters) and decreases gradually towards the central part of the grid to 400 square meters (20 * 20 meters). The grid has been rotated 25 degrees in a counter clockwise direction in order to incorporate the anisotropy in the model (Griffioen et al., 2003, Figure 5.1).
The model comprises fourteen layers. The upper seven layers each have a thickness of about two meters and represent the upper or first aquifer (Griffioen et al., 2003). The underlying five layers, each with a thickness of about five meters, represent the middle or second aquifer. The lowermost two layers each have a thickness of about twenty meters and represent the lower or third aquifer. The groundwater pumping wells (Chapter 2, Figure 5.1) are located in layers 9-14 in the central part of the grid, northeast of the village of Holten. Each well is situated in a separate cell.
Groundwater flow is simulated for a period of 56 years, starting January 1$^{st}$, 1950 and ending December 31$^{st}$, 2005. The total flow simulation period is divided in 56 stress periods, each with a length of one year.

The MODFLOW model consists of several packages, each of which comprises different hydrogeological parameters (Griffioen et al., 2003). Boundary conditions and initial head values for each layer are described in the BAS package, whereas the BCF package describes transmissivities of model layers and resistances between layers. The anisotropy package imposes differences in hydraulic conductivity between the x and y direction. The river package, drain package, well package and recharge package furthermore describe the model parameters. Setup and parameter values of the groundwater flow model as it is used in this study are copied from the MT3DMS study and extensively described in Griffioen et al. (2003) and Iwaco (1993). Therefore, here it is referred to these earlier studies.

### *5.1.2 Integrating MT3DMS and PHREEQC-2 in PHT3D*

Constructing a model in PHT3D starts with loading the results of an existing MODFLOW (groundwater flow) model. First, the BAS package and the BCF package are stated. A third package, the Flow Model Interface (FMI) package, needs to be defined in order to link MODFLOW to MT3DMS. Secondly, position (upper left x-coordinate and y-coordinate) and orientation (rotation with respect to the x-axis and y-axis) of the model grid is set. Finally, the date at which the simulation starts is defined (Van Der Grift et al., 2003). In this modeling exercise, the simulation starts January 1$^{st}$, 1950.
Within the groundwater flow model now loaded, scenarios are constructed by defining the chemical calculation module. At this stage in the model construction, it is stated whether multi-component geochemical transport is calculated (macrochemistry) or single-solute transport of only one component (microchemistry). Setting the macrochemistry module, as it is done in this study, implies that PHREEQC-2 is incorporated in the model and that the coupling between MT3DMS/MODFLOW and PHREEQC-2 has been completed, resulting in a PHT3D scenario.
Furthermore, when defining a scenario, data from an existing scenario or recharge composition data can be loaded. As it is aimed to qualify the effect of different loadings at surface level, as a result of different land use, on groundwater quality, recharge composition data, derived from the load at surface level (Chapter 3), are loaded in this study.

Within the constructed PHT3D scenario, PHREEQC-2 exists in the form of a package (PHR package). A Basic Transport (BTN) package has been prepared as well during the model construction. These will be described in the next sections.

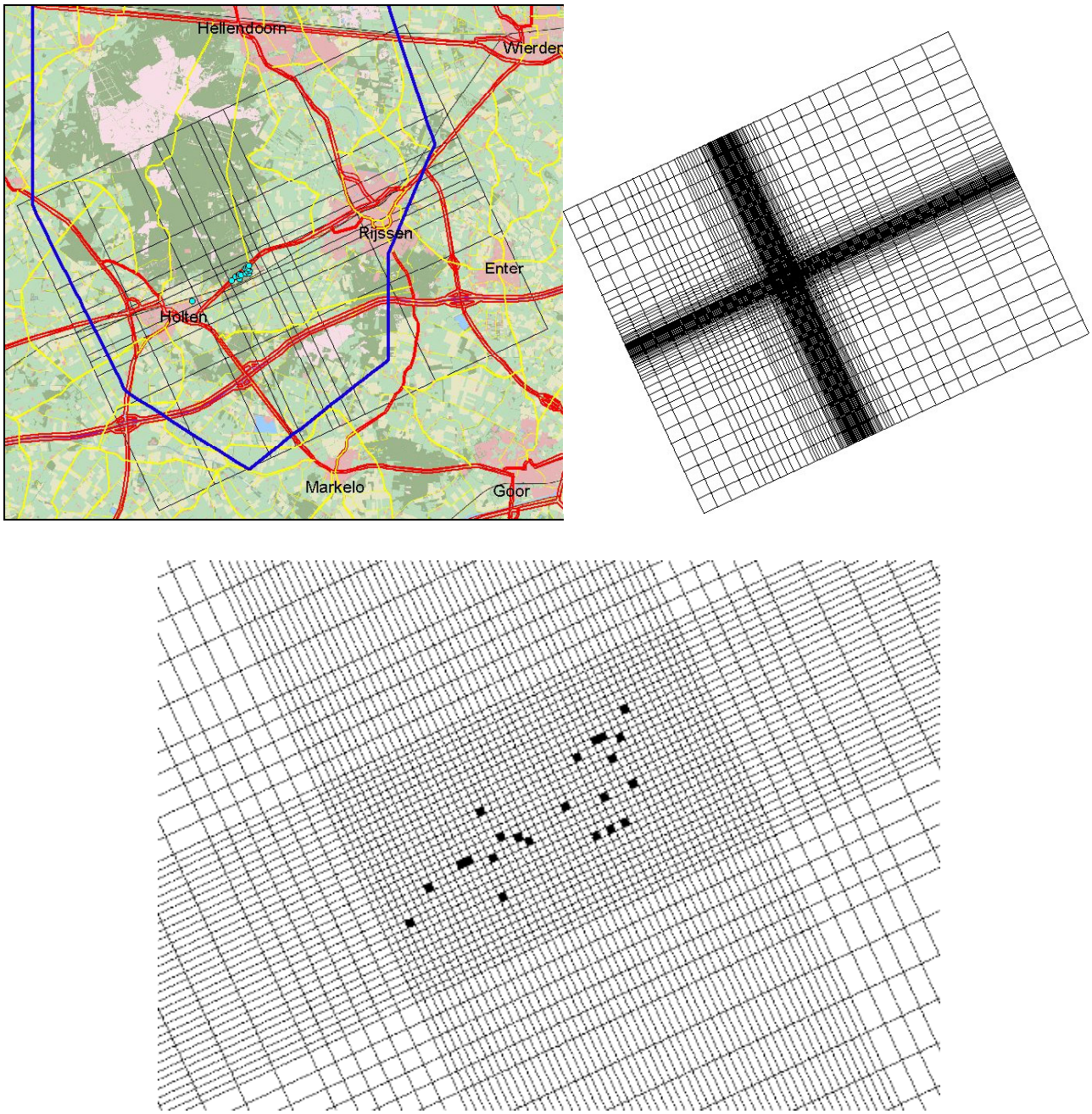


Figure 5.1 - The MT3DMS model grid in the area around Holten. In the upper left picture, only the boundaries and the main lines of the model grid have been displayed. The pumping wells are represented by the blue dots. (The topographic map in Appendix D shows the exact location of the pumping wells.) In the upper right picture, the complete model grid is displayed. Central columns and rows are too small to be separately visible. The lower picture zooms to the smallest grid cells (400 $m^2$) in the central part of the model grid. The pumping wells are located in the black grid cells.

### *5.1.3 PHT3D: PHREEQC-2 (the PHREEQC package)*

The PHREEQC-2 part of PHT3D carries out the multi-component geochemical transport calculations. First, it is stated in the PHREEQC-2 (PHR) package whether an iterative or sequential operator-splitting scheme is used. In this study, the flow and geochemical calculations are carried out sequentially, which implies that chemical equilibrium is calculated in each grid cell after every time step in which the flow has been calculated (see Section 5.1.4). The new equilibrium concentrations are transported in the next time step (Prommer, 2003).
Then, the database and the components, or species, for which reactive transport is simulated, are defined in the PHR package. The PHR package also imposes the reactive components determining the hydrogeochemical processes occurring in the aquifers. Furthermore, redox mode and groundwater temperature need to be specified in the PHR package. In this study, pH and pe are set to be variable and groundwater temperature is set to 10° centigrade. Finally, accuracy criteria with respect to both concentration and pH, determining whether PHREEQC-2 is activated or deactivated in a certain cell, are defined in the PHR package. PHREEQC-2 is active in all grid cells if one of the accuracy criteria (or both) is set to zero Prommer, 2003). In this modeling exercise, accuracy with respect to concentration is set to 1e-10 mol/l, whereas accuracy with respect to pH is set to 1e-4.

In this study, the default PHREEQC-2 database is used. Furthermore, this modeling exercise attempts to investigate reactive transport in the local hydrogeological setting of Holten for eight components: sodium (Na), potassium (K), calcium (Ca), magnesium (Mg), nitrate ($NO_3^-$), sulfate ($SO_4^{2-}$), chloride (Cl) and bicarbonate ($HCO_3^-$) (Table 5.1). However, in contrast to PHREEQC-2, in PHT3D all chemical species which are possibly formed need to be specified in the input. If species, while not specified beforehand, are formed in a grid cell during the geochemical calculations, PHT3D is not able to transport these species from one grid cell to another in the next time step, i.e. these species can not find their way back into the transport part. Therefore, according to the 'main' components, another eight components were defined in the PHR package: nitrite ($NO_2^-$), nitrogen gas ($N_2$), ammonium ($NH_4^+$), hydrogen sulfide ($HS^-$), methane ($CH_4$), oxygen ($O_2$) and iron ($Fe^{2+}$ and $Fe^{3+}$) (Table 5.1). Moreover, as bicarbonate is not defined as a solution master species in the default PHREEQC-2 database, carbonate ($CO_3^{2-}$) is specified instead of bicarbonate in the PHT3D input. Finally, two more components, bromide (Br) and lithium (Li), are defined in the PHR package. This will be explained in the next section.

As with the one-dimensional reactive transport model, the minerals calcite, pyrite, siderite and goethite form the reactive components in the model. Mineral dissolution, precipitation and oxidation are modeled in this study by imposing equilibrium phases. A second contrast with respect to PHREEQC-2 is that mineral Saturation Indices can not be directly defined in PHT3D.
Furthermore, in accordance with the one-dimensional model, cation exchange is imposed in the model and standard cation exchange coefficients from PHREEQC-2 are used. A third difference between PHREEQC-2 and PHT3D is that PHREEQC-2 imposes Cation Exchange Capacity and calculates the exchanger species and their concentrations, whereas in PHT3D exchanger species and their initial sorbed amounts need to be specified beforehand in the PHR package.

Table 5.1 Species, equilibrium phases and exchange species as defined in this model study. The amounts represent initial concentrations in the three aquifers. In the first aquifer, distinction is made between the different land use types.

| AQUIFER | 1 | | | | 2 | 3 |
|---|---|---|---|---|---|---|
| LAND USE | pasture | arable land | nature | municipal area | All | All |
| COMPONENT | | | | | | |
| Na | 4.654E-04 | 4.403E-04 | 3.076E-04 | 8.705E-04 | 2.445E-04 | 1.712E-04 |
| K | 5.852E-04 | 3.463E-04 | 8.376E-05 | 3.002E-04 | 5.683E-05 | 5.415E-05 |
| Ca | 6.592E-04 | 1.013E-03 | 2.104E-04 | 9.205E-04 | 1.389E-03 | 2.145E-03 |
| Mg | 2.196E-04 | 1.459E-04 | 8.872E-05 | 4.002E-04 | 1.586E-04 | 2.581E-04 |
| NO3- | 7.049E-04 | 1.347E-03 | 9.082E-04 | 1.901E-04 | 7.686E-05 | 0 |
| NO2- | 5.211E-16 | 1.255E-16 | 1.161E-15 | 5.711E-17 | 8.281E-15 | 0 |
| N2 | 5.494E-10 | 7.927E-15 | 7.233E-08 | 1.744E-13 | 4.201E-06 | 0 |
| NH4+ | 0 | 0 | 0 | 3.302E-06 | 0 | 0 |
| (SO4)2- | 3.087E-04 | 3.570E-04 | 3.592E-04 | 6.203E-04 | 3.644E-04 | 1.371E-04 |
| HS- | 0 | 0 | 0 | 0 | 0 | 5.625E-11 |
| Cl | 3.245E-04 | 3.245E-04 | 2.821E-04 | 8.705E-04 | 3.244E-04 | 3.175E-04 |
| (CO3)2- | 3.686E-03 | 1.399E-03 | 1.260E-03 | 2.385E-03 | 2.801E-03 | 4.616E-03 |
| CH4 | 0 | 0 | 0 | 0 | 0 | 1.316E-12 |
| Fe(2) | 8.259E-20 | 3.783E-21 | 5.144E-19 | 2.384E-20 | 1.315E-23 | 4.057E-07 |
| Fe(3) | 3.272E-13 | 1.158E-13 | 7.524E-13 | 2.130E-13 | 4.074E-15 | 5.344E-15 |
| O2 | 6.133E-07 | 3.860E-05 | 2.052E-07 | 3.709E-06 | 2.885E-11 | 0 |
| Li | 0 | 0 | 9.365E-04 | 0 | 3.551E-04 | 0 |
| Br | 9.660E-04 | 5.241E-04 | 0 | 1.317E-03 | 0 | 3.912E-04 |
| pH | 5.200 | 5.650 | 4.851 | 5.393 | 7.699 | 7.339 |
| Pe | 16.000 | 16.000 | 16.231 | 16.003 | 12.420 | -2.956 |
| Calcite | 0 | 0 | 0 | 0 | 1.542E-02 | 1.547E-01 |
| Pyrite | 0 | 0 | 0 | 0 | 0 | 7.735E-02 |
| Siderite | 0 | 0 | 0 | 0 | 0 | 0 |
| Goethite | 1.044E-01 | 1.044E-01 | 1.044E-01 | 1.044E-01 | 3.134E-02 | 1.106E-02 |
| CaX2 | 8.278E-04 | 9.424E-04 | 8.203E-04 | 7.769E-04 | 7.046E-04 | 1.750E-02 |
| MgX2 | 1.737E-04 | 8.549E-05 | 2.181E-04 | 2.131E-04 | 5.057E-05 | 1.318E-03 |
| FeX2 | 5.238E-20 | 1.780E-21 | 1.027E-18 | 1.021E-20 | 2.761E-24 | 1.301E-06 |
| NaX | 1.481E-05 | 1.207E-05 | 1.733E-05 | 2.291E-05 | 4.225E-06 | 5.880E-05 |
| KX | 1.023E-04 | 5.215E-05 | 2.591E-05 | 4.338E-05 | 5.401E-06 | 1.024E-04 |

### *5.1.4 The Basic Transport package*

In the Basic Transport (BTN) package an overview is given of the groundwater flow (MODFLOW) model (Section 5.1.1). Non-spatial parameters specifying inactive grid cells and defining output format are set in the BTN package as well. If the simulation is steady state, changes in the time discretization with respect to the MODFLOW model can be introduced in the BTN package. In this study, each stress period has a length of one year (365.25 days) and within each stress period three time steps have been defined. After every time step, PHREEQC-2 calculates the chemical equilibrium. The maximum number of transport steps allowed within one time step is set to 10000, whereas the transport step size is set to zero, implying that the model-calculated transport step size, based on the Courant number, is used in the simulation.

Furthermore, the BTN package defines several spatial parameters: cell type, top elevation, thickness, porosity, observation points and initial concentration. 'Cell type' specifies whether grid cells are variable (active) concentration cells, constant concentration cells or inactive concentration cells. Figure 5.2 shows the cell type distribution: active concentration cells are located in the central part of the model grid in order to focus the multi-component reactive transport model to the area near the pumping wells. The location of the active concentration cells corresponds to the area for which the recharge concentrations were calculated (Chapter 3). This area is depicted in Figure 3.1. The remaining cells are specified as inactive concentration cells. Moreover, in order to facilitate the model calculation at the transition from active to inactive cells, the cells corresponding to the boundary of the digital land use map were defined as constant concentration cells.
'Top elevation' defines the elevation of the top of all cells in the first layer relative to a reference elevation, whereas 'thickness' and 'porosity' define the thickness (Section 5.1.1) and porosity of all model layers respectively. Porosity is set to 0.35 in all model layers. 'Observation Points' indicates the grid cells for which output data, in this study concentration-time series, are saved. The grid cells in which the pumping wells are located are specified as observation points.
'Initial concentrations' sets the initial concentration for each component and each layer. In this study 29 components have been defined (Table 5.1). In the first aquifer (layer 1-7) initial concentrations have been specified per land use type according to the land use map (Figure 3.1). No distinction in initial concentrations between land use types is made in the second (layer 8-12) and third (layer 13-14) aquifer, as it is assumed that in the year 1950, when the model simulation starts, effects of different land use types are not noticeable at these depths (about 14 meters below ground level and deeper). Within an aquifer unit, no distinction in initial concentration between model layers is made.
Section 4.4 describes how the initial concentrations of sodium, potassium, calcium, magnesium, nitrate, sulfate, chloride and bicarbonate in the aquifers and beneath the different land use types have been determined. The initial concentrations of nitrite, nitrogen gas, ammonium, hydrogen sulfide, methane, oxygen, iron and carbonate were determined in the same model run as described in Section 4.4 (Table 5.1) as PHREEQC-2 calculates the concentration of all solution species during a simulation.
Initial contents of the minerals in the three aquifers are based on measurements by Griffioen et al. (2003) and Maas (2002) (Chapter 2). However, as the one-dimensional model showed that imposing an initial siderite content in the aquifers resulted in excessive and unrealistic siderite oxidation (Chapter 4), initial siderite contents are set to zero in the three-dimensional model, implying that the mineral may only be formed (Table 5.1). Furthermore, exchange species and their initial contents in the three aquifers are based on a speciation calculation in PHREEQC-2 in which the Cation Exchange Capacities (Chapter 2) and initial aquifer compositions (solutes and minerals, Table 4.1) were specified. The simulations determined that in these aquifer settings the exchange species are $CaX_2$, $MgX_2$, NaX, KX and $FeX_2$.

It was already mentioned in the previous section that bromide and lithium are defined in the PHR package. These two species are added in order to meet the condition of electrical charge balance. Total positive and negative electrical charge need to be equal since electrical charge imbalances are neutralized by means of pH changes in PHT3D (Prommer et al., 2003). Starting the model run with electrically balanced aquifer compositions is therefore necessary. (In Section 5.1.6, it is explained that recharge compositions, forming the input of the model, need to be electrically balanced as well.)

Moreover, PHT3D is not able to cope with large electrical imbalances: if the imbalances are too large, the model simulation will crash due to converging errors.
As bromide and lithium both are modeled as conservative species and therefore do not influence the reactive transport simulations, these species are selected to neutralize electrical imbalances in the initial aquifer compositions. After determining the initial aquifer compositions without Br and Li, total positive or negative electrical charge was calculated for each aquifer and land use type. A surplus of positive electrical charge was counterbalanced by the negatively charged bromide ion ($Br^-$), whereas a surplus of negative electrical charge was counterbalanced by the positively charged lithium ion ($Li^+$).

Finally, in the BTN package, three more packages can be activated: the Advection (ADV) package, the Dispersion (DISP) package and the Sink and Source Mixing (SSM) package. In this study, the ADV package and the SSM package are activated, whereas the DISP package is left out of consideration. The next sections describe the ADV and SSM package.

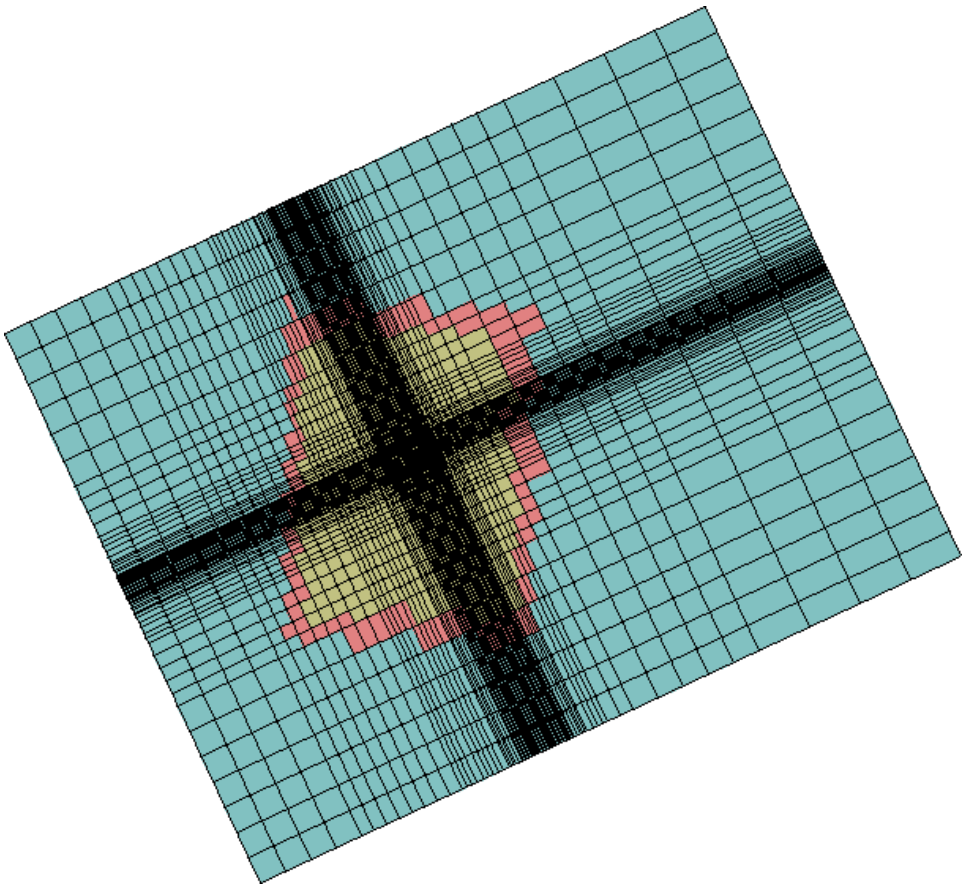

Figure 5.2 - Cell type distribution: brown cells are defined as variable concentration cells, red cells are constant concentration cells and blue cells are defined as inactive concentration cells.

### *5.1.5 The Advection package*

The Advection (ADV) package defines which solution scheme is used to calculate the advective transport of solutes: Method Of Characteristics (MOC), Modified Method Of

Characteristics (MMOD), Hybrid Method Of Characteristics (HMOC), the Upstream Finite Difference Scheme or the ULTIMATE scheme (third-order Total-Variation-Diminishing (TVD) method). In this study, the ULTIMATE scheme is used, in which the upstream weighing scheme is defined and the Courant number is set to 0.75.

### *5.1.6 The Sink and Source Mixing package*

In the Sink and Source Mixing (SSM) package, concentrations are assigned to the sink and source packages of the groundwater flow model: the well package, the drain package, the river package, the constant head package and the recharge package. In this modeling exercise, recharge concentrations are defined for each component, each land use type and each stress period. The well package, drain package, river package and constant head package are not specified in this study.
Chapter 3 describes how the recharge concentrations for sodium, potassium, calcium, magnesium, nitrate, sulfate, chloride and bicarbonate have been determined. However, as is the case with initial aquifer concentrations, concentrations of all chemical species which may be present in the recharge water need to be specified in PHT3D. Moreover, recharge concentrations need to be charge balanced. Therefore, recharge concentrations of nitrite, nitrogen gas, ammonium, hydrogen sulfide, methane, oxygen, iron, carbonate, lithium and bromide were determined as well. Again, a PHREEQC model was constructed in which for each year (or stress period) and for each land use type the concentrations of sodium, potassium, calcium, magnesium, nitrate, sulfate, chloride and bicarbonate and pH and pe were loaded. PHREEQC then carried out speciation calculations for the loaded water compositions. The output consists, for each land use type and each stress period, of eighteen components, as the concentrations of nitrite, nitrogen gas, ammonium, hydrogen sulfide, methane, oxygen, iron ($Fe^{2+}$ and $Fe^{3+}$) and carbonate were calculated, whereas concentrations of sodium, potassium, calcium, magnesium, nitrate, sulfate, chloride and pH and pe slightly changed (in the order of tens of micromoles and hundredths of pH/pe units). The calculations for the land use types pasture, arable land and nature show that the recharge concentrations are (nearly) zero for nitrite, nitrogen gas, ammonium, hydrogen sulfide, methane and iron. In the urban areas, the recharge water contains small amounts of ammonium and iron(II), whereas the nitrite, nitrogen gas, hydrogen sulphide, methane and iron(III) concentrations in the recharge water are zero. Bromide and lithium concentrations were subsequently determined by means of the surplus of positive or negative electrical charge respectively.
Furthermore, recharge concentrations of calcite, pyrite, siderite and goethite, as well as recharge concentrations of the exchange species, $CaX_2$, $MgX_2$, NaX, KX and $FeX_2$, were set to zero for each stress period and each land use type as the recharge water is supposed to represent water, which has not yet been in contact with the aquifer material. Consequently, recharge concentration series, i.e., for four land use types and 56 years, were defined for 29 components. As mentioned already, recharge data were loaded during the definition of the scenario. However, first the recharge concentration series were converted to a format compatible for PHT3D, i.e., a format in which recharge concentrations are, for each component and each stress period, arranged in a grid cell configuration. This format incorporates the four land use types within one file. Therefore, after the conversion, the recharge concentration is defined in 29 (for each component) times 56 (for each stress period) files. These recharge concentration files were then loaded into the PHT3D scenario.

## 5.2 Validation and representation of the model results

In contrast to the one-dimensional model simulations, the three-dimensional model simulations can be compared to field measurements. As the MODFLOW model properly represents the hydrogeology in the area around Holten (Griffioen et al., 2003), it is assumed that simulated concentrations at a certain site and time can be directly compared to observed concentrations at the corresponding site and time. After every stress period, simulated concentrations were saved in cells corresponding to the pumping wells and defined as observation points (Section 5.1.4). The model output thus comprises a concentration time series (1950-2005) for every solute in each pumping well.

However, the following complication should be taken into consideration when simulated concentrations are compared to observed concentrations. In the field, the pumping wells extract groundwater from different depths since the wells comprise more than one filter and each filter has a length of several meters. Consequently, groundwater with different ages and compositions is mixed. In the model, each pumping well also comprises two or three model layers as a result of the model discretisation. In comparing simulated to observed concentrations and linking the groundwater quality to the load at surface level, it should thus be kept in mind that 'averaged' data rather than point data are considered.
Furthermore, as the pumping wells are located only in the second and third aquifer, field data from the first aquifer are lacking. Therefore, simulation results of the first aquifer can not be compared to field measurements.

In Figures 5.3 – 5.9, simulated concentrations of several components are plotted against time. The modeled nitrate, sulfate and chloride concentrations are depicted both as an average value of all pumping wells and for each well separately. Furthermore, on the base of their importance in the model, their chemical characteristics and their 'expected' behavior, calcium, potassium, iron(II) and pH were selected for analysis in this section, whereas sodium and magnesium are left out of consideration. The calcium and potassium concentrations are analyzed per cluster of individual wells in the second aquifer, whereas the iron (II) concentration and the pH evolution are considered per individual well in the third aquifer.
In averaging the concentrations of all pumping wells by weight, the fractions per layer of the total extraction of an individual well are taken into account, since the wells withdraw groundwater from several layers. Furthermore, amounts of groundwater extracted per individual well and their changes in time are taken into account in calculating the average concentration. Finally, the fraction per well of the total extraction, i.e., from all wells, is considered in averaging the concentrations. The averaged model results are compared to field observations which have been averaged by weight as well. Moreover, recharge concentrations which were averaged by weight for the four land use types, based on their surface area, are depicted for reference.
Due to the fact that the pumping wells start to extract groundwater in 1955 (Vitens) and therefore no groundwater extraction occurs from 1950 until 1955, all simulated well concentrations are zero in the period 1950-1955. This period is therefore left out of consideration in the analyses of the averaged simulation results in the next sections.
The calculation of groundwater quality per individual well takes into account the fraction per layer of the total well discharge. The simulated groundwater quality per individual well is compared to the measured groundwater quality of the well in

question. The wells are arranged in four clusters according to the area from where the groundwater is extracted. The wells in Cluster 1 extract groundwater beneath nature area in the north, whereas the wells in Cluster 2 withdraw groundwater from agricultural areas in the south. Cluster 3 represents wells extracting their groundwater from both nature and agricultural areas (mixed). All wells in Clusters 1, 2 and 3 started to extract groundwater during the 1960s and early 1970s and pump groundwater from the second aquifer. The wells in Cluster 4 were brought into use in 1985 and extract groundwater from the third aquifer. These wells do not withdraw groundwater from a specific area.

## 5.3 Simulation results of the reactive transport model PHT3D

### *5.3.1 Nitrate*

As can be seen, the simulated nitrate concentration, averaged for all wells, starts to rise around 1960, in accordance with the increasing load at surface level (Figure 5.3a, Chapter 3). The response of the nitrate concentration in the groundwater to the increasing load at surface level is thus considerably fast. However, although the nitrate concentrations in the recharge water decrease around 1985, the concentrations in the groundwater keep rising towards a value of 0.4 mmol/l until approximately 2000. This implies that the maximum nitrate load at surface level, which is approximately 4 mmol/l, arrives at least 15 years later in the pumping wells. Furthermore, the simulations show that nitrate concentrations in the groundwater have decreased with respect to the concentrations in the recharge water.
The observations averaged for all wells show a rise in nitrate concentrations around 1960 as well, although it is difficult to accurately determine when the observed concentrations start to rise, as no data from 1950 to 1960 are available. Furthermore, it can be seen in Figure 5.3a that the observed nitrate concentrations agree well with the modeled concentrations.
However, it should be mentioned that for nitrate a correction factor of 4.43 has been applied to the model results. This correction factor takes into account a miscalculation of the nitrate load at surface level, which caused the load to be too large (in Figure 5.3a, the correction factor has been applied to the load at surface level as well). Nevertheless, despite the overestimation, the modeled mass balance for all solutes including nitrate is correct, implying that the total input of each component is equal to the total output and that the model simulation is confident.
The concentrations simulated by RT3D (Chapter 1) have been depicted as well in Figure 5.3. As can be seen, Griffioen et al. (2003) simulated several scenarios with different initial concentrations for a period of 80 years (1950-2030). The red data points in the lower plot in Figure 5.3b represent the field measurements and are equal to the red data points in Figure 5.3a.
Comparing the PHT3D results to the RT3D results shows that the (corrected) nitrate concentrations simulated in PHT3D better agree with the observations than the nitrate concentrations simulated in RT3D. This is due to the incorporation of the several geochemical processes in PHT3D. Moreover, the differences between the models can be explained by the fact that in RT3D, the stress periods have a length of 10 years (the simulated time period is from 1950 until 2030), whereas in PHT3D, the stress periods

have a length of 1 year. However, although smaller, differences between the PHT3D simulations and the observations still exist, particularly in the period from 1976 to 1988.

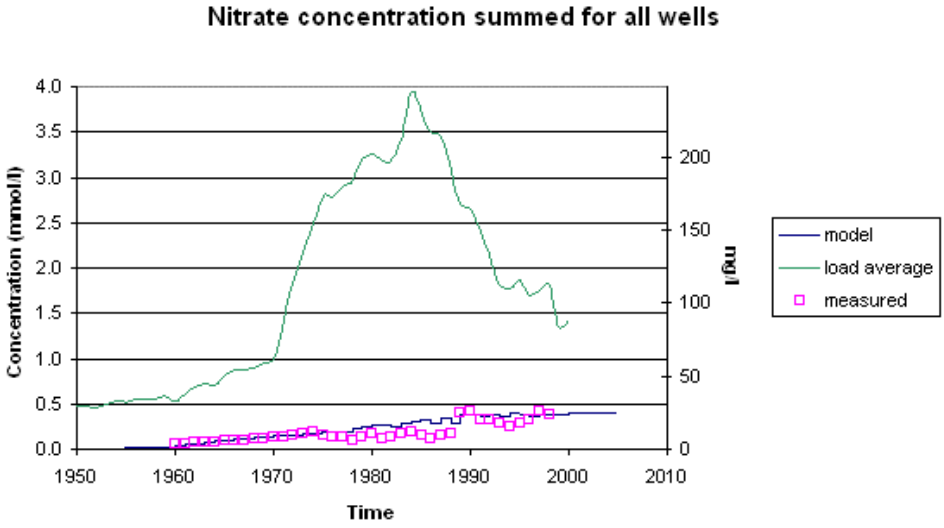


a

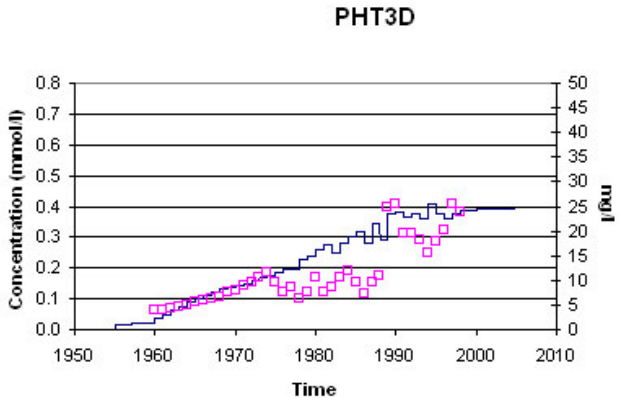


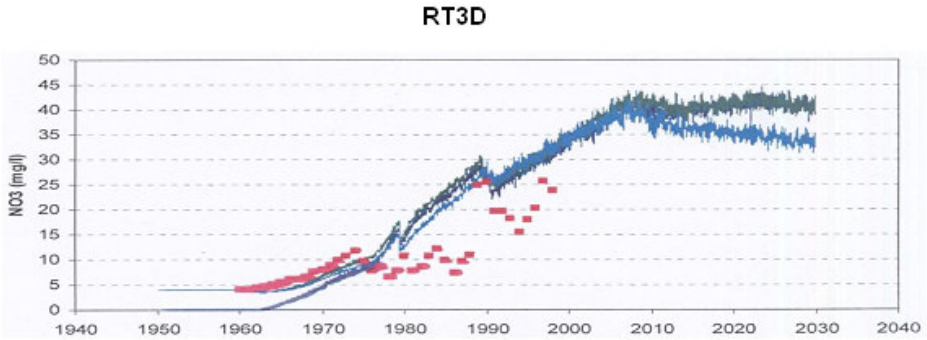


b

Figure 5.3a - Simulated and observed nitrate concentrations averaged for all wells. The load at surface level averaged for all land use types has been depicted for reference. b PHT3D results (scaled) compared to RT3D results. Coloured lines in RT3D plot represent several scenarios, red data points represent field measurements. In PHT3D plots field measurements are represented by open data points in order to properly display model results.

The PHT3D model results for the wells in Cluster 1 (nature) show a more gradual increase in nitrate concentrations (Figure 5.3c). Moreover, maximum concentrations in Cluster 1 are around 0.7 mmol/l, i.e., higher than the maximum concentration for all wells averaged (Figure 5.3a), whereas it is not clear from the model results whether the maximum nitrate load at surface level has already arrived in wells 72-22 and 71-20. The fact that the simulated nitrate concentrations are higher in the wells beneath nature than in all wells averaged will be explained further on, when the simulated concentrations in the wells in Cluster 4 are considered. The simulated nitrate concentrations in Cluster 1 agree relatively well with the observed concentrations in this Cluster 1 and are considerably better than the RT3D results for Cluster 1 (Figure 5.3c).

Nitrate concentrations in the wells which extract groundwater from beneath agricultural lands (Cluster 2) are in average higher than in Cluster 1. In particular well 61-08, in which modeled nitrate concentrations amount to approximately 2.25 mmol/l, shows a relatively high nitrate concentration (Figure 5.3d). Obviously, with respect to the difference between Cluster 1 and 2, the different land use functions are distinctly reflected in the nitrate concentrations in the groundwater.

Nitrate concentration in wells 61-08, 59-05 and 71-21 increases less smoothly than the nitrate concentration in the wells in Cluster 1, whereas the concentration in wells 61-07 and 72-27 does not distinctly rise after approximately 1990. All wells, except well 61-08, show a relatively good agreement between simulated and observed concentrations. In the period 1950-1980, the RT3D results for wells 59-05, 61-07, 71-21 and 72-27 in Cluster 2 show approximately equal nitrate concentrations as the PHT3D results. However, from 1980, the PHT3D simulations better agree with the field measurements than do the RT3D simulations. The RT3D simulations show a larger difference with respect to the field measurements, particularly in wells 61-07 and 72-27. For well 61-08, the simulated concentrations are considerably higher than the field measurements in both the PHT3D and RT3D model. However, the concentrations in well 61-08 simulated by RT3D are in general lower than the concentrations simulated by PHT3D and therefore agree relatively better to the field measurements.

Furthermore, modeled nitrate concentrations for the wells in Cluster 3, extracting groundwater from both nature and agricultural areas, are relatively low compared to Cluster 1 and 2 and the field measurements (Figure 5.3e). The nitrate concentrations simulated by RT3D better agree with the observations than the nitrate concentrations simulated by PHT3D.

The deep wells (Cluster 4) show that hardly any nitrate reaches the wells in the third aquifer: modeled concentrations are smaller than one µmol/l (Figure 5.3f). This is due to the presence of pyrite in the third aquifer. The fact that nitrate concentrations are nearly zero in the third aquifer explains the, with respect to Cluster 1, relatively low concentrations if all wells are averaged (Figure 5.3a).

Although a few orders of magnitude larger, the observations agree with the model results, as most of the observed nitrate concentrations fluctuate around the detection limit, which varies between 0 and 8 µmol/l. The nitrate concentrations simulated by RT3D are until approximately 2000 rather low as well and in the same order of magnitude as the nitrate concentrations simulated by PHT3D. However, from 2000 until 2005, the concentrations in the RT3D model are higher than the concentrations in the PHT3D model in all wells except well 77-32. With respect to this period therefore, the PHT3D model results are better than the RT3D model results. Furthermore, as the PHT3D model simulated the hydrogeochemistry only until 2005, the further increase in nitrate concentrations simulated by RT3D can not be ‘checked’.

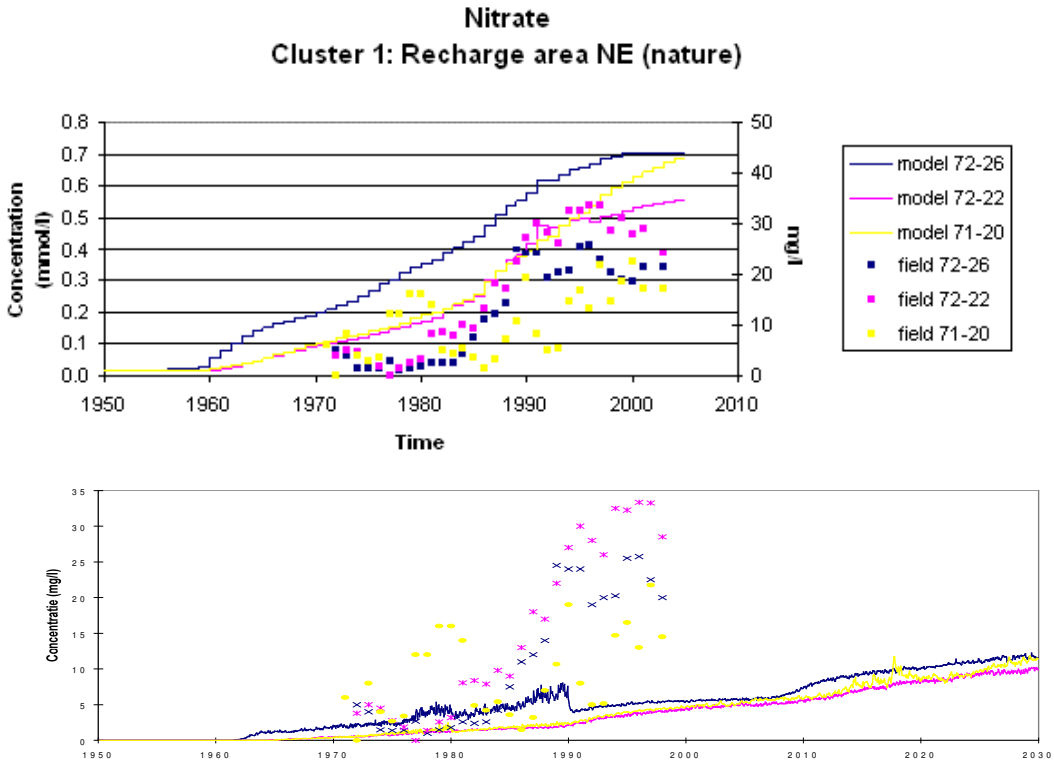


Figure 5.3c - Simulated and observed nitrate concentrations for the wells in Cluster 1. The upper plot represents the PHT3D simulation results, the lower plot represents the RT3D simulation results. The colours representing the different wells are equal in both plots, in the RT3D plot the several symbol represents the field measurements.

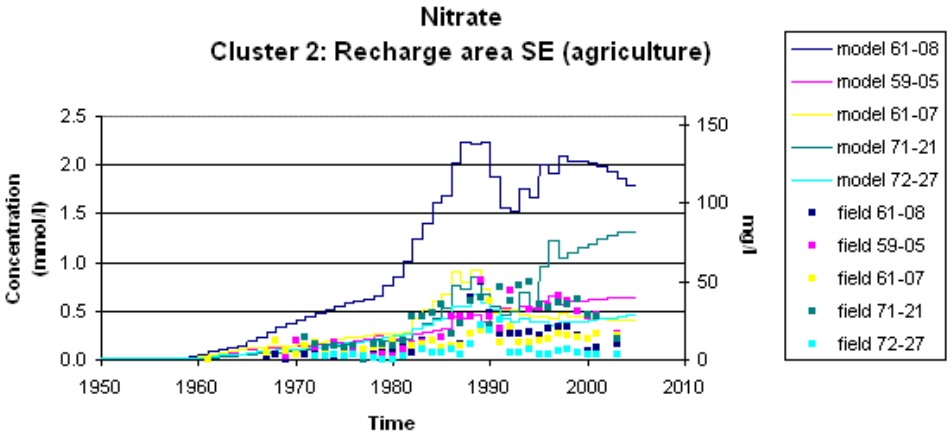


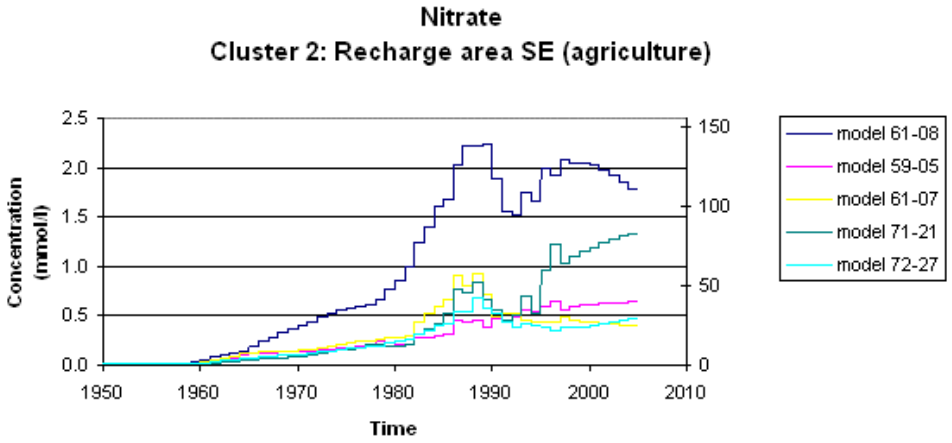


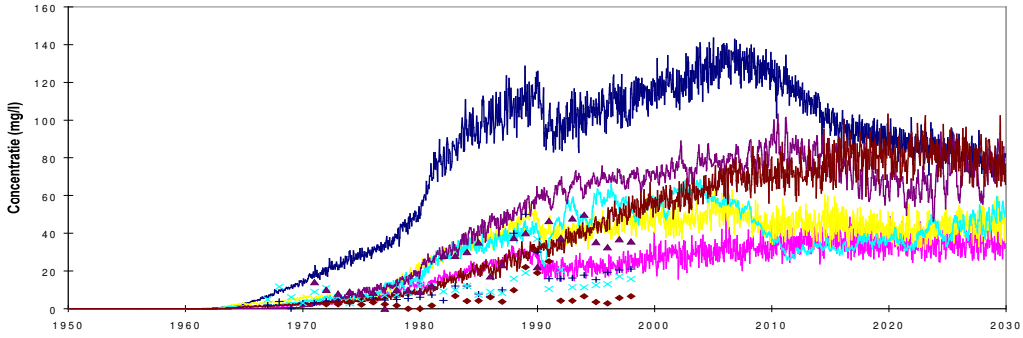


Figure 5.3d - Idem Figure 5.3 c for the wells in Cluster 2. In order to properly represent the model results, the observations have been left out in the middle plot.

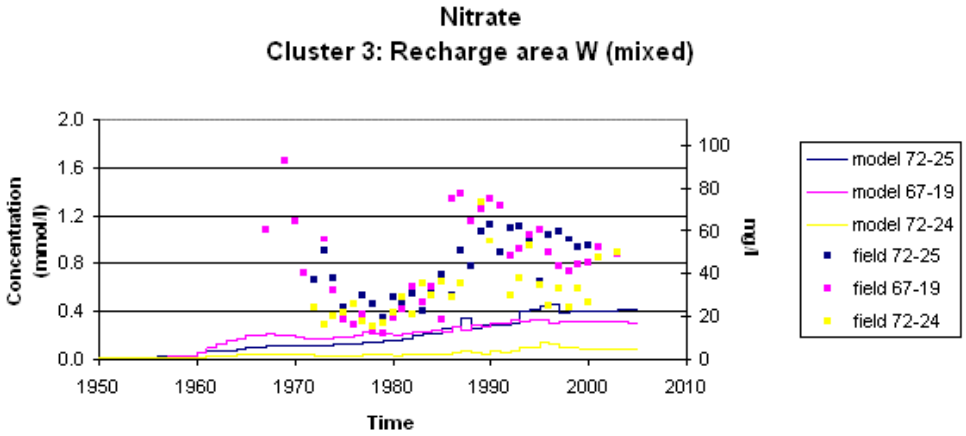


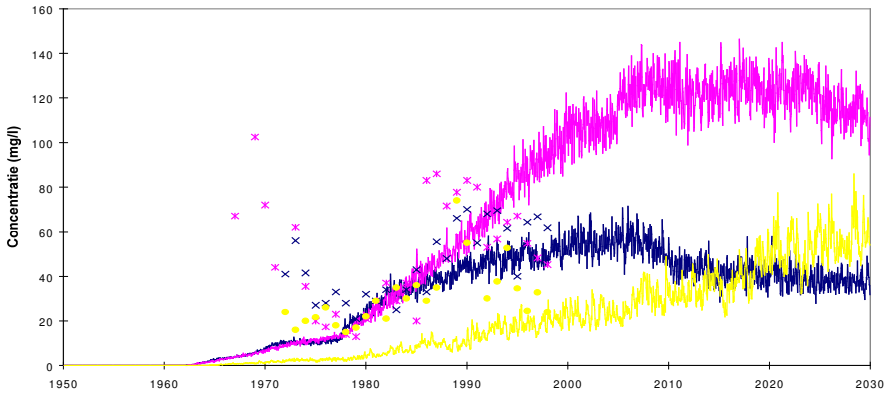


e

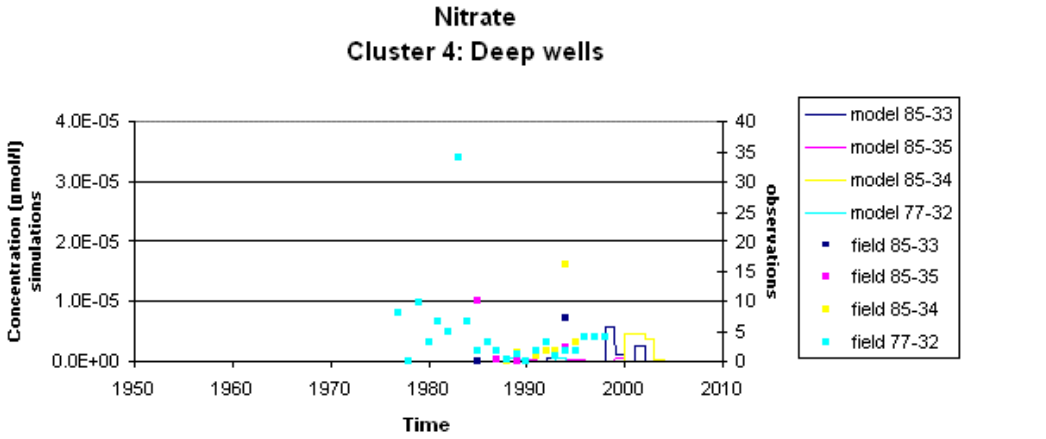


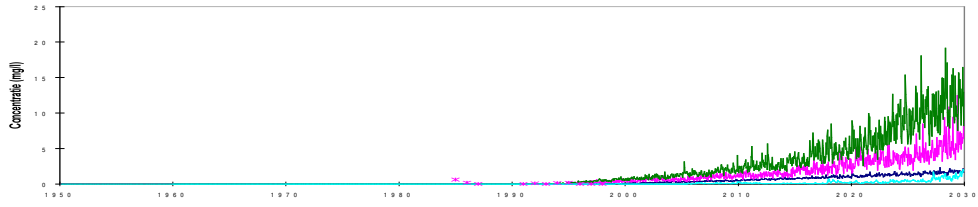


f

Figure 5.3e - Idem Figure 5.3 c for the wells in Cluster 3. f Idem Figure 5.3 c for the wells in Cluster 4. Mind that concentrations are in µmol/l on both the left and right y-axis in the PHT3D plot, whereas concentrations are in mg/l in the RT3D plot. For reference: 10 µmol/l is equal to 0.62 mg/l. In RT3D plot, well 85-33, 85-35, 85-34 and 77-32 are represented by a dark blue, red, green and light blue line, respectively. The x-symbol represents field measurements in well 85-35

Figure 5.3g shows a vertical cross section through the model, in which the nitrate concentration is depicted for several time steps. The upper cross section shows the nitrate concentration in 1953, slightly after the beginning of the simulation, the next cross sections show the nitrate concentration after 15, 29 and 43 years, i.e., in 1965, 1979 and 1993, respectively, and the lower cross section shows the nitrate concentration at the end of the simulation (2005). The concentration is displayed as a colour range between red (high concentration) and yellow (low (or zero) concentration). The green rectangles represent the pumping wells.

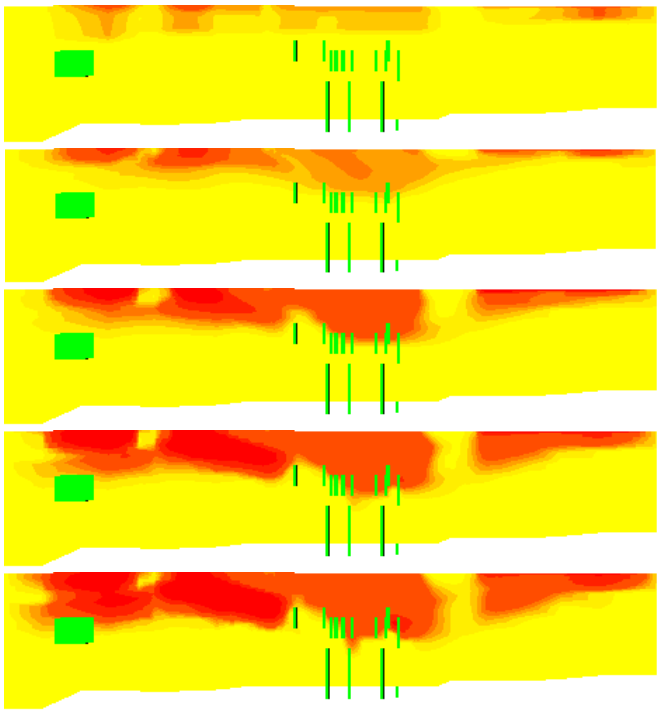

Figure 5.3g - Vertical cross section through the model showing the nitrate concentration in 1953, 1965, 1979, 1993 and at the end of the simulation (2005). Red and yellow represent high and low (or zero) concentrations, respectively. The green rectangles are the pumping wells.

As can be seen, in the upper part of the cross section (in the first and second aquifer), the nitrate concentrations increase during time as a result of the higher load at surface level. Nitrate is transported through the first and second aquifer towards the pumping wells. The concentrations in the lower part of the cross section (in the third aquifer) are zero at all time steps, as all nitrate entering the third aquifer is reduced by pyrite oxidation.

### *5.3.2 Nitrogen gas*

The initial concentrations and the model results for nitrogen gas in the third aquifer (Cluster 4; Table 5.1; Figure 5.4) indicate that nitrate is reduced, thereby forming nitrogen gas: initially there was no nitrogen gas present, whereas it starts to form around 1985. In this model setting, no processes besides nitrate reduction are able to produce nitrogen gas. Obviously, the travel time of nitrate from the groundwater level to the wells in the third aquifer is approximately 35 years in the model.

By comparing the nitrogen gas and sulfate (Figure 5.4; see also next section) model results it becomes clear that the nitrate reduction occurs by pyrite oxidation, thereby producing sulfate according to equation (1) in Chapter 2. As the nitrate concentrations in the deep wells are (nearly) zero, it may be stated that, according to equation (6), all nitrate entering the third aquifer is being reduced. Obviously, pyrite acts as a strong electron acceptor in the model.

$$NO_3 \text{ reduction} = ((N_2 - N_{2(initial)})*2) / (NO_3 + (N_2 - N_{2(initial)})*2) \approx 100\ \% \qquad (6)$$

However, it can also be seen in Figure 5.4 that the increase in sulfate is not only due to pyrite oxidation: the expected production of nitrogen gas based on the production of sulfate (equation (7), see equation (1)) is higher than the actual production of nitrogen gas according to Figure 5.4 (Table 5.2). This implies that the sulfate concentration in the third aquifer increases as a result of the load at surface level as well.

$$N_2 = 0.7 * (SO_4 - SO_{4(initial)}) \qquad (7)$$

Table 5.2 Nitrogen gas production based on sulfate production versus actual nitrogen gas production in the model.

| Well | $N_2$ based on $SO_4$ (eq(7)) (mmol/l) | $N_2$ in Figure 5.4 (mmol/l) |
|---|---|---|
| 85-33 | 0.068 | 0.052 |
| 85-35 | 0.037 | 0.011 |
| 85-34 | 0.085 | 0.062 |
| 77-32 | 0.022 | 0.004 |

Nevertheless, it should be kept in mind that the miscalculation in the nitrate load has also affected the production of sulfate by pyrite oxidation (equation (1)), i.e., the sulfate production is overestimated. This is not taken into account in the correction factor for sulfate.

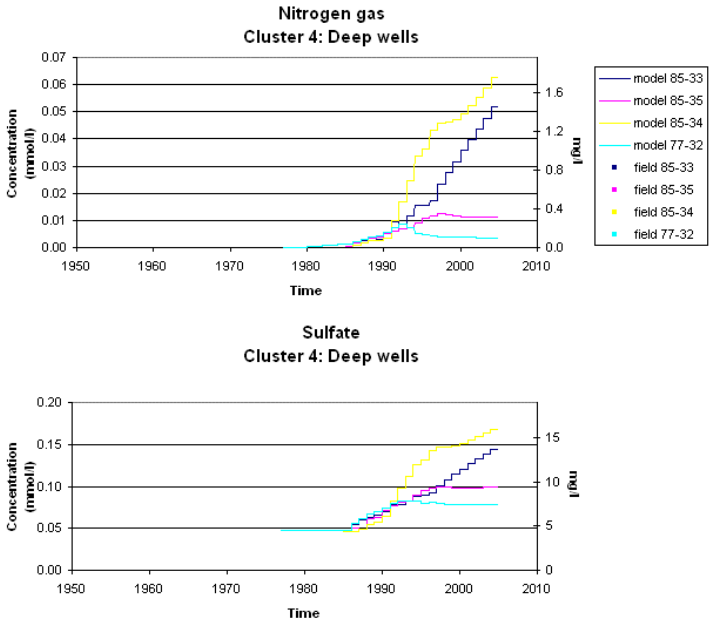


Figure 5.4 - Simulated and observed nitrogen gas and sulfate concentrations in the wells in Cluster 4.

The simulated nitrogen gas concentrations in the second aquifer are (nearly) zero, which indicates that nitrate reduction does not occur in this aquifer. This explains the fact that the model results show that nitrate is still available in the second aquifer. In the model therefore, the decrease in the nitrate concentration in the groundwater with respect to the nitrate concentration in the recharge water is due to a physical process, i.e., hydrodynamic dispersion, rather than to chemical processes.

### *5.3.3 Sulfate*

The simulated sulfate concentrations are depicted in Figure 5.5. As is the case with nitrate, a correction factor of 2.99 has been applied to the simulated concentrations in order to take into account a miscalculation in the sulfate load at surface level (the correction factor has been applied to the load at surface level as well in Figure 5.5a). Furthermore, as it was already mentioned, the miscalculation of the nitrate load has affected the simulated sulfate concentrations as well. The model results averaged for all wells show that the sulfate concentration gradually increases from 0.12 mmol/l in the early 1960s to a value of approximately 0.18 mmol/l at the end of the 1970s (Figure 5.5a). Subsequently, the sulfate concentration decreases to a value of 0.15 mmol/l and from approximately 1990 it slightly increases again to 0.16 mmol/l. These subtle ‘trends’ in the groundwater, i.e., two ‘peaks’ of which the second is slightly lower than the first, were observed in the recharge concentration as well (Figure 5.5a; Chapter 3). It was mentioned in Chapter 3 that the first peak in the recharge water is due to atmospheric deposition, and the second peak is due to the use of manure. However, the sulfate concentrations in the groundwater have considerably decreased with respect to the sulfate concentrations in the recharge water and the peaks in the recharge water have become rather smooth in the groundwater. As was the case with the nitrate concentrations, the peaks in the sulfate load at surface level arrive approximately 15 years later in the pumping wells.

The observed sulfate concentrations averaged for all wells are slightly higher than the simulated sulfate concentrations in the period from 1960 to 1985 (Figure 5.5a). Moreover, the observations also show a gradual increase from 1960, where the data series starts, until approximately 1975. From 1985, the differences between simulated and observed concentrations become larger. The ‘peaks’ in the sulfate concentrations as they were simulated can not be discerned in the observations.

With respect to the RT3D model results, the observed sulfate concentrations are slightly lower in the period from 1965 to 1985 (Figure 5.5b). After 1985, the simulated sulfate concentrations agree relatively well with the field measurements. In general thus, the RT3D model results are better than the PHT3D model results if the concentrations in all wells are averaged.

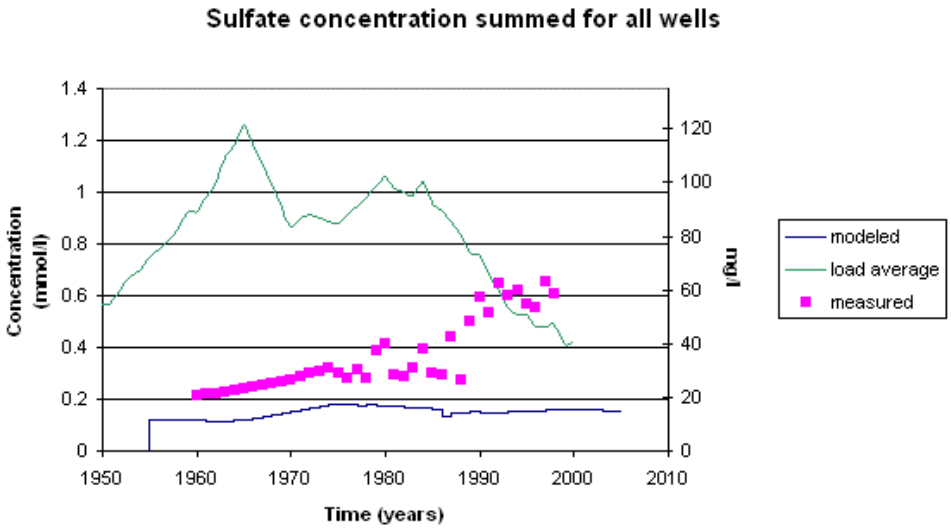


a

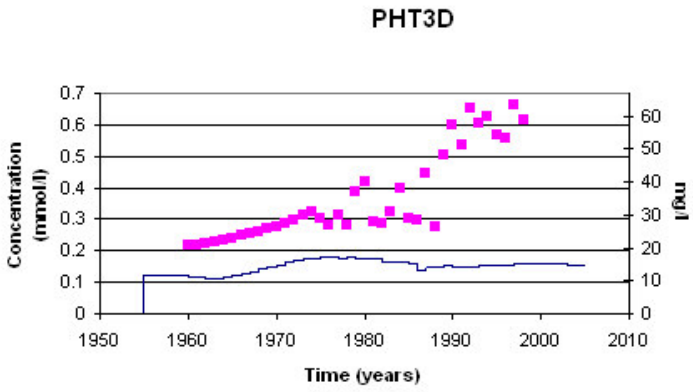


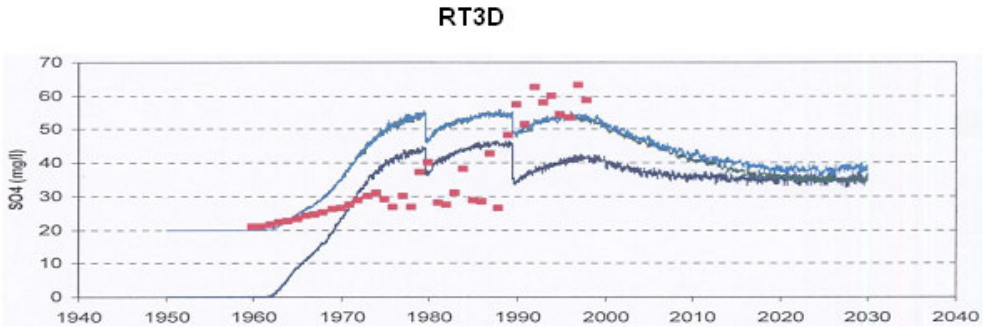


b

Figure 5.5a - Simulated and observed sulfate concentrations averaged for all wells. The load at surface level averaged for all land use types has been depicted for reference. b PHT3D results (scaled) compared to RT3D results. Blue line in RT3D plot represents the simulated concentration red data points represent field measurements.

The model results for well 72-26 in Cluster 1 (nature) show approximately the same pattern as the model results averaged for all wells (Figure 5.5c). The ‘peaks’ as they were described before, are also visible in the modeled concentration in well 72-26. However, the ‘peaks’ are not visible in the model results for wells 72-22 and 71-20:

although the sulfate concentrations show a slight bend between approximately 1980 and 1985, they keep rising until the early 1990s.
The observed sulfate concentrations in the wells in Cluster 1 agree relatively well with the modeled sulfate concentrations. Furthermore, in contrast to the simulations for all wells averaged, the PHT3D model results better agree with the observations than do the RT3D model results (Figure 5.5c).
The simulated concentrations in all wells, except 71-21, in Cluster 2 show the subtle 'peaks' as well (Figure 5.5d). The concentration in well 71-21 shows the same pattern as the concentration in wells 72-22 and 71-20 in Cluster 1: although a slight bend is visible between 1980 and 1985, the concentration keeps rising until the end of the simulation.
Cluster 2 furthermore shows that, despite the fact that these wells extract water from beneath agricultural lands, the simulated sulfate concentrations in well 61-08 are only slightly higher, whereas the other wells in Cluster 2 have comparable simulated sulfate concentrations with respect to those in Cluster 1 (nature). Although it is expected that the wells in Cluster 2 show higher simulated sulfate concentrations than those in Cluster 1, they show in general thus a relatively low concentration. As appears from the above, the relatively high sulfate load at surface level in the agricultural areas does not right away result in relatively higher sulfate concentrations in the groundwater in the model, or, the land use functions nature and agriculture are not distinctly reflected in the sulfate concentrations in the groundwater. Nevertheless, it should be mentioned that the differences in load at surface level between agricultural areas and nature are smaller for sulfate than for nitrate (Figure 3.2).
In contrast to the simulated sulfate concentrations, the observed sulfate concentrations in the wells in Cluster 2 are considerably higher than the observed concentrations in the wells in Cluster 1 and considerable differences exist between observed and simulated concentrations in Cluster 2. Furthermore, although in general relatively low as well with respect to Cluster 1, the concentrations simulated by RT3D better agree to the observations in the wells in Cluster 2.
Furthermore, the simulated concentrations in well 67-19 in Cluster 3 represent, although rather subtly, the peaks in the recharge concentration, whereas the simulated concentrations in wells 72-25 and 72-24 keep rising until approximately 1995 (Figure 5.5e). However, in contrast to the concentration for all wells averaged, the peaks in the sulfate load at surface level arrive only 10 years later in the groundwater in well 67-19. This is explained by the fact that well 67-19 is situated in the second aquifer, whereas in averaging all wells, also wells in the third aquifer, to which travel times are longer, are taken into account.
As is the case with the wells in Cluster 2, the modeled sulfate concentrations in the wells in Cluster 3 are relatively low compared to the observed concentrations in these wells, whereas the concentrations simulated by RT3D show a better agreement with the observations (Figure 5.5e).
As it was already mentioned in relation to the nitrate reduction in the third aquifer, modeled sulfate concentrations in the deep wells (Cluster 4) start to increase around 1985 (Figure 5.5f). Concentrations in wells 85-33 and 85-34 keep rising until the end of the simulation, whereas the concentrations in wells 85-35 and 77-32 are constant from the late 1990s until 2005. A good agreement exists between the simulated and observed concentrations with respect to the time at which they start to rise. However, the simulations show considerably lower concentrations than the observed concentrations. The concentrations simulated by RT3D start to rise only in 1995, whereas with respect to the observations the simulations are considerably low as well.

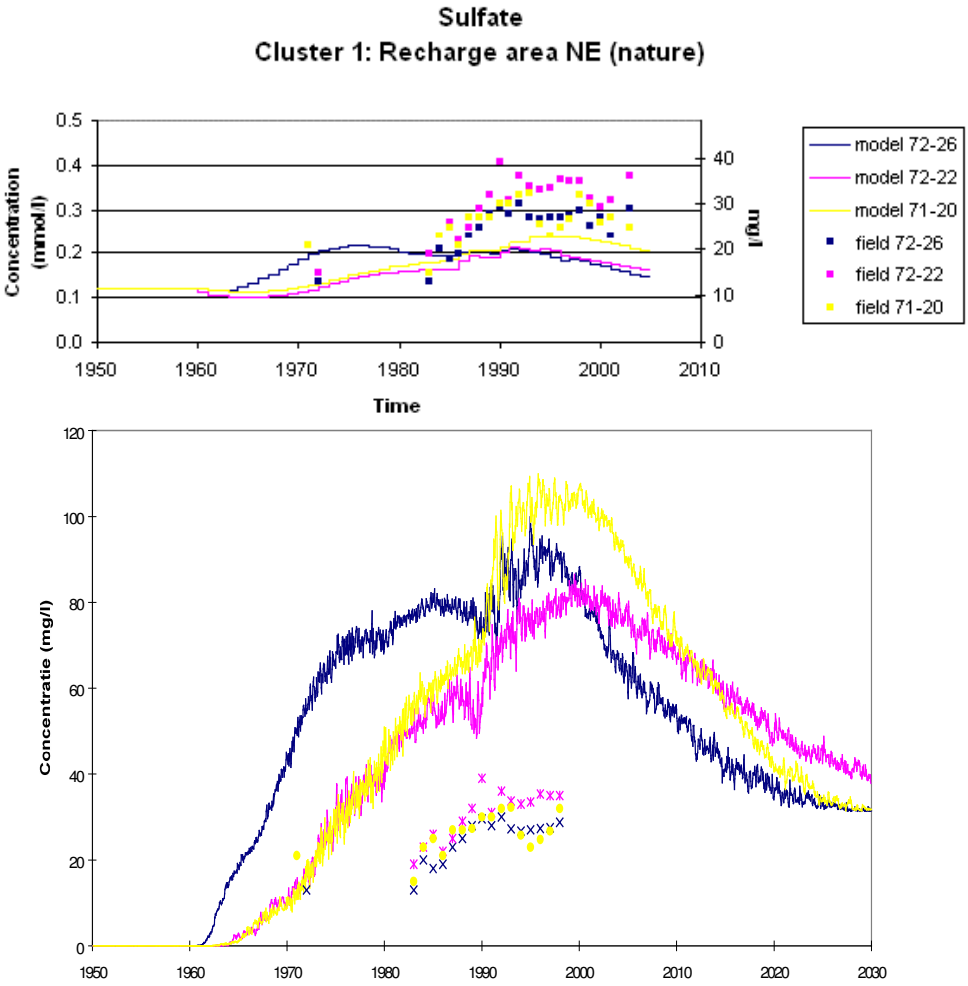


Figure 5.5c - Simulated and observed sulfate concentrations for the wells in Cluster 1. The upper plot represents the PHT3D simulation results, the lower plot represents the RT3D simulation results. The colours representing the different wells are equal in both plots, in the RT3D plot the several symbols represent the field measurements.

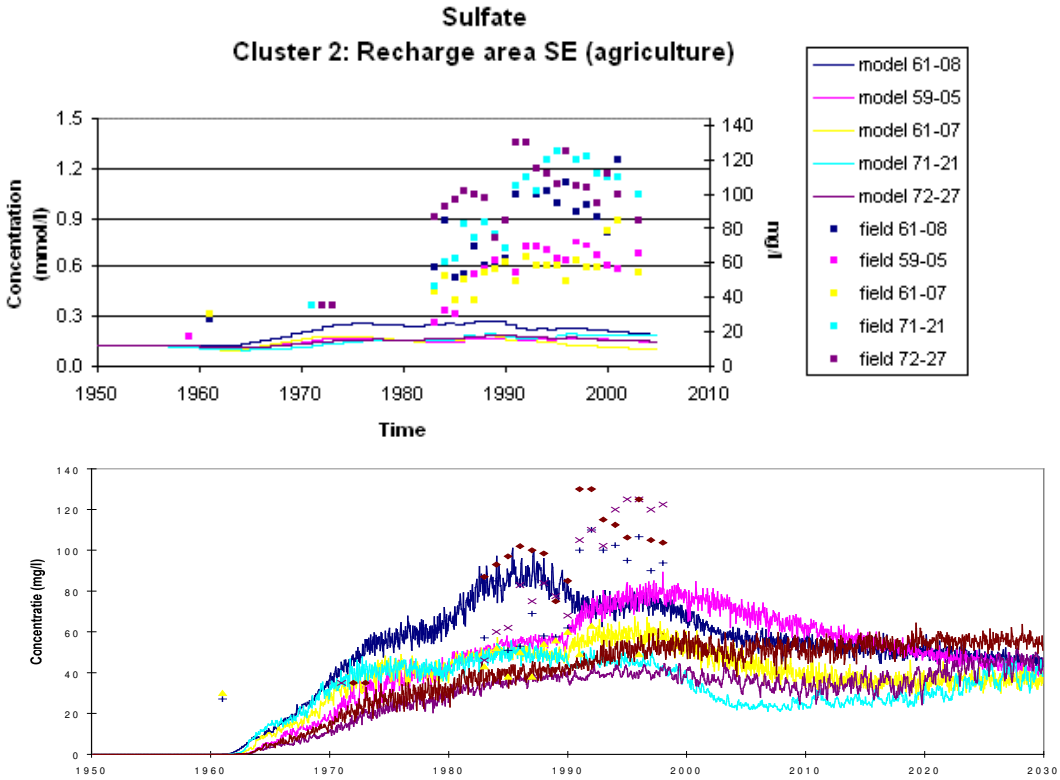


Figure 5.5d - Idem Figure 5.5 c for the wells in Cluster 2.

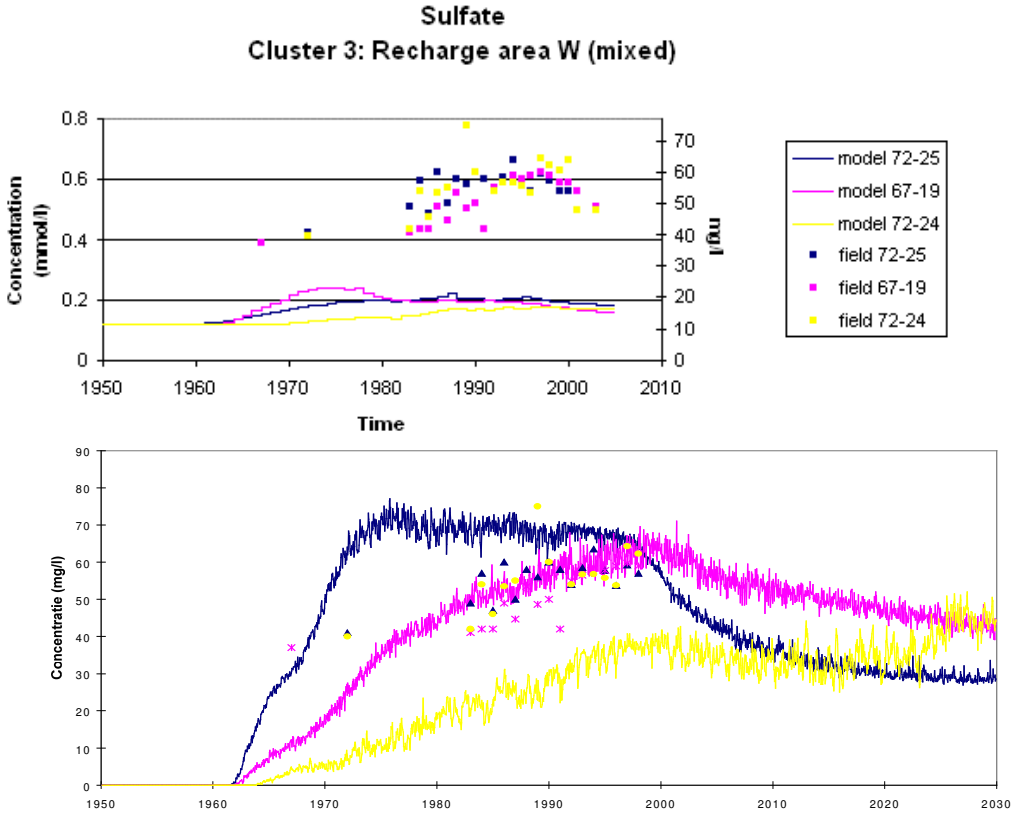


Figure 5.5e - Idem Figure 5.5 c for the wells in Cluster 3.

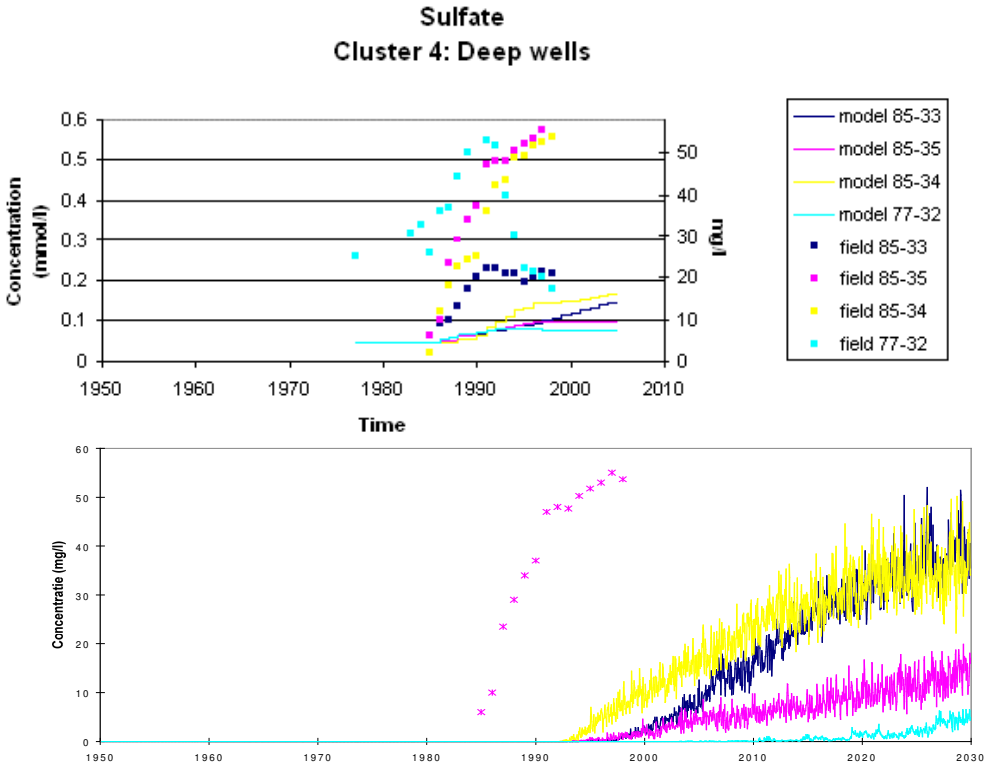


Figure 5.5f - Idem Figure 5.5 c for the wells in Cluster 4. The x-symbol represents field measurements in well 85-35.

Figure 5.5g shows a vertical cross section through the model in which the sulfate concentrations are depicted for several time steps. The time steps for which the sulfate concentrations are displayed are equal to those in Figure 5.3g (1953, 1965, 1979, 1993 and 2005). The concentration is again displayed as a colour range between red (high concentration) and yellow (low (or zero) concentration). The green rectangles represent the pumping wells.

The pictures from 1953 and 1965 in Figure 5.5g show that the sulfate concentrations increase in all aquifers, whereas the pictures from 1979, 1993 and 2005 show a decreasing sulfate concentration in the upper part of the cross section (first aquifer) and an increasing sulfate concentration in the middle and lower parts of the cross section (second and third aquifer). The decrease in the first aquifer is due to the decrease of the sulfate load at surface level.

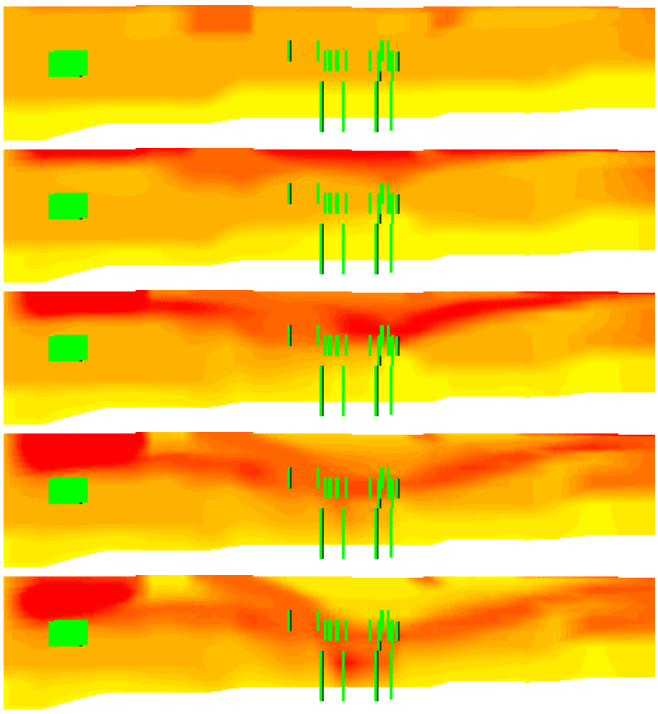

Figure 5.5g - Vertical cross section through the model showing the sulfate concentration in 1953, 1965, 1979, 1993 and 2005. Red and yellow represent high and low (or zero) concentrations, respectively. The green rectangles are the pumping wells.

### *5.3.4 Chloride*

The simulated chloride concentrations averaged for all wells, as they are depicted in Figure 5.6a, start to gradually increase in the early 1960s. The simulated chloride concentration is about 0.35 mmol/l in 1960 and keeps rising to about 0.60 mmol/l in the late 1990s. Subsequently, the concentration is constant until the end of the simulation (2005). As it is supposed that the constant chloride concentration around 2000 represents the maximum load at surface level (Chapter 3; Figure 5.6a), the simulated time lag between infiltration and arrival in the pumping wells is, as was the case with nitrate and sulfate averaged for all wells, approximately 15 years. Furthermore, the simulated chloride concentrations show a decrease and smoothening with respect to the chloride concentrations in the recharge water.

The observed chloride concentrations averaged for all wells increase from 1960 as well. However, since data from 1950 to 1960 are not available, it can not be determined when exactly the chloride concentrations start increasing. Nevertheless, observed chloride concentrations rise faster than simulated chloride concentrations and from approximately 1970, the observed concentrations are considerably larger than the simulated concentrations.

Although the RT3D simulations are relatively low as well with respect to the observations (Figure 5.6b), the concentrations simulated by RT3D show in general a better agreement with the observations.

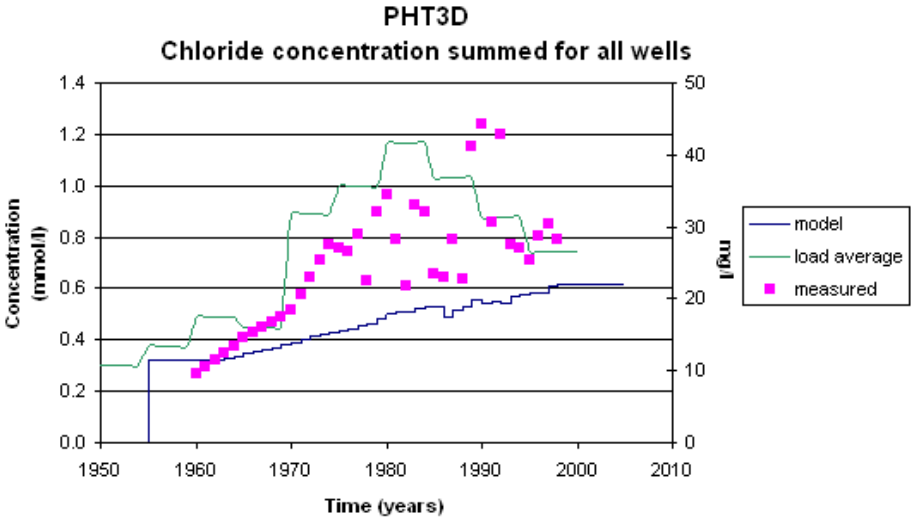


a

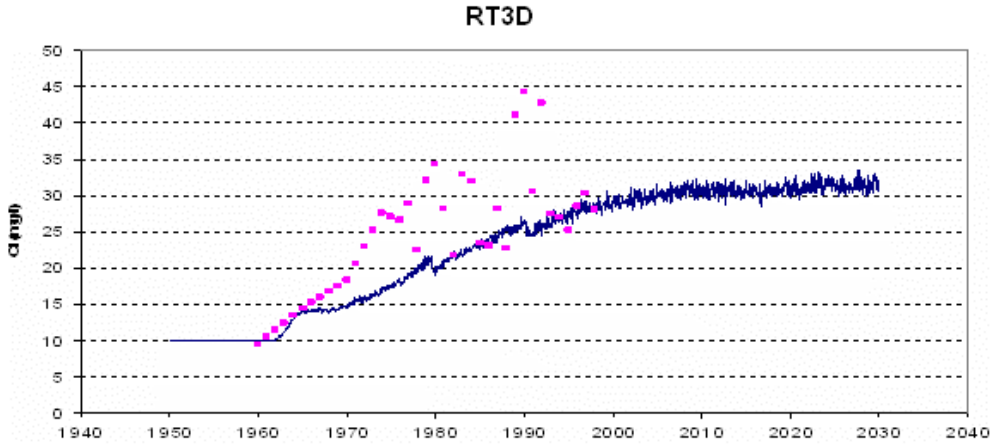


b

Figure 5.6a - Chloride concentrations simulated by PHT3D and observed chloride concentrations averaged for all wells. The load at surface level averaged for all land use types has been depicted for reference. b Chloride concentrations simulated by RT3D averaged for all wells. The blue line represents the simulated concentration, the red data points represent the field measurements.

Although the overall simulated chloride concentrations are higher in the wells in the Clusters 1, 2 and 3, the pattern of the gradual increase in the concentrations from 1960 until the late 1990s is approximately the same in these clusters as it is for all wells averaged (Figure 5.6a, c-e). Moreover, all wells, except wells 72-22 and 71-20, show a constant concentration from the late 1990s until 2005. The concentrations in wells 72-22 and 71-20 keep rising until the end of the simulation.

As was the case with sulfate concentrations, the wells which extract groundwater from beneath agricultural lands (Cluster 2) do not show higher chloride concentrations than the wells which extract groundwater from beneath forest (Cluster 1). Obviously, considering nitrate, sulfate and chloride, nitrate concentrations most evidently reflect differences in land use in the groundwater. This is in accordance with the differences in the load at surface level between the land use types agriculture and nature, which were most evident for nitrate as well.

The observed chloride concentrations agree relatively well with the simulated concentrations for the wells in Cluster 1, where wells 72-26 and 72-22 show the best agreements in the period from 1970 to 1990 and well 71-20 shows the best agreements in the period from 1990 to 2005 (Figure 5.6c). Furthermore, the PHT3D simulations show better results than the RT3D simulations in the wells in Cluster 1. The observed and simulated chloride concentrations in the wells in Cluster 2 correspond moderately well: in the period 1960 to 1990, the simulations are relatively low with respect to the observations, whereas from 1990 to 2005 the agreements are relatively good (Figure 5.6d). The concentrations simulated by RT3D are, with respect to the observations, relatively low from 1960 to 1975 and from 1975 relatively high. In general therefore, the PHT3D results are better than the RT3D results in Cluster 2.

Furthermore, the simulated concentrations for well 67-19 in Cluster 3 agree well with the observed concentrations. However, in wells 72-25 and 72-24, the simulated concentrations are considerably lower than the observed concentrations. The concentrations simulated by RT3D show with respect to the observations approximately the same pattern as the concentrations simulated by PHT3D, except for well 67-19, in which the RT3D concentration increases from 1990, whereas the observed concentrations decrease.

The simulated chloride concentrations in the deep wells in Cluster 4 appear to be almost constant during time (Figure 5.6f). However, although rather slightly, the simulated concentrations do increase from approximately 1985 in wells 85-34 and 85-35, simultaneously with the observed concentrations in these wells. Nevertheless, the simulated increases are about an order of magnitude smaller than the observed increases. The concentrations simulated by RT3D show approximately the same pattern, except that the concentrations in wells 85-34 and 85-35 only start to rise from the late 1990s. The fact that the PHT3D simulations as well as the RT3D simulations are smaller than the observations can be explained by an underestimation of the chloride load at surface level.

Since chloride behaves conservatively in both the PHT3D model and the RT3D model, the differences in simulated chloride concentrations between the models is caused by differences in the chloride load at surface level or in the initial chloride concentrations in the aquifers. Obviously, as the PHT3D results are in general better than the RT3D results with respect to chloride, the load at surface level or the initial concentrations in the aquifers determined for the PHT3D study were in general better than those determined for the RT3D study.

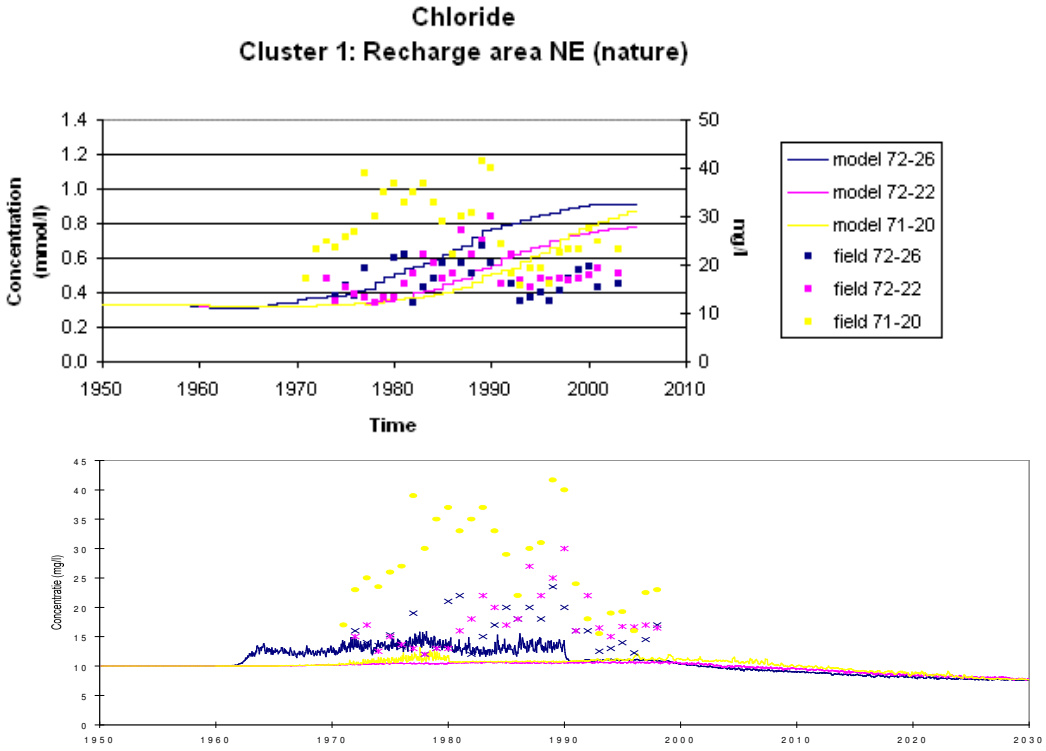


Figure 5.6c - Simulated and observed chloride concentrations for the wells in Cluster 1. The upper plot represents the PHT3D simulation results, the lower plot represents the RT3D simulation results. The colours representing the different wells are equal in both plots, in the RT3D plot the several symbols represent the field measurements.

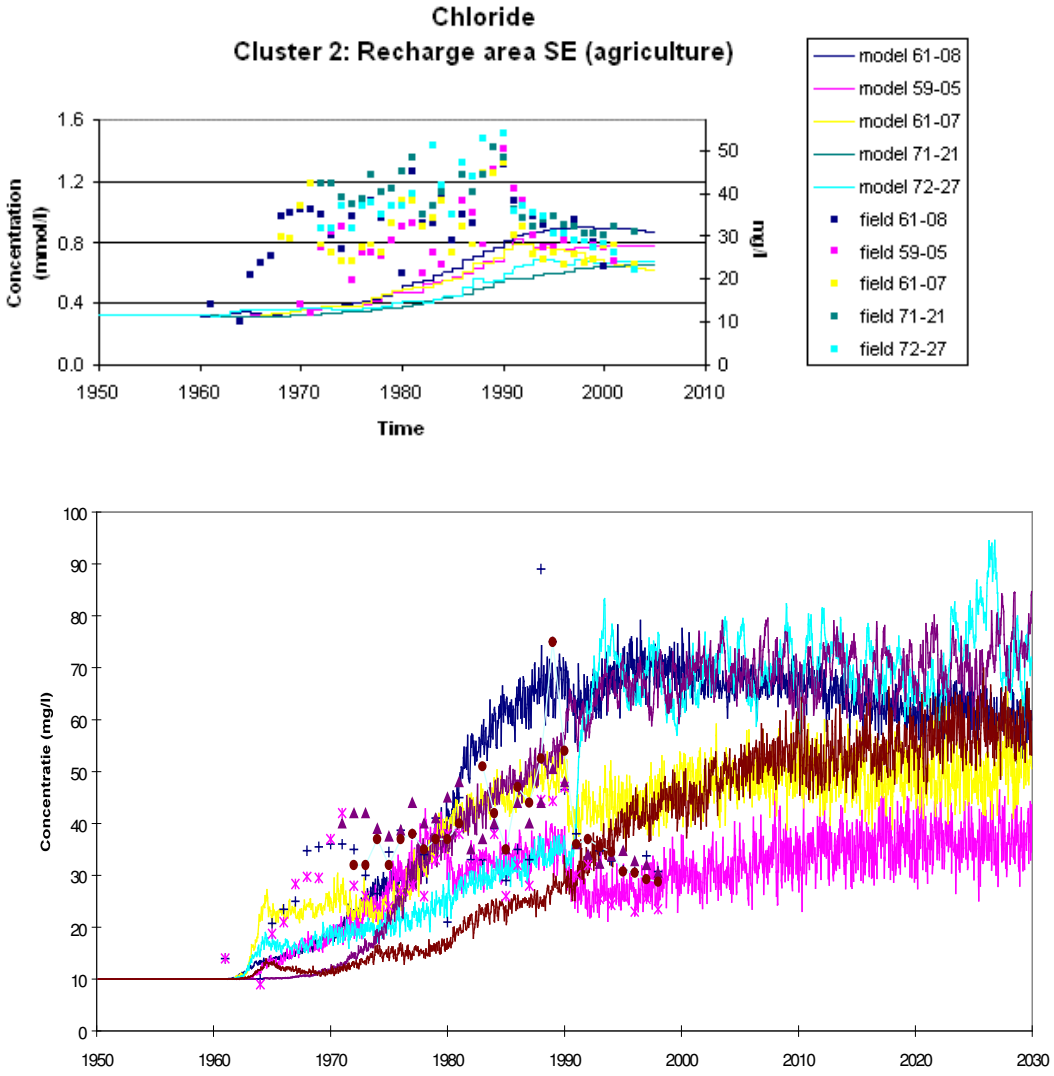


Figure 5.6d - Idem Figure 5.3 c for the wells in Cluster 2.

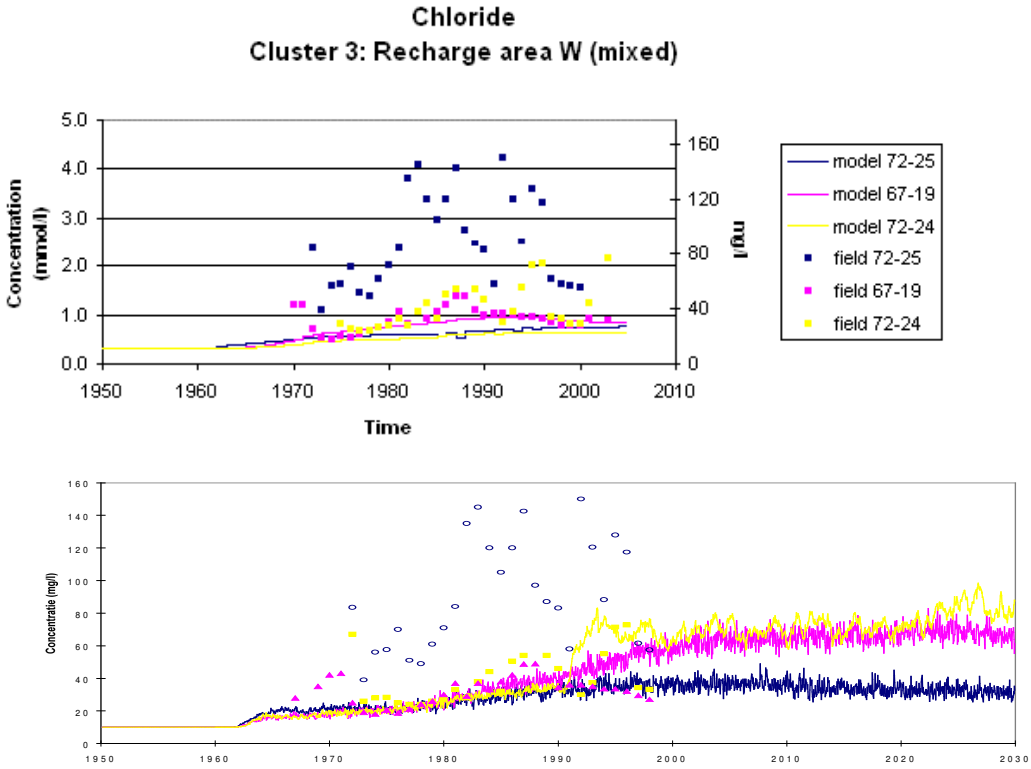


Figure 5.6 e - Idem Figure 5.6 c for the wells in Cluster 3.

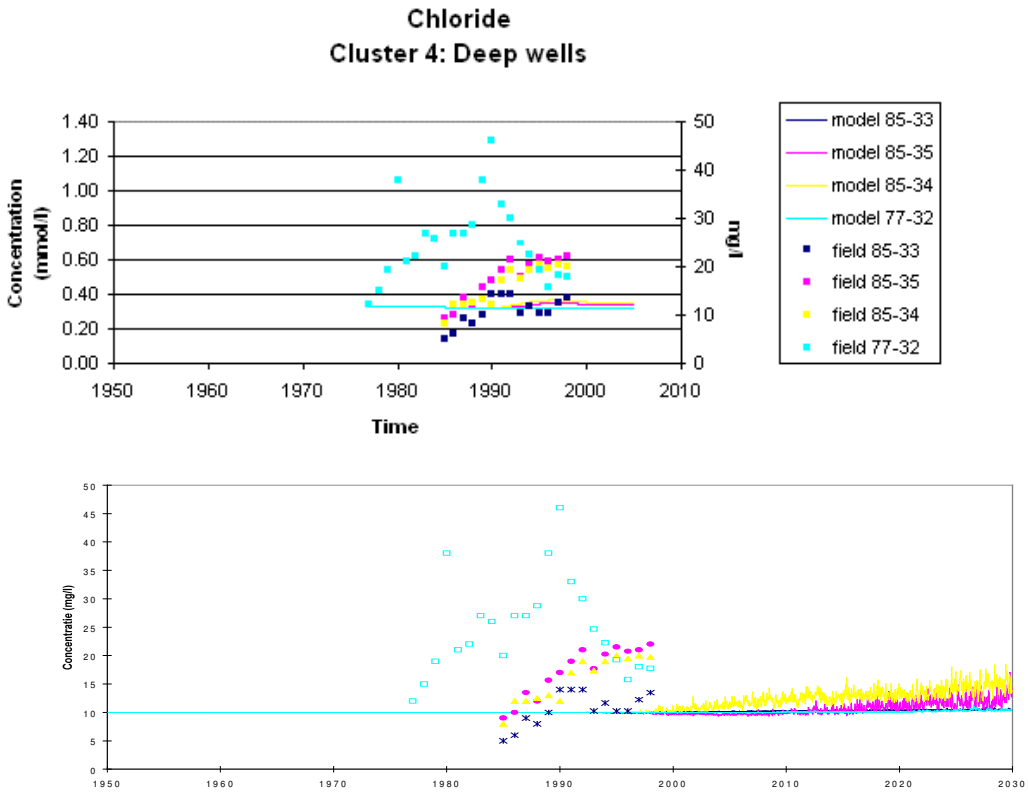


Figure 5.6f Idem Figure 5.6 c for the wells in Cluster 4. In the lower plot, field measurements are represented by several types of symbols.

### 5.3.5 *Calcium and potassium*

The simulated and observed calcium and potassium concentrations for the wells in the Clusters 1 (nature) and 2 (agriculture) are displayed in Figures 5.7 and 5.8, respectively. The load at surface level for nature and agricultural areas are depicted for reference, where the load at pasture and arable land are, based on their surface areas, averaged by weight to obtain the load at agricultural areas. As it can be seen, both calcium and potassium load at agricultural lands is considerably higher than in nature. The difference in load between Cluster 1 and 2 is, although decreased, reflected in the simulated potassium concentrations in the groundwater. However, the simulated calcium concentrations in the groundwater show only a slight difference between Cluster 1 and 2. Obviously, differences in land use are better expressed in potassium concentrations in the groundwater than in calcium concentrations. This is explained by the fact that for calcium, differences in land use are obscured by the process of calcite dissolution, releasing calcium in the groundwater. However, although the differences for potassium between the wells in Cluster 1 and 2 are clear, it can be seen that potassium concentrations in the groundwater beneath nature do increase despite the nearly constant load, and therefore still are affected by the higher potassium concentrations in the agricultural areas. Obviously, the wells grouped as a nature cluster (Cluster 1) are not strictly 'separated' and withdraw groundwater from agricultural areas as well.

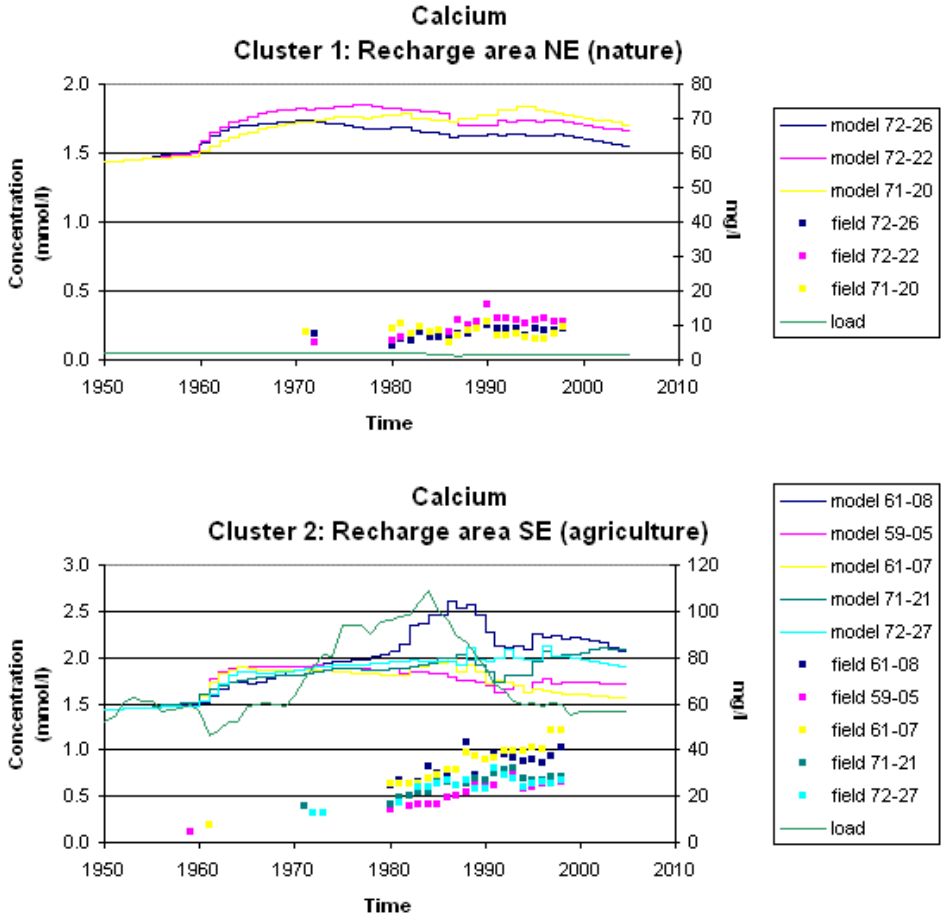


Figure 5.7 Simulated and observed calcium concentrations for the wells in Cluster 1 and 2. The load at surface level for nature and agriculture are depicted for reference.

Furthermore, all wells in Cluster 2, except well 61-08, show a slight increase in potassium concentrations in the early 1970s (Figure 5.8). The concentrations keep rising during the remaining part of the simulation. The one-dimensional model showed that potassium is retarded for 11 years. As the conditions with respect to cation exchange are equal in the one-dimensional and three-dimensional models, it is expected that the maximum potassium load at surface level will arrive around 2006, i.e., ~21 years instead of 10 years later, in the wells in the second aquifer. Well 61-08 shows, as was the case for nitrate and sulfate, a faster increase in the potassium concentration. Obviously, this well experiences changes in load at surface level to a larger extent than the other wells in Cluster 2. This can be explained by the fact that well 61-08 extracts groundwater from shallower depths than do the other wells in Cluster 2 and therefore the decreases in the concentrations as a result of groundwater mixing are smaller.
Moreover, the wells in Cluster 2 show higher potassium concentrations than the wells in Cluster 1 (Figure 5.8). With respect to potassium therefore, the differences in the land use functions nature and agriculture are clearly visible. Finally, in Cluster 1, the simulations are relatively high with respect to the observations, which is due to an overestimation of the load at surface level. The simulated and observed potassium concentrations in the wells in Cluster 2 agree relatively well to each other.

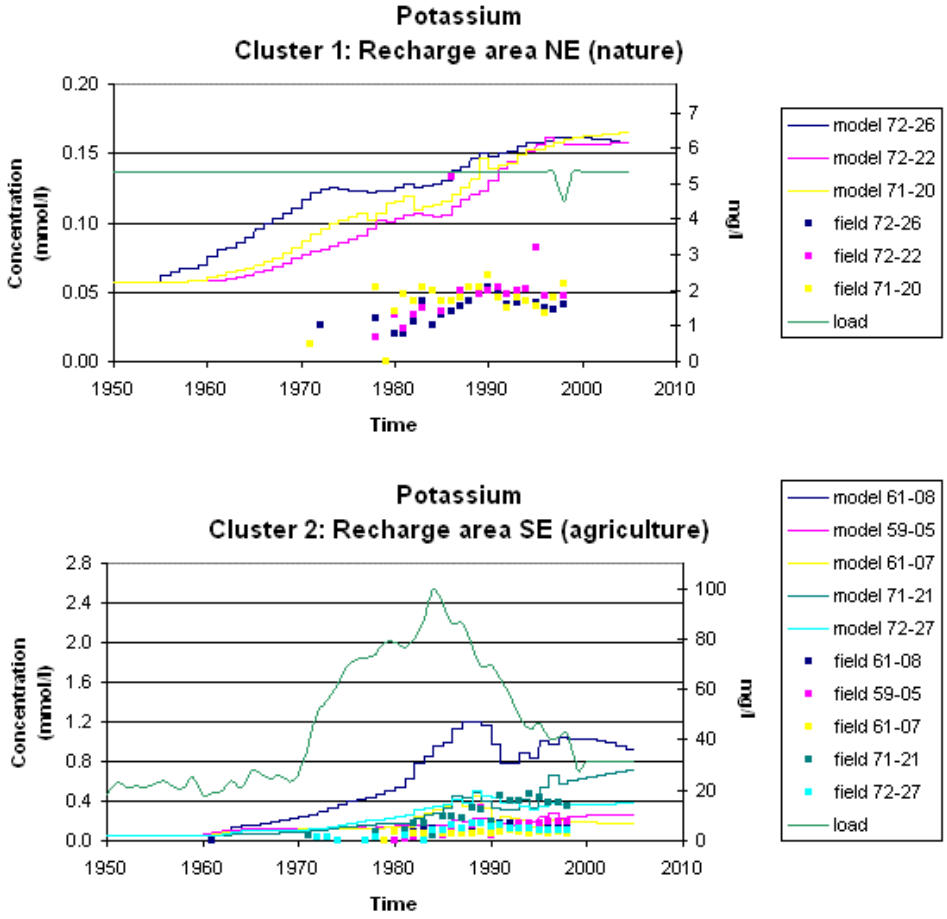


Figure 5.8 Simulated and observed potassium concentrations in the wells in Cluster 1 and 2. The load at surface level for nature and agriculture are depicted for reference.

The simulated calcium concentrations in the groundwater show in all wells in Cluster 1 and 2 an increase from 1960 until 1965 (Figure 5.7). Then, the concentrations are constant until approximately 1985. During the remaining 20 years of the simulation, the calcium concentrations gradually decrease in most wells. However, the concentration in wells 71-20, 61-08, 71-21 and 72-27 shows a different behavior. Well 71-20 shows that the calcium concentration increases from 1985 until 1995. From 1995 until the end of the simulation, the concentration decreases. The calcium concentration in well 61-08 increases relatively fast from the late 1970s until approximately 1985. While the calcium concentration in most wells varies between approximately 1.5 and 2.0 mmol/l, it reaches a value of about 2.5 mmol/l in well 61-08 in the model. Subsequently, from 1985 the concentration unsmoothly decreases in well 61-08. Furthermore, the concentration in well 71-21 shows an increase again from 1990, whereas the concentration in well 72-27 stays relatively constant from 1965 until the end of the simulation in 2005.
Finally, in Cluster 1, the simulated calcium concentrations are considerably higher than the observed concentrations. In Cluster 2, the simulated calcium concentrations better agree with the observations, although they are still relatively high.

### *5.3.6 Iron(II)*

In Figure 5.9a, the simulated iron(II) concentrations in the wells in Cluster 4 (in µmol/l) are displayed. The iron(II) concentrations start to decrease in 1985. Obviously, simultaneously with pyrite oxidation, both iron(II) which is originally present in the third aquifer and iron(II) which is formed by pyrite oxidation are oxidized by nitrate. It was already mentioned before that the oxidized iron precipitates as iron hydroxide (FeOOH).

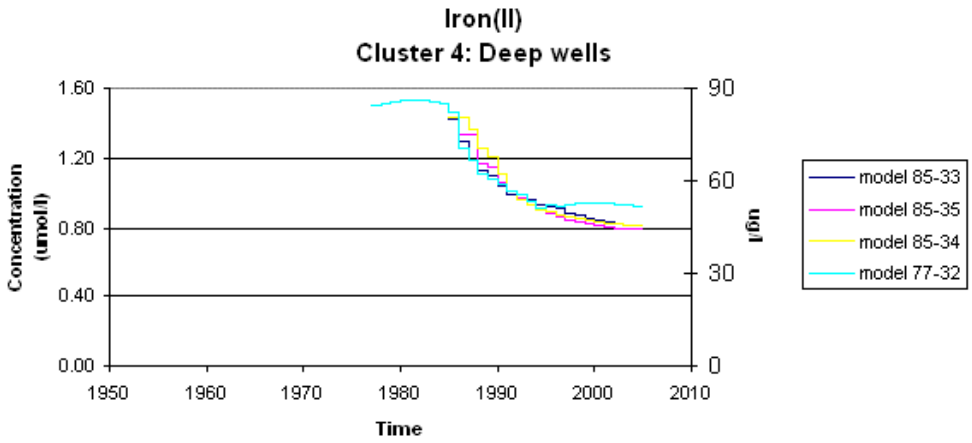


Figure 5.9a - Simulated iron concentration in the wells in Cluster 4.

Furthermore, Figure 5.9b shows a vertical cross section through the model in which the iron(II) concentrations are depicted for several time steps. The time steps for which the iron(II) concentrations are displayed are equal to those in Figure 5.3g (1953, 1965, 1979, 1993 and 2005). The concentration is again displayed as a colour range between red (high concentration) and yellow (low (or zero) concentration). The green rectangles represent the pumping wells.

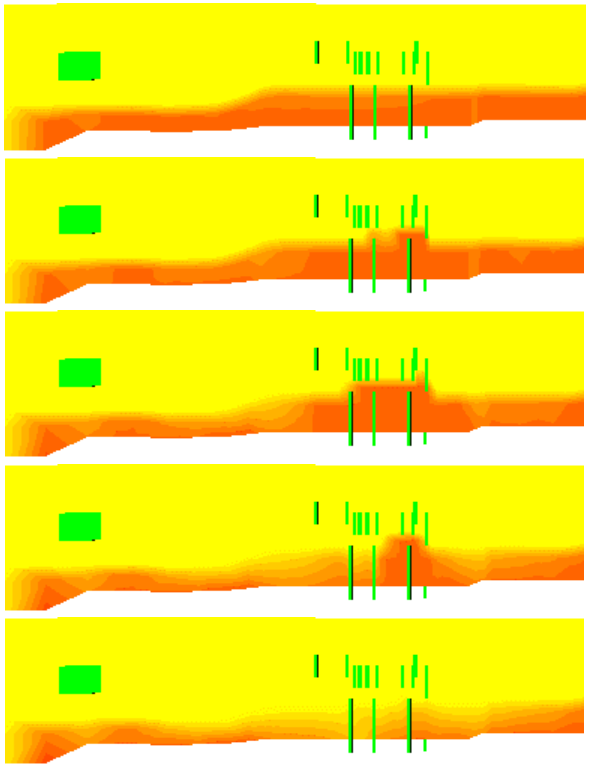

Figure 5.9b Vertical cross section through the model showing the iron concentration in 1953, 1965, 1979, 1993 and 2005. Red and yellow represent high and low (or zero) concentrations, respectively. The green rectangles represent the pumping wells.

In the upper picture, the iron(II) concentration is (nearly) zero in the upper and middle parts of the cross section (first and second aquifer), whereas in the lower part of the cross section (third aquifer), the iron concentration is relatively high. The pictures showing the nitrate concentrations in 1965 and 1979 show that the pumping wells in the second aquifer, which were brought into use from 1955, extract part of their water from the third aquifer, thereby taking along the iron(II) dissolved in the water. The lower two pictures show that in 1993 and 2005, the wells in the second aquifer extract, with respect to 1979, a relatively low amount of groundwater from the third aquifer, as at these time steps the pumping wells in the third aquifer are in use as well. Furthermore, the 1993 and 2005 picture show that, in accordance with Figure 5.9a, the iron(II) concentration in the third aquifer decreases. This is the result of the arrival of nitrate in the third aquifer from 1985, which oxidizes the iron(II).

### *5.3.7 pH and alkalinity*

Figure 5.10 shows the simulated and observed pH values in the deep wells in Cluster 4. In considering the simulated pH values, it should be kept in mind that, as already mentioned, electrical charge imbalances are neutralized by means of pH changes in PHT3D (Prommer et al., 2003). Although the initial and recharge compositions were charge balanced, during the calculation imbalances might have developed and therefore the simulated pH values might have been affected by the neutralizing effect of the model.

As can be seen, pH only slightly increases from 1985 until 2005. Obviously, the hydrogeochemical processes occurring in the third aquifer influence the pH values in the model only to a certain extent. Moreover, as the pH changes are rather slight it is difficult to determine whether hydrogeochemical processes, charge balancing effects or a combination of both cause the changes. Furthermore, the observed pH values are in the same order of magnitude and agree relatively well with the simulations.

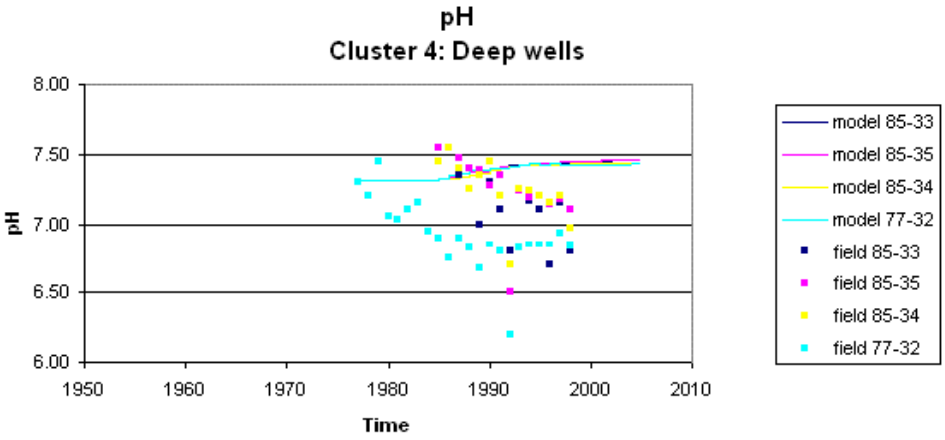


Figure 5.9 Simulated and observed pH values in the wells in Cluster 4. The pH in the recharge water is depicted for reference.

As is the case with pH, PHT3D may change the alkalinity in order to neutralize electrical charge imbalances (Prommer et al., 2003). The alkalinity data might thus be subject to uncertainty as well. Furthermore, $CO_3^{2-}$ was the only carbonate species specified in the model input (Section 5.1.3). It is therefore hard to determine the alkalinity by means of the model output. Consequently, alkalinity is not considered in the description of the simulation results.

## 5.4 Discussion and conclusions

Considering the nitrate, sulfate and chloride concentrations simulated by PHT3D and RT3D it becomes clear that with respect to nitrate and chloride, PHT3D yields better results than RT3D, whereas with respect to sulfate both PHT3D and RT3D do not fully represent the concentration changes in time. Nitrate concentrations simulated by PHT3D show better agreements with observed nitrate concentrations in all wells except well 61-08 (Cluster 2) and the wells in Cluster 3, while chloride simulations show better agreements with the observations in all wells.
However, although for nitrate and chloride the PHT3D results are in general better than the RT3D results, the concentrations simulated by PHT3D do show differences with the observed concentrations as well. The simulated nitrate concentration in well 61-08 (Cluster 2) is relatively high and the nitrate simulations in the wells in Cluster 3 are relatively low with respect to the observations. Furthermore, the simulated chloride concentrations are in general lower than the observed concentrations. With respect to sulfate, the simulated concentrations are lower than the observed concentrations as well. The wells in Cluster 3 show for nitrate, sulfate and chloride the largest differences between simulations and observations.

The reason that differences between simulations and observations still exist is explained by the fact that only one scenario has been calculated in this study. Due to its size and complexity it took a rather long time to get the model running. Therefore, tuning with the parameter values in order to calibrate the model has not been carried out, causing the current scenario to not yet fully represent the hydrogeochemistry as it is observed around pumping station Holten.
The differences between simulated and observed concentrations are due to an underestimation of the load at surface level, an underestimation of the initial concentrations in the aquifers, improper simulation of the hydrogeochemical processes or a combination of these factors. Furthermore, it should be mentioned here that, with respect to the miscalculations in the nitrate and sulfate load at surface level, care has to be taken in comparing the simulated and observed concentrations.

If the simulated nitrate concentrations would be relatively low as a result of excessive nitrate reduction, the simulated sulfate concentrations would be relatively high with respect to the observations (equation (1) in Chapter 2). However, the simulated sulfate concentrations are relatively low as well. Furthermore, sulfate reduction is not likely to occur as siderite is not initially present in the aquifers. Therefore, the relatively low nitrate and sulfate concentrations must be caused by an underestimation of the load at surface level or an underestimation of the initial concentrations in the aquifers. The initial nitrate and sulfate concentrations imposed in the aquifers agree with the observations in most wells (Table 5.1 and Figure 5.3 and 5.5). It is therefore concluded that the low nitrate and sulfate concentrations are due to an underestimation of the load at surface level.
Well 61-08 shows relatively high nitrate and sulfate concentrations with respect to the other wells. Moreover, other components have relatively high concentrations in well 61-08 as well. The relatively high concentrations are explained by the fact that well 61-08 extracts groundwater from shallower depths than do the other wells in Cluster 2. The decreases in the concentrations as a result of mixing are smaller in groundwater at shallow depths than in deeper groundwater.

As chloride behaves conservatively in the model, the relatively low simulated concentrations are caused by an underestimation of the load at surface level or an underestimation of the initial chloride concentration in the aquifers. Figure 5.6 and Table 5.1 suggest that the initial chloride concentration in the aquifers as imposed in the model agrees with the observations. Therefore, an underestimation of the load at surface level caused the relatively low chloride concentrations in the model.

In this study, load at surface level was calculated by means of the available data about atmospheric deposition, applied manure and fertilizers on agricultural lands and data about sinks in the unsaturated zone determining the leaching to the groundwater. The load at surface level was subsequently converted into recharge concentrations (Chapter 3).
In this conversion, the relatively deep groundwater tables at the Holterberg were not taken into account. However, the depth of the groundwater table does influence the load at surface level, in that the load degradation capacity in the unsaturated zone is dependent on the groundwater level. An earlier study determined nitrate, sulfate and chloride in the recharge water by taking into account these differences in the degradation capacity in the unsaturated zone (Beekman, 1998). Moreover, this study considered local heterogeneities in the sediments in the determination of the load at surface level. The nitrate and sulfate concentrations in the recharge water determined by

Beekman (1998) are expected to result in more accurate calculations of groundwater quality in the area around Holten. Nevertheless, these data were not available during this study and could therefore not be used.

The simulated calcium concentrations in Cluster 1 are considerably higher than the observed calcium concentrations. Furthermore, although smaller, differences between simulations and observations exist in Cluster 2 as well. Obviously, as the load at surface level in nature areas is rather low (Figure 5.7), the relatively high simulated concentrations are caused by either excessive calcite dissolution or an overestimation of the initial calcium concentration in the second aquifer or both of these processes. An explanation for excessive calcite dissolution lies in the bicarbonate concentration in groundwater. As a result of low bicarbonate concentrations in groundwater the amount of calcite able to dissolve is large. A large amount of calcite dissolution in turn results in high calcium concentrations. Since the bicarbonate concentrations in the recharge water are rather low for Cluster 1 and bicarbonate is not produced by geochemical processes, the occurrence of excessive calcite dissolution is a plausible explanation for the high simulated calcium concentrations in the second aquifer. Moreover, as Figure 5.7 and Table 5.1 indicate that the initial calcium concentrations imposed in the second aquifer are relatively high with respect to the observations, the high calcium concentrations simulated by the model are due to an overestimation of the initial calcium concentration in the second aquifer as well.
In Cluster 2, the load at surface level is in the same order of magnitude as the simulated calcium concentrations. Therefore, in Cluster 2, the relatively high calcium concentrations are besides excessive calcite dissolution and an overestimation of the initial calcium concentration in the second aquifer, due to an overestimation of the calcium load at surface level.

Simulated potassium concentrations in Cluster 1 are relatively high with respect to the observations. According to Figure 5.8, this is due to both an overestimation of the initial potassium concentrations in the second aquifer and an overestimation of the load at surface level. The simulated and observed potassium concentrations in the wells in Cluster 2 agree relatively well with the observations, except for well 61-08. This implies that for the agricultural areas, the load at surface level and the initial concentration in the second aquifer are correct. Moreover, it is concluded that the cation exchange process has been simulated properly in the second aquifer. It is therefore expected that in the first aquifer, the process of cation exchange has been simulated properly as well and did not cause the relatively high simulated potassium concentrations.

From the iron(II) simulation results it can be concluded that the nitrate entering the third aquifer is reduced by the oxidation of pyrite, the oxidation of in situ iron(II) and the oxidation of iron(II) released by pyrite oxidation. Furthermore, the simulated pH values are in the same order of magnitude as the observed pH values in the wells in Cluster 4, implying that the initial pH value in the third aquifer and the pH value of the recharge water are correct and the hydrogeochemical processes in general have been simulated properly in the third aquifer.

Arranging the wells in clusters according to the provenance of the groundwater showed that the differences in the land use types agriculture and nature are best reflected by the nitrate and potassium concentrations in the groundwater. However, the nitrate and potassium loads at surface level show the largest differences between agriculture and

nature as well (Figure 3.2). Furthermore, the chloride loads at surface level are equal for the land use types agriculture and nature, which explains the fact that the chloride concentrations in the groundwater beneath the land use types agriculture and nature are nearly equal. Finally, the small differences in the calcium concentrations in the groundwater beneath agricultural areas and nature are explained by the dissolution of calcite, which obscures the differences in the load at surface level.

# 6 General conclusions

The one-dimensional model study (Chapter 4) has shown that groundwater quality in the area around Holten depends on the composition of the load at surface level, whereas the reactive components in the aquifers in and around Holten determine the groundwater quality as well. The one-dimensional model study furthermore showed that the equilibria of calcite, pyrite, siderite and iron hydroxide are strongly related to each other in the geochemical setting of the Holten aquifers.

The three-dimensional model study in PHT3D has shown comparable results: both the load at surface level and reactive components in the aquifers determine the groundwater quality in the area around Holten. On the one hand, the evolution of the concentration of conservative or less reactive species such as chloride and potassium are (largely) determined by the load at surface level. On the other hand, the evolution of the nitrate, sulfate, calcium and iron(II) concentrations is, besides the load at surface level, determined by hydrogeochemical reactions, particularly in the third aquifer.
Although the observed nitrate concentration averaged for all pumping wells shows an increasing trend (Figure 5.3a), indicating that the increasing load at surface level is the main factor in determining the groundwater quality, the model reveals that the reduction of nitrate in the third aquifer plays an important part as well. The model results in Figure 5.3 show that, if nitrate reduction would not occur in the third aquifer, the nitrate concentration averaged for all pumping wells would be considerably higher.
With respect to sulfate, the model results of the third aquifer also show that the increasing concentrations are due to both the production of sulfate by pyrite oxidation and the increasing load at surface level (Figure 5.4 and 5.5). Furthermore, the calcium concentration is influenced by calcite dissolution, while the iron(II) concentration in the third aquifer is influenced by oxidation by nitrate.

Furthermore, it was already mentioned that the PHT3D model yields better results than the RT3D model with respect to the nitrate and chloride concentrations in the groundwater. Moreover, PHT3D yields a broader view of the hydrogeochemistry as it is able to take into account many components and hydrogeochemical processes occurring in the aquifers. As the nitrate concentrations in the recharge water in PHT3D are in the same order of magnitude as in RT3D, it is concluded that imposing nitrate reduction by pyrite oxidation and iron(II) as well as imposing iron hydroxide in PHT3D played an important part in the improvement of the nitrate simulations with respect to RT3D. It is therefore furthermore concluded that the differences between simulations and observations in RT3D are caused by the fact that, besides pyrite oxidation by nitrate reduction, no hydrogeochemical processes are incorporated, rather than by wrong estimates of the nitrate concentration in the recharge water.
The sulfate concentrations simulated in PHT3D do not show an improvement with respect to the sulfate concentrations simulated in RT3D. It is therefore hard to determine whether wrong estimates of the recharge concentration or the fact that, besides pyrite oxidation by nitrate reduction, no hydrogeochemical processes were incorporated in the model caused the differences between simulations and observations in RT3D. However, the most important geochemical process affecting the sulfate concentration in the study area, pyrite oxidation, was incorporated in RT3D. It is therefore expected that the differences between simulated and observed sulfate concentrations in RT3D were caused by wrong estimates of the sulfate load at surface level or improper modeling of sulfate leaching from the unsaturated zone.

Chloride was modeled conservatively in both the RT3D and the PHT3D model. Therefore, hydrogeochemical processes did not influence the chloride concentrations in the models. It is thus concluded that the improvements in the PHT3D simulations with respect to the RT3D simulations are due to a better estimation of the chloride load at surface level. However, it should be mentioned that in PHT3D the chloride load at surface level is underestimated as well.

Besides the advantages, it should be mentioned that PHT3D has several disadvantages as well. Constructing a scenario in PHT3D costs relatively much time, due to the fact that the initial aquifer concentrations and the recharge concentrations need to be electrically balanced in PHT3D. Furthermore, changing the scenario and loading the new initial aquifer concentrations and recharge concentrations takes a lot of time as well. Finally, a PHT3D simulation takes a relatively long calculation time. In this study, the calculation time was in the order of one day. Nevertheless, the models size and complexity in this study contribute to the considerable time needed for preparation and calculation as well.

# 7 Recommendations for further research

It was mentioned before that underestimations of the load at surface level caused the differences between simulated and observed nitrate and sulfate concentrations. As it is assumed that the recharge concentration data for nitrate and sulfate determined by Beekman (1998) might result in more accurate calculations of groundwater quality and its changes in time in the area around Holten, it is recommended, if they would be available, to run the PHT3D-model with these recharge data as input.

Furthermore, the PHT3D model results for other components also indicate that the scenario as it is described in Chapter 5 does not yet fully represent the hydrogeochemistry in the subsurface of Holten. However, as was mentioned in Chapter 5, constructing and loading a new scenario in the PHT3D model costs relatively much time. Therefore, in this study, only one scenario could be calculated in PHT3D.
Consequently, it is recommended to further improve the current PHT3D scenario. On the one hand, the initial concentrations in the aquifers and the load at surface level should be adapted for chloride, calcium and potassium. On the other hand, other components should be incorporated in the model. Soil organic matter (SOM) was not taken into account as the behavior of organic matter was not in the scope of this study. However, SOM is likely to be an important component in the study area as brought forward by respiration experiments using the micro-oxymax (Griffioen et al., 2003). It is therefore recommended to expand the model exercise by incorporating SOM as a chemical component and adding SOM oxidation as a geochemical process.
It was mentioned before that besides overestimations of the initial concentrations and the load at surface level, the high calcium concentrations in the model are caused by excessive calcite dissolution as a result of an underestimation of the bicarbonate concentration in the recharge water. It is therefore recommended to improve the bicarbonate concentration in the recharge water. Moreover, it is advised to better estimate the initial bicarbonate concentration in the aquifers. The incorporation of SOM in the model will contribute to a better representation of the bicarbonate concentration in the aquifers as well, as the oxidation of SOM yields bicarbonate in the groundwater.

It is also recommended to measure reduced sulfur species and methane concentrations in the groundwater. This would lead to a better understanding of the oxidation and reduction processes occurring in the aquifers, which would in turn result in a better model definition.

Furthermore, it is advised to determine groundwater age at several sites by means of e.g. tritium measurements. If groundwater ages would be known, field observations and model results could more accurately be compared and therefore it would be easier to calibrate the model. Subsequently, this would result in more efficient adjustments of the model input.

Finally, if the simulation period would be increased with a few tens of years, a realistic prediction can be made of the future evolution of the groundwater quality in the aquifers in and around Holten.

# References

Appelo, C.A.J. & Postma, D., [1993]. Geochemistry, groundwater and pollution. Balkema, Rotterdam.

Beekman, W., [1998]. Beschrijving SPREAD. Voorspelling van nitraat, hardheid, chloride en sulfaat in het ondiepe grondwater. KIWA/VEWIN.

Van den Brink, C. & Van Immerzeel, C.H., [2002]. Ruimtelijke ontwikkeling en grondwaterbeheer DR 4. MD-SAT: Berekening van de uitspoeling uit de onverzadigde zone – Handleiding en Toepassingen. Royal Haskoning.

Clement, T.P., [1997]. RT3D. A Modular Computer Code for Simulating Reactive Multispecies Transport in 3-Dimensional Groundwater Aquifers. Pacific Northwest National Laboratory, Richland, Washington.

Coppoolse et al., [1993]. Zware metalen in oppervlaktewater: bronnen en maatregelen. Riza, nota 93.012.

Griffioen, J., Buijs, E.A., Den Otter, C., Keijzer, T.J. & Van den Brink, C., [2002]. Ruimtelijke ontwikkelingen en Grondwaterbeheer. Grondwaterkwaliteit, belasting en (geo)chemische processen (DR 3). NITG-TNO & Royal Haskoning.

Griffioen, J., Van den Brink, C., Van der Grift, B., Roelofsen, F., Zaadnoordijk, W.J. & Frapporti, G., [2003]. Ruimtelijke ontwikkelingen en Grondwaterbeheer. Uitgangssituatie drinkwaterwinning Holten (DR 5). NITG-TNO & Royal Haskoning.

Van der Grift, B. & Van Beek, C.G.E.M., [1996]. Hardheid van onttrokken grondwater. 4, indicatieve voorspellingen. KIWA/VEWIN.

Van der Grift, B., Griffioen, J. & Beekman, W., [2003]. Handleiding Geïntegreerd Transportmodel voor Grondwaterkwaliteit. Versie 3.1. NITG-TNO & KIWA.

Harbaugh, A.W., & McDonald, M.D., [1996]. User's documents for MODFLOW-96, an update to the U.S. Geological Survey modular finite-difference ground-water flow model. U.S. Geological Survey Open File Report 96-485.

Hotsma et al., [1997]. Gehalten aan zware metalen in meststoffen. IKC, Ede.

Hotsma et al., [1999]. Gehalten aan zware metalen in kalkmeststoffen. Meststoffen 1999.

[1993] Onderzoek intrekgebieden drinkwaterwinningen Overijssel. Iwaco, eindrapport fase 2, nr 22.0641.0.

Maas, D.J., [2002]. Acidification and subsurface reactive transport of cadmium at groundwater pumping station Holten. NITG-TNO.

Meeuwessen, P.C. & Van Erp, P.J., [1995]. Invloed van het meststoffengebruik op de zware metalenaanvoer in de Nederlandse landbouwgronden. Heidemij Advies, Arnhem.

Parkhurst, D.L. & Appelo, C.A.J., [1999]. User's guide to PHREEQc (Version 2) – A computer program for speciation, batch-reaction, one-dimensional transport, and inverse geochemical calculations. U.S. Geological Survey, Water-Resources Investigations Report 99-4259.

Prommer, H., Barry, D.A. & Zheng, C., [2003]. MODFLOW/MT3DMS based reactive multi-component transport modeling. Ground Water 42 (2).

Pronk, A., [1994]. Jaarstatistiek van de Kunstmeststoffen 1993/'94. Periodieke rapportage 66-93/94. LEI-DLO, Den Haag.

Raven, K.P. & Loeppert, R.H., [1997]. Trace element composition of fertilizers and soil amandements. J. Environ. Qual. 26, pp 551-557.

[1994] Risico's van wonen en woningbouw in grondwaterbeschermingsgebieden. Tauw.

Zheng, C. & Wang, P.P., [1998]. MT3DMS. A modular Three-Dimensional Multispecies Transport Model. The University of Alabama.

# A Translations English – Dutch

| English | Dutch |
|---|---|
| Agricultural Economic Institute - | Landbouw Economisch Instituut - Dienst |
| Agricultural Survey | Landbouwkundig Onderzoek |
| arable land | bouwland |
| breeding sows | fokzeugen |
| calcium fertilizers | kalkmeststoffen |
| horned cattle | rundvee |
| load at surface level | maaiveldbelasting |
| maize | mais |
| moorland | heidegrond |
| nitrogen fertilizers | stikstofmeststoffen |
| pasture | grasland |
| phosphor fertilizers | fosfaatmeststoffen |
| porkers | mestvarkens |
| potassium fertilizers | kalimeststoffen |
| poultry | pluimvee |
| residential neighborhood | villawijk |
| Statistics Netherlands | Centraal Bureau voor de Statistiek (CBS) |

# B Converting load data in kg $m^{-2}$ $year^{-1}$ to moles $l^{-1}$

| **units** | **calculation** | **units** |
|---|---|---|
| kg $ha^{-1}$ $year^{-1}$ | divide by $1e^4$ | kg $m^{-2}$ $year^{-1}$ |
| kg $m^{-2}$ $year^{-1}$ | multiply by $1e^3$ | g $m^{-2}$ $year^{-1}$ |
| g $m^{-2}$ $year^{-1}$ | divide by 250* | g $l^{-1}$ |
| g $l^{-1}$ | divide by gram formula weight | moles $l^{-1}$ |

*Annual recharge in l $m^{-2}$ $year^{-1}$ (Griffioen et al., 2003).

# C Short version of input file used in PHREEQC-2

```
DATABASE d:\Phreeqc\InputPhreeqc\phreeqc.dat
TITLE  Holten multi species one-dimensional reactive transport model

SOLUTION 0      # input load 1950-1951
  units  mol/l
  temp   10.0
  pH     5.4
  pe     16.0   O2(g)  -0.7
  Na     6.663e-04
  K      4.657e-04
  Ca     1.298e-03
  Mg     2.421e-04
  Cl     3.036e-04
  Alkalinity    1.998E-05 as HCO3-
  S(6)   5.686e-04
  N(+5)  4.719e-04  as NO3-

SOLUTION 1-20   # Aquifer 1
  units  mol/l
  temp   10.0
  pH     5.4
  pe     15.962
  Na     4.653e-04
  K      5.851e-04
  Ca     6.591e-04
  Mg     2.196e-04
  Cl     3.244e-04
  Alkalinity    1.965e-04 as HCO3-
  S(6)   3.086e-04
  N(+5)  7.048e-04 as NO3-

SOLUTION 21-80  # Aquifer 2
  units  mol/l
  temp   10.0
  pH     5.6
  pe     -0.66
  Na     2.393e-04
  K      5.115e-05
  Ca     2.283e-04
  Mg     7.817e-05
  Fe     8.953e-06
  Cl     3.244e-04
  Alkalinity   1.912e-04 as HCO3-
  S(6)   3.644e-4
  N(+5)  8.105e-5 as NO3-
```

```
SOLUTION 81-200 # Aquifer 3
  units  mol/l
  temp   10.0
  pH     7.45
  pe     -3.04
  Na     1.673e-04
  K      5.115e-05
  Ca     1.752e-03
  Mg     2.232e-04
  Fe     1.343e-04
  Cl     3.174e-04
  Alkalinity   3.361e-03 as HCO3-
  S(6)   2.252e-04
  N(+5)  0.0 as NO3-

EXCHANGE 1-20
   X    0.00212
   -equilibrate 1-20
EXCHANGE 21-80
   X    0.00152
   -equilibrate 21-80
EXCHANGE 81-200
   X    0.0378
   -equilibrate 81-200
EQUILIBRIUM_PHASES 1-20
   Goethite 3.0    0.1044
EQUILIBRIUM_PHASES 21-80
   Goethite 3.0    0.03132
   Calcite  0.0    0.01668
   Siderite 0.5    0.007731
EQUILIBRIUM_PHASES 81-200
   Pyrite   0.0    0.07731
   Goethite 3.0    0.01044
   Calcite  0.0    0.1557
   Siderite 0.5    0.07731

TRANSPORT
   -cells  200
   -shifts  2
   -time_step  15.768e6
   -lengths  0.35
   -dispersivities 0
   -print_frequency 100
   -punch_frequency 100

SELECTED_OUTPUT
      -file              complete run.prn
      -state              true
      -pH                 true
      -pe                true
      -alkalinity          true
```

```
    -totals              Na K Ca Mg Cl C(4) C(-4) Fe(2) O(0)
    -molalities          NO3- SO4-2 HCO3- CaX2 MgX2 FeX2 NaX KX
    -equilibrium_phases   pyrite goethite siderite calcite
    -saturation_indices   pyrite goethite siderite calcite

PRINT
    -equilibrium_phases   true
    -exchange             true
END

SOLUTION 0     # input load 1951-1952
  units  mol/l
  temp   10.0
  pH     5.4
  pe     16.0   O2(g)  -0.7
  Na     5.621e-04
  K      5.872e-04
  Ca     1.366e-03
  Mg     2.777e-04
  Cl     3.036e-04
  Alkalinity   1.998e-05 as HCO3-
  S(6)   5.717e-04
  N(+5)  4.714e-04 as NO3-
TRANSPORT
   -shifts  2
END

SOLUTION 0    # input load 1952-1953
  units  mol/l
  temp   10.0
  pH     5.4
  pe     16.0   O2(g)  -0.7
  Na     5.480e-04
  K      5.331e-04
  Ca     1.507e-03
  Mg     2.846e-04
  Cl     3.036e-04
  Alkalinity   1.998E-05 as HCO3-
  S(6)   6.270e-04
  N(+5)  4.639e-04 as NO3-
TRANSPORT
   -shifts  2
END
…..
…..
…..
…..
SOLUTION 0    # input load 2000-2001
  units  mol/l
  temp   10.0
  pH     5.4
```

```
  pe     16.0   O2(g)  -0.7
  Na     7.065e-04
  K      8.098e-04
  Ca     1.407e-03
  Mg     5.642e-04
  Cl     7.432e-04
  Alkalinity   1.998E-05 as HCO3-
  S(6)   4.195e-04
  N(+5)  1.430e-03 as NO3-
TRANSPORT
   -shifts  2
END
```

# D Location of the pumping wells

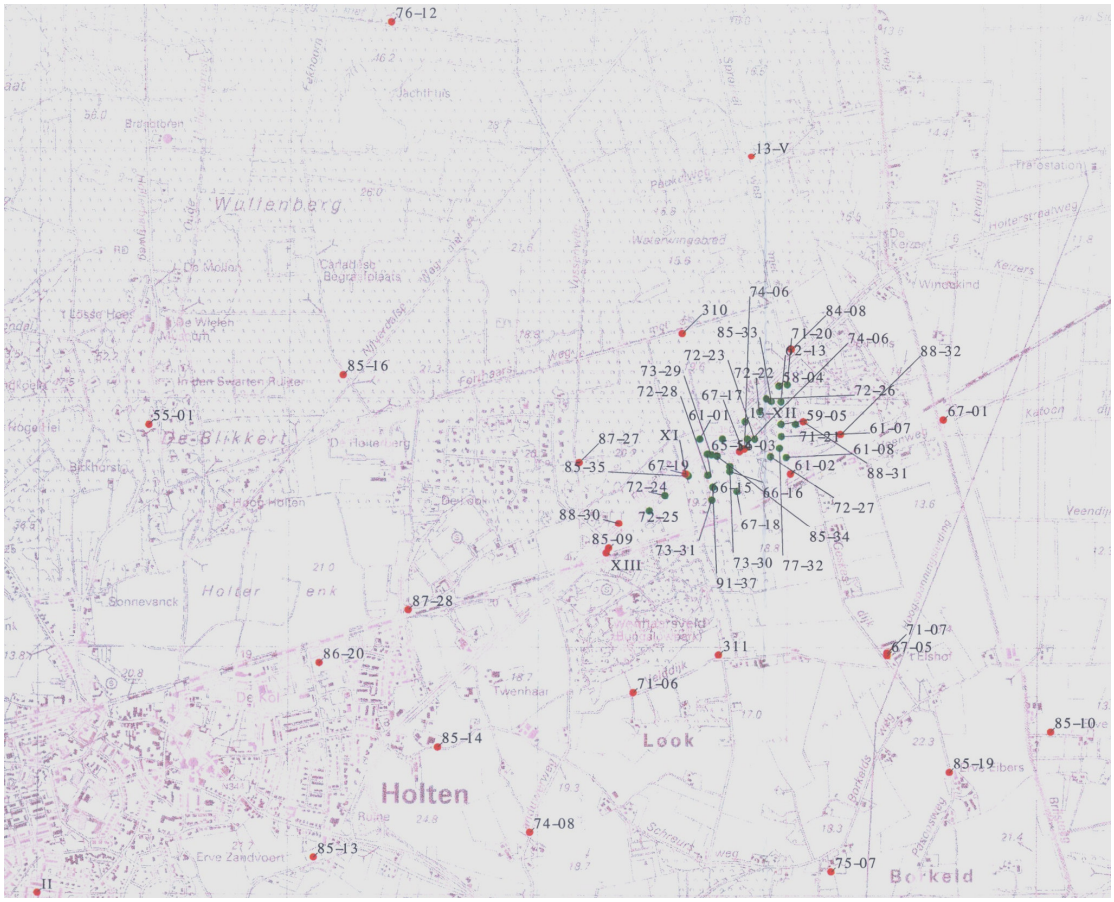


The red and green dots represent observation and pumping wells, respectively.